Nanocomposite-graphene based platform for heavy metal detection

Chandré Monique Willemse

BSc Chemistry (honours)

A thesis submitted in fulfillment of the requirements for the degree of Magister Scientiae in the Department of Chemistry, University of the Western Cape

Supervisor: Dr. N. Jahed

Co- Supervisor: Prof. E. I. Iwuoha

November 2010

Nanocomposite-graphene based platform for heavy metal detection

Chandré Monique Willemse

KEYWORDS

Square-wave anodic stripping voltammetry

Heavy metal detection

Trace metal analysis

Thin metal film

Glassy carbon electrode

Detection limit

Nanocomposite

Graphene

Nafion

Metal sensor

ABSTRACT

Amongst the various environmental pollutants, heavy metals such as lead, cadmium, copper and zinc are considered the most important due to their high stability and their ability to bioaccumulate. Heavy metals are extremely dangerous for all biological organisms but especially to human life. Thus it is of great importance to analyze and quantify these toxic heavy metals in the environment. This study reports the synthesis of graphene by oxidizing graphite to graphite oxide using H_2SO_4 and $KMnO_4$ and reducing graphene oxide to graphene by using $NaBH_4$. Graphene was then characterized using FT-IR, TEM, AFM, XRD, Raman spectroscopy and solid state NMR. Nafion-Graphene in combination with a mercury film electrode, bismuth film electrode and antimony film electrode was used as a sensing platform for trace metal analysis in 0.1 M acetate buffer (pH 4.6) at 120 s deposition time, using square-wave anodic stripping voltammetry (SWASV). Detection limits were calculated using 3σblank/slope. For practical applications recovery studies was done by spiking test samples with known concentrations of metal ions and comparing the results to inductively coupled plasma mass spectrometry (ICP-MS). This was then followed by real sample analyses. The Nafion-G mercury film electrode still proved to be the most sensitive since it was the only platform able to detect traces of Zn^{2+}, Cd^{2+} and Pb^{2+} in lake water, for the Nafion-G bismuth and Nafion-G antimony film electrode it was below the detection limit. Detection limit values for individual analysis on the Nafion-G mercury film electrode was; 0.07 µg L^{-1} for Pb^{2+} and Zn^{2+} and 0.08 µg L^{-1} for Cd^{2+}, on the Nafion-G bismuth film electrode it was; 0.13, 0.18 and 0.33 µg L^{-1} for Pb^{2+}, Cd^{2+} and Zn^{2+} respectively and lastly on the Nafion-G antimony film electrode it was; 0.03, 0.07 and 0.32 µg L^{-1} for Pb^{2+}, Cd^{2+}

and Zn^{2+} respectively. These detection limits found at a deposition time of 120 s for each metal, were more sensitive when compared to previously reported literature.

DECLARATION

I declare that **"*Nanocomposite-graphene based platform for heavy metal detection*"** is my own work, that is has not been submitted for any degree or examination in any other university, and that all the resources I have used or quoted have been indicated and acknowledges by complete references.

UNIVERSITY *of the*
WESTERN CAPE

Chandré Monique Willemse   November 2010

Signed…………………………………………………

# ACKNOWLEDGEMENTS

LIST OF PUBLICATIONS

1. **Chandré M. Willemse**, Khotso Tlhomelang, Nazeem Jahed, Priscilla G. Baker and Emmanuel I. Iwuoha, Metallo-Graphene Nanocomposite Electrocatalytic Platform for the Determination of Toxic Metal Ions, Sensors, 2011, 11, 3970-3987.

UNIVERSITY *of the*
WESTERN CAPE

LIST OF ABBREVIATION

- ➢ AdSV   Adsorptive stripping voltammetry

- ➢ AFM   Atomic force microscopy

- ➢ ASV   Anodic stripping voltammetry

- ➢ BiFE   Bismuth film electrode

- ➢ CNT   Carbon nanotube

- ➢ CSV   Cathodic stripping voltammetry

- ➢ CVD   Chemical vapor deposition

- ➢ DPP   Differential pulse polarography

- ➢ DPSV   Differential pulse stripping voltammetry

- ➢ EPA   Environmental protective agency

- ➢ FAAS   Flame atomic absorption spectrophotometry

- ➢ FET   Field-effect transistor

- ➢ FT-IR   Fourier transformed infrared

- ➢ GCE   Glassy carbon electrode

- ➢ GFAAS   Graphite furnace atomic absorption spectroscopy

- ➢ GO   Graphite oxide

- ➢ HgFE   Mercury film electrode

- ➢ HMDE   Hanging mercury drop electrode

- ➤ ICP-OES   Optical emission inductively coupled plasma spectrometry

- ➤ ICP-MS   Inductively coupled plasma mass spectrometer

- ➤ LCD   Liquid crystal display

- ➤ LSSV   Linear scan stripping voltammetry

- ➤ Nafion-G   Nafion-Graphene

- ➤ OLED   Organic light emitting diode

- ➤ PSA   Potentiometric stripping analysis

- ➤ ppb   Parts per billion

- ➤ QHE   Quantum Hall Effect

- ➤ SbFE   Antimony film electrode

- ➤ SiC   Silicon carbide

- ➤ ssNMR   Solid state nuclear magnetic resonance

- ➤ SV   Stripping voltammetry

- ➤ SWASV   Square-wave anodic stripping voltammetry

- ➤ SWV   Square wave voltammetry

- ➤ TEM   Transmission electron microscopy

- ➤ TMFE   Thin mercury film electrode

- ➤ XRD   X-ray diffraction

LIST OF FIGURES

LIST OF TABLES

TABLE OF CONTENTS

1. INTRODUCTION

1.1 Heavy metals and their effect on health and the environment?

The term "heavy metals" is used to define any metal that has a relatively high density and is toxic at low concentration [1]. Of the more than 20 heavy metals, four are of particular concern to human health namely lead, cadmium, mercury and arsenic. These belong to a class of pollutants that produce undesirable health effects, even if present in minuscule quantities [2]. Heavy metals tend to accumulate in the food chain and human body and are stored in soft and hard tissue [1]. They are natural components of the earth's crust and are extremely toxic and poisonous at low concentrations, and thus cannot be degraded or destroyed. Some heavy metals such as copper, selenium and zinc are essential for maintaining the metabolism of the human body, however when the concentration of these heavy metal exceed a certain threshold amount poisoning can occur. Heavy metal poisoning occurs via the intake of contaminated drinking water (e.g. lead pipes), food or atmosphere (emissions from factories) and industry is the main source of high amounts reaching the environment.

The Environmental Protective Agency (EPA) has set a maximum contamination level (MCL), for cadmium, lead, copper and zinc at 5 ppb, 15 ppb, 1.3 ppm and 5 ppm respectively [3]. Yearly, approximately 25,000 tones of cadmium is released into the environment of which half is

released into rivers through weathering of rocks, some is released into the air through forest fires and volcanoes [1]. Exposure to lower amounts of cadmium causes renal dysfunction, bone degradation, lung insufficiently liver damage and hypertension in humans with both acute and chronic toxicity [2, 3]. Lead on the other hand, is one of four metals that have the most damaging effect. Most of the lead found in the environment is as a result of human activities. Exposure to lead causes brain and/ or kidney damage, disruption of the nervous system, miscarriages and subtle abortions. Lead is known to affect the nervous system of unborn children. Under or over exposure of zinc also causes health problems. If too little, zinc is absorbed by the human body loss of appetite, decreased sense of taste and smell; slow wound healing and skin sores [1] and birth defects occur. Very high levels of zinc damages the pancreas and are dangerous to unborn and newborn children especially when mothers have absorbed large concentrations of the metal, it reaches unborn children through blood and young children through mother's milk [1]. Copper is released into the environment by both natural and human activities. It enters the air mainly during the combustion of fossil fuels. Furthermore since, copper is found in a variety of food, drinking water and air, we absorb eminent quantities each day by eating, drinking and breathing [1]. Over exposure of copper may cause liver and/ or kidney damage and even death and is also associated with Wilson's disease which is an autosomal recessive genetic disorder in which copper accumulates in tissue [2].

In considering the toxic effects of these heavy metals it is wise to know or at least be familiar with the metal content in various matrices, owing to the fact that there is a very narrow "concentration window" which exists between toxic and essential levels for these metals [4]. It is wise to have a thorough understanding of the effects of trace metal analysis, which depends

largely on the availability of sensitive and reliable analytical techniques such as, atomic absorption spectroscopy (AAS), plasma emission spectrophotometry (ICP), X-Ray fluorescence and Stripping Voltammetry.

1.1.1 Why use stripping voltammetry?

Electrochemical stripping analysis has been recognized as a powerful tool for heavy metal analysis [5, 6]. It is capable of measuring four to six samples simultaneously at concentration levels down to the sub-parts per billion (sub-ppb) in addition the instrumentation required to perform the analysis is inexpensive. Its spectroscopic competitor the graphite furnace atomic absorption spectrometer (GFAAS) has nearly the same sensitivity but it is much more expensive. Inductively coupled plasma atomic emission spectroscopy (ICP-AES) can also determine metals simultaneously but in the higher ppb range and at a much higher cost. Stripping analysis instrumentation is small in size, has a very low power demand (small carbon footprint), and requires no special installation or additional instrumentation.

A major criticism leveled at ASV is the use of mercury working electrodes which are extremely toxic, thus the technique is making use of more environmentally friendly materials such as antimony and bismuth. Thus far, bismuth has been considered as the best alternative to the mercury electrode [7], due to its low toxicity, its reasonably wide potential window [8] and its ability to form alloys with many metals. Antimony on the other hand revealed an attractive electroanalytical performance for measuring trace heavy metals and its application as a substitute

for the mercury analogue is particularly beneficial considering, e.g., approximately 30 times lower toxicity than the mercury electrode [9]. The advantage of using a thin film is that it offers a large surface area to volume ratio that provides a high amalgam concentration during the deposition step. It has a high plating efficiency which results in high sensitivity and this plating efficiency is enhanced due to the electrode which can be used under vigorous conditions, unlike in the case of the hanging mercury drop electrode (HMDE). The number of publications based on bismuth and antimony has been few, 121 publications based on bismuth and 14 based on antimony.

1.1.2 Graphene

Graphene took the physics community by storm when the first paper appeared in 2004. The man who discovered graphene along with his colleague, Kostya Novoselov is Andre Geim. Graphene, a single- atom-thick sheet of hexagonally arrayed sp2-bonded carbon atom has recently been getting a lot of attention due to its excellent electronic [10-12], thermal [13] and mechanical [14, 15] properties. This material is remarkable in terms of thinness and resiliency and is also said to be the strongest material in nature; roughly 200 times the strength of steel [15]. The advantages of using graphene are its strong adsorptive capabilities, huge specific surface area due to the nano-sized graphene sheet and nano-scale thickness of these sheets and also its good conductivity [16]. Graphene has been attracting a great deal of interest to explore its fascinating application since it was experimentally produced in 2004 [17]. It is suggested to be a very important material, not only for fundamental research but also for device applications.

Graphene's availability and processability has been the rate-limiting step in the evaluation of graphene applications [17, 18]. Researchers reported numerous works based on growth and exfoliation [19-22]. Currently micromechanical cleavage is the most effective and reliable method to produce high-quality graphene sheets [23]. The disadvantage of this method however, is its low productivity, which makes it unsuitable for large-scale applications. To produce good quality graphene sheets, high yield productions are desirable for applications such as composite materials and conductive films [23]. Exfoliation of graphite oxide either by rapid thermal expansion or ultrasonic dispersion has been one of the best approaches to obtain graphene in bulk [24, 25]. In comparison to other production techniques, this method is best because of its reliability, amenability to large-scale production and exceptionally low material costs [23].
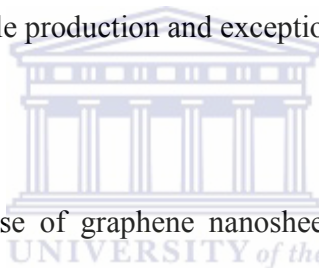
Li et al. [26] demonstrated the use of graphene nanosheets for the development of a high-performance electrochemical sensor for dopamine and electro-catalytic oxidation of methanol. Worden et al. [27] reported the use of a high performance glucose biosensor based on the exfoliated graphite nanoplatelets as a viable and inexpensive alternative to carbon nanotubes (CNT). The purpose of this work is to create a sensing platform for the determination of selected metals based on the Nafion-graphene nanocomposite (Nafion-G) modified electrode, in combination with an *in situ* plated thin metal film.

1.2 Rationale and Motivation

Due to the low levels and toxic nature of heavy metals it is imperative to monitor the concentration thereof in the environment, to identify and/ or limit threats to human health and natural ecosystems, investigate trends in pollution and to identify future problems. To meet these requirements much research has been conducted over the years to develop sensitive and selective equipment and analysis procedures capable of determining trace level (μg L^{-1} range) of heavy metals in the environment. Stripping analysis is the most widely used technique for trace analysis. Mercury based electrodes are commonly used as the working electrode because of its excellent reproducibility and high sensitivity [28]. However due to its toxic nature, numerous attempts have been made to replace it with new mercury-free and reliable electrodes. Recently the bismuth film and antimony film electrodes has been drawing increasing attention in the field of stripping analysis due to their low toxicity and many other advantages they have, which has proved to be equal to or even more superior to that of the mercury film electrodes [7, 9]. Recent literature suggests that using a graphene based nanocomposite would improve the sensitivity of metal detection. Li et al. [29] developed a cadmium sensing platform with the HgFE based on the graphene nanosheets. Although the sensing platform showed ultra-sensitivity for the detection of cadmium, its wide use was limited due to the toxicity of mercury. So Li et al. [16] did some further studies and employed graphene nanosheets in combination with the *in situ* bismuth film electrode to fabricate a sensitive and mercury-free electrochemical platform for the analysis of lead and cadmium. They concluded that the prepared Nafion-G nanocomposite film not only exhibited improved sensitivity for the metal ion detection, but also alleviated the interferences due to the synergistic effect of graphene nanosheets and Nafion [16].

6

1.3 Objectives

The focus of this study is to synthesize the Nafion-G nanocomposite and investigate its applicability towards the detection of metals at various metal thin film electrodes. To achieve this, the following must be met:

i. Synthesis of graphene by subjecting graphite to a harsh oxidation process using H_2SO_4 and $KMnO_4$, to produce graphite oxide, which is then intern reduced using $NaBH_4$ to graphene.

ii. Characterize graphene using FT-IR, XRD, TEM, AFM, solid state NMR, and Raman spectroscopy.

iii. Modify the GCE with the Nafion-G nanocomposite and plate a metal thin film (Hg, Bi or Sb) electrochemically on the Nafion-G surface. And investigate its applicability towards the detection of trace metals.

iv. Do a comparative study of the different Nafion-G metal films.

v. Do recovery studies to test the accuracy of the analysis followed by real sample analysis.

1.4 Thesis structure

This thesis is comprised of five chapters and is structured as follows:

Chapter 1   Introduction

Chapter 1 gives an introduction to stripping analysis and graphene. The rationale and motivation of this project are also given as well as the objectives that must be met.

Chapter 2   Literature Review

Chapter 2 presents the literature review, which covers relevant aspects of graphene, trace metals and stripping voltammetry; as well as the characterization techniques used to characterize graphene.

Chapter 3   Materials and Method

Chapter 3 gives an account on the specific equipment used in the analysis, before explaining in detail the protocols involved in the synthesis, characterization and electrochemistry of the analysis.

Chapter 4   Results and Discussion

Chapter 4 presents the results and discussion with relevant references to literature. The main trends of the results are discussed and connecting the results with the literature and any correlation that has emerged in the data are highlighted.

Chapter 5   Conclusion and Future work

Chapter 5 concludes this thesis by summarizing the main points highlights the novelty of the research and provides conclusions and recommendations as well as future work.

2. LITERATURE REVIEW

2.1 GENERAL BASIS OF VOLTAMMETRY

2.1.1 Voltammetry

Voltammetry is a general name of electroanalytical methods used in analytical chemistry and various industrial processes. In voltammetry, the current is monitored as the potential of the electrode is changed [30, 31]. Voltammetry measurements are usually carried out using a two or three electrode system. The cell consists of a working electrode, reference electrode and auxiliary electrode. The auxiliary electrode is only incorporated in a three electrode system shown in Fig. 2.1 [32]. In voltammetry the "working electrode" serves as the electrode at which the reaction of interest takes place. The potential of this electrode serves as the driving force for the electrochemical reaction, meaning, it is the controlled parameter that causes the chemical species in solution to be reduced or oxidized at the surface [4]. Then there is the reference electrode, whose purpose is to provide a known and stable potential that is insensitive to the composition of the solution and with which the potential of the working electrode is compared [4]. The third electrode namely the auxiliary electrode completes the three electrode system. It is employed to minimize errors from cell resistance.
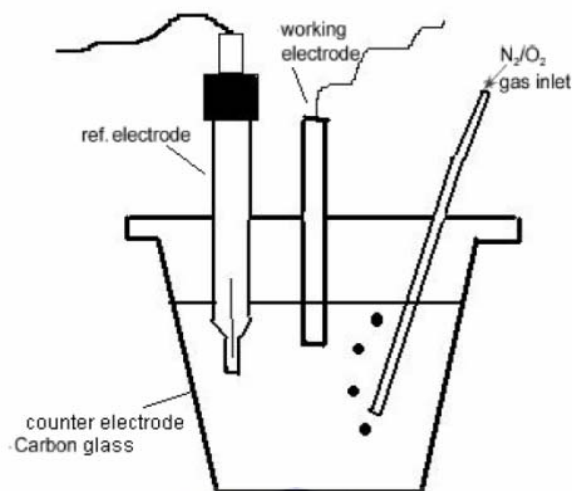
Figure 2.1: Three electrode system for voltammetry.
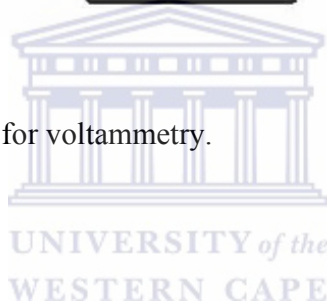
2.1.2 Stripping Voltammetry

Stripping voltammetry is a sensitive electroanalytical technique for measuring trace heavy metal ions. The unusual high sensitivity and selectivity are based on the fact that the analyte is accumulated before it is determined and that both accumulation and determination are electrochemical processes whose progress can be controlled. When compared with other polarographic work, determinations by stripping voltammetry are generally more sensitive by a factor of 10^3 to 10^5, so that the detection limits are between 10^{-9} and 10^{-11} mol L^{-1} and in some cases even 10^{-12} mol L^{-1}. This indicates that stripping analysis is one of the most sensitive instrumental analysis methods.

Stripping analysis consists of three steps. Metal ions are accumulated (deposited) onto an electrode which is held at the reduction potential of the metal being analyzed. This potential is called the "deposition potential" and the time in which deposition occurs is called the "deposition time". The solution is stirred during deposition to maximize the amount of metal deposited. In the second step, the stirring is stopped so that the solution becomes quiet and this is known as the "rest period". The third step involves the metals being stripped out from the amalgam at specific half-wave potentials. The current observed during the stripping step can be related to the amount of metal ion in the solution. There are various types of stripping analysis techniques namely Anodic Stripping Voltammetry, Cathodic Stripping Voltammetry and Adsorptive Stripping Voltammetry.

2.2 WHY USE STRIPPING ANALYSIS

Usually analytical chemists prefer to use the techniques which they know and have had the opportunity of studying and working with. The discussion that follows is a comparison of the different techniques used for trace metal analysis and does not propose that stripping analysis replace these techniques. Each technique in its own offers its advantages and disadvantage and it is the work of the analyst to decide which technique is best for a particular problem or analysis.

2.2.1 Comparison between Stripping Voltammetry, Graphite Furnace Atomic Absorption Spectroscopy and Inductively Coupled Plasma Spectrometry

Detection limits and reproducibility of stripping analysis compare favorably with that of GFAAS and ICP spectrophotometry. Stripping voltammetry is an electrochemical technique and GFAAS and ICP spectrometry are optical techniques. Only metals (and sulphur and phosphorus) in solution are analyzed with optical techniques, while stripping analysis allows to analyze also oxidizable or reducible anions and organic compounds [33].

2.2.1.1 Graphite Furnace Atomic Absorption Spectrometry (GFAAS)

The detection limits for the GFAAS fall in the ng L^{-1} range for most elements. The sample is atomized in a very short period of time, concentrating the available atoms in the heated cell, which causes an observed increase in sensitivity [34]. This technique only makes use of micro liter sample volumes; however, the small sample size is compensated by the long residence time in the light path, which results in detection limits similar to techniques which use much larger samples. The disadvantage however is that the GFAAS requires a great number of lamps and for better reproducibility an automatic sampler and injection system is strictly necessary [33]. Also the instrumentation needs a frequent replacement of graphite tubes and it also wastes a lot of inert gas (argon) and the instrumentation is much more expensive and time consuming.

2.2.1.2 Inductively Coupled Plasma Spectrophotometry (ICP)

Inductively coupled plasma (ICP) spectrophotometry is applicable to the determination of a large number of elements. The detection limit for this technique is generally in the $\mu g\ L^{-1}$ (ppb) range and it also offers simultaneous analysis, longer linear dynamics and fewer condensed phase interferences [35]. However ICP spectrophotometry wastes a great deal of argon and it uses very dilute solutions. Also the injection system gets dirty or broken very easily and the instrumentation is very expensive as well as time consuming.

2.2.1.3 Stripping Voltammetry (SV)

Stripping analysis is capable of measuring four to six trace metals simultaneously in the sub parts per billion range. Its instrumentation is inexpensive and small in size. This technique also has a low power demand (small carbon footprint), requires no additional instrumentation or special installation [4]. No other technique for trace metal analysis can compete with stripping analysis on the basis of sensitivity per money invested. Other advantages of stripping analysis include species characterization, its suitability for automatic on-line monitoring and for *in situ* measurements. Figure 2.2 indicates the different detection limits for different metal analysis techniques [33].
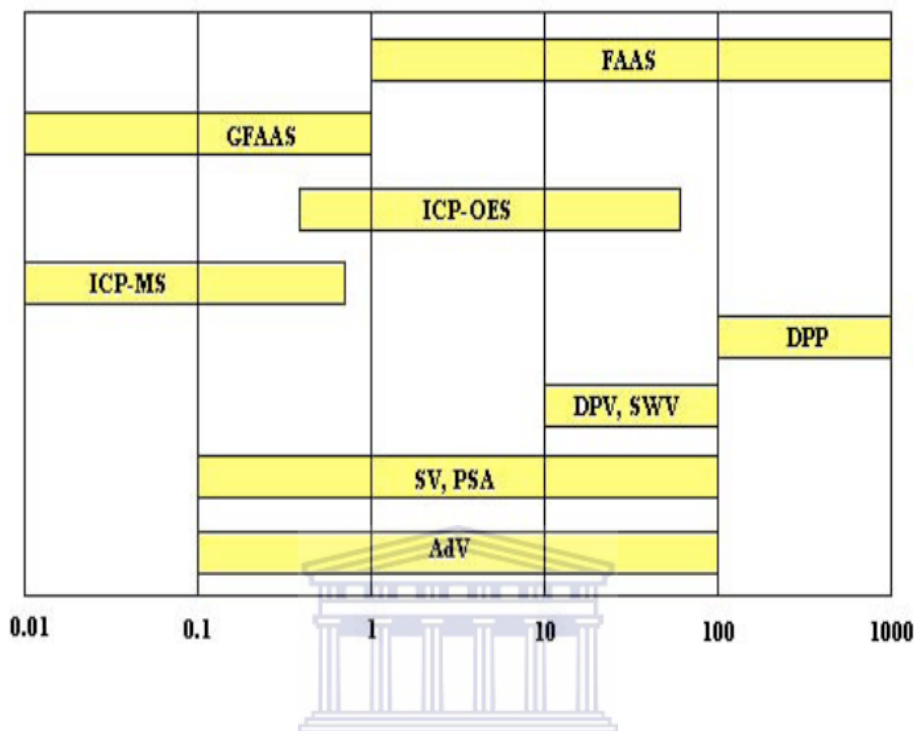
Fig 2.2: Detection limits ($\mu g \ L^{-1}$) of the principal techniques for trace analysis. Refer to list of abbreviations.

2.3 PRINCIPLES OF STRIPPING VOLTAMMETRY

2.3.1 Deposition step

Stripping voltammetry is a powerful electroanalytical technique, whose low detection limit is attributed to the pre-concentration that takes place during the deposition step. The deposition step is carried out at a fixed/ controlled potential for a definite time under reproducible mass transport conditions in the solution [36] . During the deposition step the analyte of interest is electroplated onto/into the working electrode forming an amalgam with the mercury. In the anodic variant of

stripping analysis the analyte is accumulated by their reduction into or onto the working electrode and as for the cathodic variant of stripping analysis, it utilizes the deposition of various organic and inorganic species as sparingly soluble compounds on the surface of the electrode. Whichever method is employed, the deposition potential imposed on the working electrode depends on the metal ion species to be determined and is maintained for a certain deposition time depending on their concentrations [36]. The formation of an amalgam depends on the solubility of the metal in mercury (Table 2.1).

Table 2.1: Solubilities of metals in mercury [4].

Element	Solubility in Hg (atomic %)	Element	Solubility in Hg (atomic %)
Ag	0.066	Mg	2.5
Al	0.015	Mn	0.007
Au	0.133	Na	4.8
Ba	0.48	Ni	2.1×10^{-3}
Bi	1.1	Pb	1.3
Cd	10.0	Pu	0.013
Co	3.0×10^{-4}	Pt	0.10
Cu	0.006	Sb	4.7×10^{-5}
Ga	3.6	Sn	1.26
In	70.0	Tl	43.0
K	2.0	Zn	5.83

2.3.2 Rest period

After the deposition step, the stirring of the solution is stopped and the solution is allowed to become quiescent. This causes the concentration of metal in the amalgam to reach uniformity [4]. The purpose of the rest period is also to ensure that the stripping step which is to follow is performed in a quiescent solution.

2.3.3 Stripping step

During the stripping step, the deposited metal is oxidized (stripped) back into solution by oxidation into the ionic form:

$$M\ (Hg) \rightarrow M^{n+} + ne$$
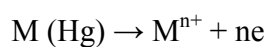
The voltammogram recorded during this step provides the analytical data of interest. The potential at which the stripping occurs is related to the redox potential of the metal. Peak potentials serve to identify the metals in the sample. In the following section the nature of the stripping step is discussed.
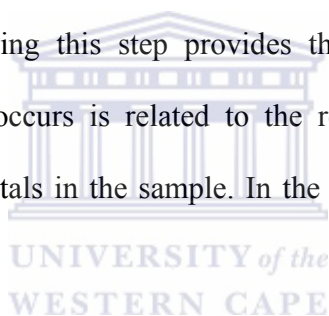
2.3.3.1 Linear scan stripping voltammetry (LSSV)

There are a number of ways in which the potential can be scanned and linear scan stripping voltammetry is one of them (LSSV). In LSSV the current of the working electrode is measured, while the potential between the working electrode and the reference electrode is scanned linearly as a function of time. The oxidation or reduction of species is registered as a peak in the current at the potential at which the species begins to be oxidized or reduced.

2.3.3.2 Differential pulse stripping voltammetry (DPSV)

Differential pulse stripping voltammetry (DPSV) is probably one of the most widely used stripping modes, designed to compensate the charging background current [4]. In DPSV, a series of regular pulses of equal amplitude are superimposed on an anodic potential scan (Fig. 2.3[37]). In most cases the basic potential scan rate is slow so that the ramp potential does not change much during the pulse life [4]. The currents are measured twice before the pulse and at the end of the pulse. The first current is subtracted instrumentally from the second one, and the current difference is plotted as a function of potential. A voltammogram is obtained, with the peak potential corresponding to the maximum rate of metal oxidation for a given potential range.
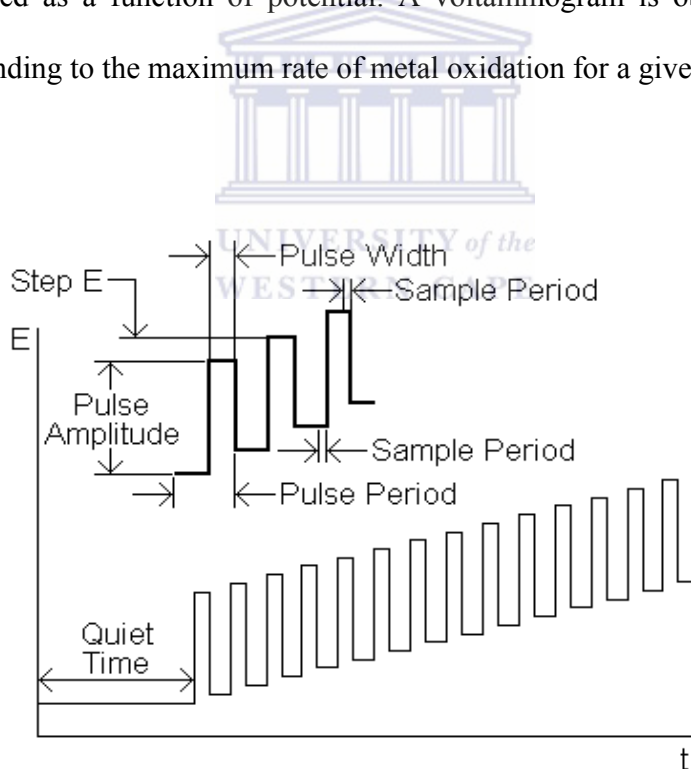
Figure 2.3: Potential wave form for differential pulse stripping voltammetry.

2.3.3.3 Staircase stripping voltammetry (SCSV)

In this stripping mode, the potential sweep is a series of stair steps. The current is measured at a given time after the potential change and then plotted versus the potential. Staircase stripping voltammetry is characterized by parameters such as step height, ΔE, and the step width, T. Even though the sensitivity of this waveform is similar to that of differential pulse stripping voltammetry it is much faster, due to its rapid potential scan [4].

2.3.3.4 Square-wave stripping voltammetry (SWSV)

This stripping mode was introduced by Barker [38], and involves the superposition of a square-wave on the potential staircase sweep. The current is measured at the end of each half-wave, just prior to the potential change (Fig.2.4[37]). The current measured on the reverse half-cycle (ir) is subtracted from the current measured on the forward half-cycle (if). The difference is plotted as a function of potential. Square-wave stripping voltammetry is often used due to its high sensitivity, speed of analysis and insensitivity of dissolved oxygen in the sample.
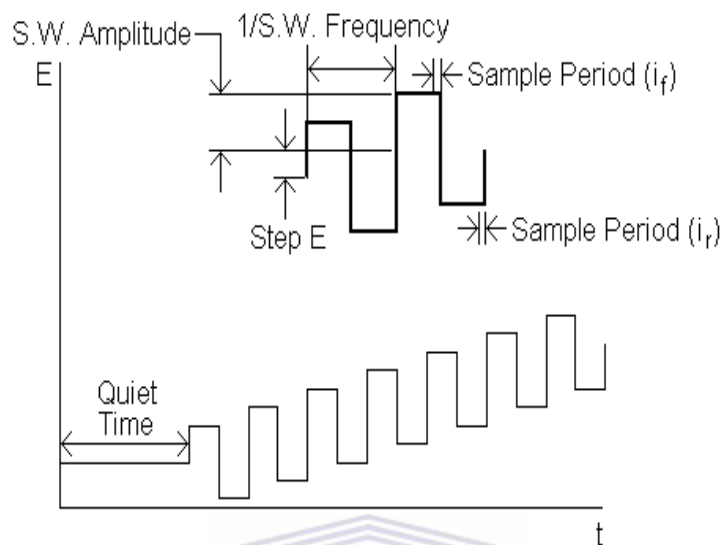
Figure 2.4: Potential wave form for square-wave stripping voltammetry.
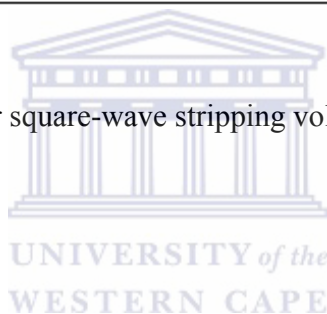
2.4 STRIPPING METHODS

2.4.1 Anodic Stripping Voltammetry (ASV)

This technique describes exactly the process that is occurring during the voltammetric scan. During deposition the analyte in the sample solution is reduced and concentrated into the mercury electrode as an amalgam. This is followed by metals being stripped from the mercury anodically to form its ions back in solution. The mechanism can be described as follows [4]:

Mechanism of anodic stripping voltammetry	
Deposition:	$M^{n+} + ne \rightarrow M \ (Hg)$
Stripping step:	$M \ (Hg) \rightarrow M^{n+} + ne$
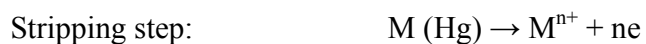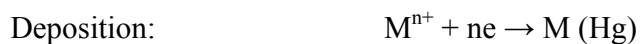
2.4.2 Cathodic Stripping Voltammetry (CSV)

CSV is used to determine a wide range of organic and inorganic compounds that form insoluble salts with the electrode material [39]. This technique is similar to anodic stripping voltammetry, except that deposition involves the oxidation of the metal ions as an insoluble film onto the working electrode. A negative potential then strips the deposited film into solution. The mechanism can be described as follows [4]:
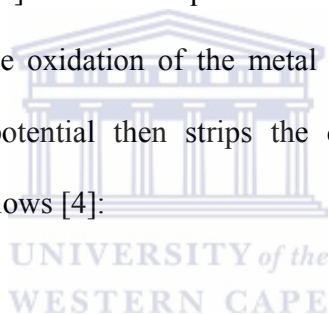
Mechanism of cathodic stripping voltammetry	
Deposition:	$M \rightarrow M^{n+} \ ne$ $M^{n+} + A^{n-} \rightarrow MA$
Stripping step:	$MA + ne \rightarrow M + A^{n-}$

2.4.3 Adsorptive Stripping Voltammetry (AdSV)

This technique is similar to anodic and cathodic stripping voltammetry. The difference is that the analyte is deposited by adsorption on the working electrode surface, rather then by electrolysis. Chemically modified electrodes are often used.

2.5 INSTRUMENTATION USED FOR STRIPPING ANALYSIS

2.5.1 Working Electrodes

The working electrode, is the electrode at which the reaction of interest is occurring [30-32]. Sensitivity and reproducibility plays a major role in the selection of working electrode used for stripping analysis. The ideal working electrode should be easy to handle, have a low background current, favorable electrochemical behavior of the analyte(s) of interest, a reproducible surface area or easy to re-condition, long-term stability, i.e., no fatigue or poisoning phenomena as a result of electrochemical reactions. Mercury based electrodes (HMDE, MFE) are most frequently used as the working electrodes, due to their excellent reproducibility, high sensitivity [40] and wide cathodic range.

2.5.1.1 The Hanging Mercury Drop Electrode (HMDE)

The hanging mercury drop electrode was developed by Wiktor Kemula, a famous Polish chemist, electrochemist, polarographist in the late 1950s [41]. It is one of the most popular working electrodes for stripping analysis. It produces a partial drop of controlled geometry and

surface area at the end of a capillary. The drop is usually dislodged at the end of the stripping step, and a new drop is dispensed for the next experiment [4]. However, there are several disadvantages to the HMDE. The first one being that it has a low surface area to volume ratio. The small area of the drop reduces the plating efficiency and the large volume yields a low concentration of metal in mercury $C_a = i_L t_d / nFV_{Hg}$ [4]. This is the same reason why intermetallic interferences are minimized. Due to the large volume, peak broadening occurs as well as loss of selectivity. Not very long deposition times are used because the metals may diffuse up into the mercury column in the capillary, resulting in further peak broadening and a decrease in peak current [4]. Another disadvantage of the HMDE is that vigorous stirring cannot be applied to the solution because it would lead to the drop falling off prematurely.
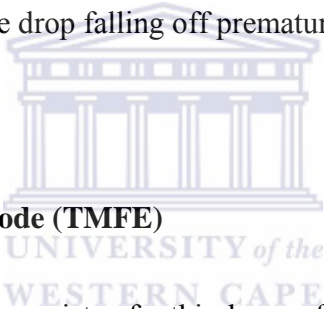
2.5.1.2 Thin Mercury Film Electrode (TMFE)

The mercury film electrode (MFE) consists of a thin layer of mercury covering an inert support. An advantage of thin films is that they offer a large surface to volume ratio at least three orders of magnitude greater than the HMDE [42], which results in a high amalgam concentration during the deposition step. Due to the high plating efficiency, high sensitivity is obtained. The plating efficiency and sensitivity is enhanced because vigorous stirring may be applied. A good example of a substrate for a mercury film is the glassy carbon [28], due to its good electrical conductivity, high hydrogen over-potential and chemical inertness. One of the problems associated with TMFE is the frequent cleaning/polishing of the glassy carbon surface to ensure reproducible behavior even though during the analysis a cleaning step is applied, this may not be sufficient.

2.5.2 More environmentally friendly thin film electrodes

Mercury based electrodes has most commonly been used over the years for stripping analysis, due to its excellent reproducibility and high sensitivity [40], but due its toxic nature its use has been restricted and numerous attempts have been made to replace it with new mercury-free and more environmentally friendly electrodes.

2.5.2.1 Bismuth film electrode (BiFE)

Recently the bismuth film electrode has drawn increasing attention in the field of stripping analysis and is said to be a successful replacement for the "toxic" mercury electrode and is by now widely accepted in many electroanalytical laboratories worldwide [43]. The utility of bismuth as an electrode is based on its ability to form alloys with many metals [44]. Because bismuth film electrodes have such favorable electroanalytical characteristics many scientists have been encouraged to further study bismuth as a promising alternative for the toxic mercury. As a results, *in situ* as well as *ex situ* formed BiFE have been studied [45]. Many different types of materials have been used as substrates for BiFE, including glassy carbon [43], wax-impregnated graphite [46], carbon paste [47], carbon fibers [45] etc.

2.5.2.2 Antimony film electrode (SbFE)

The use of antimony/ antimony oxide electrodes as potentiometric sensors for pH measurements was first reported by Uhl Kestranek [9]. However, only a small number of work concerning the

successful application of the antimony film electrodes for electrochemical stripping analysis of trace metals has been published. The most promising characteristic of the SbFE is its convenient operation in acidic solutions of pH 2 or lower, which is more superior to that reported for BiFEs [32]. Another advantage of SbFE is that it provides a markedly lower background characteristic in the vicinity of the anodic potential limit in comparison to that of bismuth and mercury based electrodes. From the work done by Hocevar et al. [32], application of the antimony film electrode as a substitute for the mercury analogue is particularly beneficial, since it is 30 times less toxic than mercury chloride [32].

2.6 INTERFERENCES

Interferences are a common problem, not only for stripping analysis but also for any other analytical technique and it usually affects the accuracy and precision of the measurements. General interferences are those such as contamination or loss of analyte (adsorption) and the more difficult ones include intermetallic interferences or overlapping peaks. They are more specific and relate to the nature of the stripping measurements. Theses errors can be eliminated, and if not it can at least be minimized but only if attention is paid to certain key operations [4].

2.6.1 Contamination

When dealing with trace and ultratrace metal analysis, the problem of contamination is always present. The reliability and validity of the analytical data depends mostly on the degree to which contamination can be minimized. Contamination usually results from impurities in reagents,

particulates in air and trace metals from the container and cell walls, and they are the primary components of the blank [4]. First, to eliminate contamination, always try to follow good laboratory practice which involves; careful sample handling and storage, proper attention to glassware cleanliness and reagent purity, must at all times be observed to obtain high accuracy and low detection limits. To reduce contamination as well as adsorption problems polyethylene containers and Teflon or polypropylene are preferred but it is still preferred to clean the containers with acid and rinse them with ultrapure water before use preferably with 6 M nitric acid, this is also to prevent leaching of metals to the cell wall. Standard solutions should be prepared daily and mercury solutions should be stored in the fridge. Try to eliminate dust as far as possible and the laboratory should be kept clean at all times.

2.6.2 Intermetallic Interferences

An inherent difficulty with stripping analysis is the interaction between metal ions within the mercury electrode. When an intermetallic compound is formed, the stripping peaks for the constituent metals may be severely depressed or shifted. Numerous intermetallic compounds have been reported; these include the following combinations.: Ag-Cd, Ag-Cu, Ag-Zn, Au-Cd, Au-Ga, Au-Mn, Au-Sn, Au-Zn, Co-Zn, Cu-Cd, Cu-Ga, Cu-In, Cu-Mn, Cu-Ni, Cu-Sb, Cu-Sn, Cu-Tl, Cu-Zn, Fe-Mn, Mn-Ni, Ni-Ga, Ni-Sb, Ni-Sn, Ni-Zn, Pt-Sb, Pt-Sn and Pt-Zn [4]. The compound would be stable if the difference between the constituent properties is large enough. One of the most common examples is the interaction of copper and zinc to form Cu-Zn intermetallic species. The Cu-Zn intermetallic compounds are oxidized at or near the sample potential as Cu, causing errors when copper and zinc are quantified simultaneously by anodic

stripping voltammetry [48]. An enhanced copper peak is observed and a diminished zinc peak. The magnitude of the zinc peak depression is determined by the ratio of the copper and zinc concentration deposited in the mercury electrode. Another intermetallic interference that has been reported and is of importance is that between copper and cadmium. When the solubility limit of copper in the mercury electrode is exceeded, a depression in the cadmium stripping peak is observed [49, 50]. The Cu-Cd intermetallic interference is not as common and pronounced as that of Cu-Zn. Various approaches have been taken to minimize or eliminate intermetallic interferences. One common approach involves the use of gallium to form preferentially the Cu-Ga intermetallic species, because a higher formation constant exists between copper and gallium than between copper and zinc [51]. Another approach for overcoming intermetallic interferences would be to adjust the deposition time to reduce the concentration of metals in the amalgam or by setting the deposition potential to a value, where only the metals of interest is deposited and detected [52].
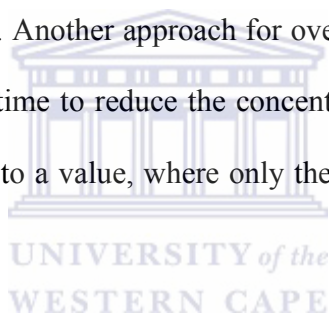
2.6.3 Overlapping Stripping Peaks

The potential range over which most metals are oxidized is relatively narrow, which makes it difficult to resolve the responses from metals that are electroactive in close proximity to one another. One example of this is the interaction between a bismuth film electrode used to determine copper. Copper is a problematic element to be directly quantified by ASV using the BiFE because it's stripping potential is so close to that of bismuth, resulting in severe overlapping of stripping peaks. Most studies report the impossibility of determining samples containing copper at the BiFE, therefore copper is usually determined individually from other

analytes by mercury based electrodes [53, 54]. Pacheco et al. reports an approach taken to minimize the overlapping of stripping peaks between copper and bismuth by the addition of hydrogen peroxide to the sample cell [55]. This resulted in the copper being determined without interference. Another approach taken to overcome overlapping stripping peaks is by lowering the deposition potential until the metal ion with the more negative peak is not deposited.

2.6.4 Organic Interference

When using stripping analysis for the determination of heavy metals in real samples one of the major complications an analysts has to deal with is the presence of organic compounds, particularly surface-active substances. These surface-active substances tend to adsorb on the mercury electrode, thus inhibiting the metal deposition and/or stripping processes [4]. This may affect the peak current as well as the peak potential [56]. The organic material has a wide variety of affects on the stripping peak currents, for example a decrease in the peak current due to hindered transport to the surface during the deposition step and the changed reversibility of the metal oxidation reaction, and this also results in peak broadening. Brezonik et al. [56] and Sagberg et al. [57] did comprehensive studies on the possible effects of surface-active compounds on the response of anodic stripping voltammetric analysis and found that not all surface-active substances exhibit a depression effect and also no general trend can be established.

Table 2.2: Summarizes selected approaches for minimizing interferences in stripping analysis [4].

Interference	Solution	Selected reference
Intermetallic compound	Addition of a third element	[51, 58]
	Using dual working-electrode approach	[59]
	Adjustment of the deposition potential	[59]
	Standard addition	[51, 60]
Overlapping peaks	Suitable choice of supporting electrolyte	[61]
	Suitable choice of exchange solution	[62, 63]
	Suitable choice of electrode or stripping mode	[49]
	Mathematical and computational approaches	[64-66]
Organic compounds adsorbed at the electrode	Destruction of organic matter	[67]
	Standard addition	[56, 68]
	Electrode coverage	[69]

2.7 APPLICATIONS OF STRIPPING ANALYSIS

Due to the low cost and high sensitivity of stripping analysis, its application has been very useful in a large number of analytical problems. The technique has proven useful for the determination of various trace metals in environmental and clinical samples, as well as for analysis of foodstuffs, beverages, gunshot residues, or pharmaceutical tablets. The following section reviews stripping analysis in the fields of its application.

2.7.1 ENVIRONMENTAL ANALYSIS

Reliable analytical measurements of environmental samples are a very important and an essential ingredient of sound decision involving many aspects of society safeguarding the public health, facilitating advances in technology and improving the quality of the environment [4]. Unlike any other pollutant, heavy metals may be the most harmful due to the fact that they are not biodegradable and are retained in the ecosystem indefinitely. Metals are present in water, air and soil as a result of both natural and anthropogenic sources.

2.7.1.1 Water Analysis

Accurate determination of trace metals in various water systems is becoming increasingly important because toxic metals tend to enter the marine food chain, and then ultimately reaching the water system. Because of the sensitivity of stripping analysis it is one of the few techniques that are sufficiently sensitive to determine heavy metals directly in natural waters. This is a very

important characteristic for the minimization of contamination possibilities and changes in the physiochemical nature of the species being measured [4]. Over the last two decades, stripping analysis has widely been used in all branches of aquatic trace metal chemistry. Much of the success in applying stripping analysis for analyzing natural waters is attributed to T. M Florence, who used it about 15 years ago to determine trace levels of lead, cadmium, copper, indium, bismuth and antimony in sea water as well as fish, seaweed, abalone and oysters inhabiting the southern coast of Australia [50]. As a result of many researchers contributions and measurements, the technique has been used widely for measuring normal and pollution levels of more than 15 trace metals in different types of natural waters, such as oceans, rivers and lakes, most of theses metals are known as important toxic or micronutrient elements [4].

2.7.1.2 Other environmental applications

Water analysis is not the only environmental application that stripping analysis is used for other important applications have also been reported, such as airborne particulate matter, fly ash, rocks, minerals and sediments. Khandekar et al. used anodic stripping voltammetry for cadmium, zinc and lead in airborne particulates collected at various locations around Bombay [70]. ASV was preferred over other techniques such as neutron activation and atomic absorption spectroscopy because of its ability to measure various metals simultaneously at the ultratrace level.

2.7.2 CLINICAL ANALYSIS

Clinical analysis has become an important application for determining trace and ultratrace concentration of metals in the human body for assessing exposure to toxic substances and relating the levels of a metal to various pathologic conditions [4]. A deficiency or excess of certain metals is associated with various diseases. An example being, elevated or decreased copper levels are associated with leukemia or Wilson's disease, respectively [71]. Monitoring trace metals in the body is therefore very important.

2.8 GRAPHENE

2.8.1 Discovery of Graphene

In 2003, one ingenious physicist by the name of Andre Geim, along with his colleague, Kostya Novoselov took a block of graphite, some Scotch tape and a lot of patience and persistence and produced a magnificent new material that is a million time thinner than paper, stronger than diamond, more conductive than copper and it is called graphene [72]. Andre Geim studied at the Moscow Physical-technical University and earned his PhD from the Institute of Solid State Physics in Chernogolovka, Russia. Geim thought, since carbon nanotubes were and are a major area of material research, it might be possible to do something similar to carbon nanotubes, only in an unfolded configuration [73]. What Geim did was; he assigned one of his students the task of polishing down a graphite block to just 10 or 100 layers thick and then studied the materials properties. The student produced a speck of graphite roughly 1000 layers thick, which was just a little short off the mark. Geim than had the idea of using Scotch tape to peel away the top layer. What happens is that, flakes of graphite come off onto the tape and the process can be repeated numerous times to achieve progressively thinner flakes, attached to the tape. He then dissolved the tape in solution, leaving him with ultra-thin flakes of graphite: just 10 layers thick. Refinement of this technique finally yielded the first graphene sheets [74]. Graphene is a mere one atom thick, perhaps the thinnest material in the universe and forms a highly quality crystal lattice, with no vacancies or dislocations in the structure. From a fundamental standpoint, graphene's most exciting capability is the fact that its conducting electrons arrange themselves

into quasi-particles that behave more like neutrinos or electrons moving close to the speed of light, mimicking relativistic laws of physics [73].

2.8.1.1 Graphene-Mother of all graphitic materials

Carbon is an interesting and important element for many reasons one particularly being its capability to form a variety of allotropes. The three dimensional (3-D) allotropes being, diamond and graphite which were known from ancient times, 0-D allotrope fullerenes which is the third form of carbon [75] and were discovered in 1985 and the 1-D allotrope of carbon, namely carbon nanotubes [76] which were discovered in 1991. Despite its lack of isolation, graphene is the best theoretically studied allotrope of carbon for more than 60 years [77]. Graphene is a single layer of carbon atoms densely packed into a benzene ring structure. Graphene sheets are one-atom thick, 2-D layers of sp^2-bonded carbon and predicted to have unusual properties. The 3-D material graphite is a later-structured material and is composed of several layers of graphene that are held together by Van der Walls forces (Fig 2.5).
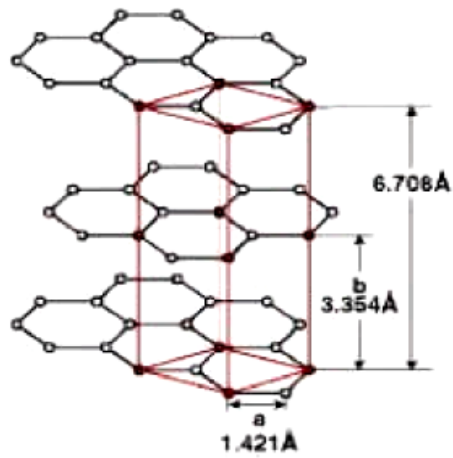
Figure 2.5: Crystal structure of graphite [78].

Graphene is the building block for carbon materials of all other dimensionalities [72], and is therefore the mother of all graphitic materials. Thus the 2-D material can be wrapped up into 0-D fullerenes, rolled into 1-D nanotubes or stacked into 3-D graphite (Fig 2.6)
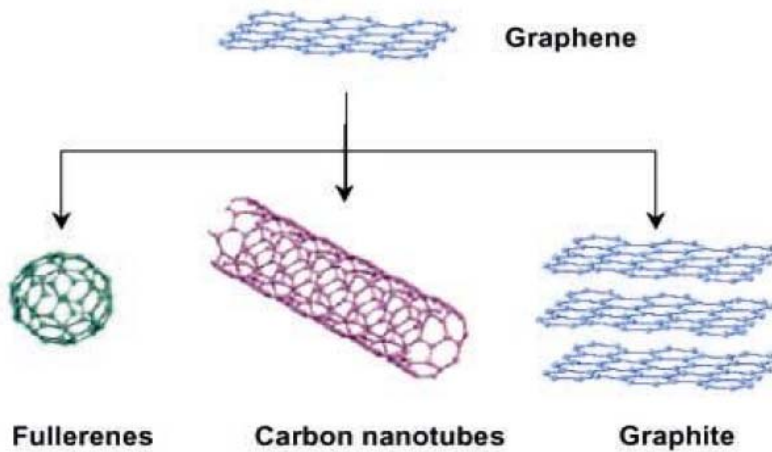
Figure 2.6: Formation of 0 D, 1 D and 3 D materials from graphene.

2.8.2 Structure and Properties

Graphene is a layer of carbon atoms, connected in a hexagonal 2-D crystalline lattice (Fig. 2.7). It can be considered as one graphite plane, separated from the voluminous crystal [79]. An ideal graphene consists exclusively of hexagonal cells. The carbon-carbon bond length in graphene is approximately 0.142 nm. Graphene is a zero gap semiconductor, where the charge carriers have a linear dispersion relation near the Dirac point, essentially giving them zero effective mass [80]. Graphene sheets have excellent electronic [11, 12, 81], thermal [13] and mechanical [14, 15] properties and are expected to provide a variety of applications in various technological fields [82], such as field effect transistors [25, 83], transparent conductors [84], electromechanical resonators [85] and drug delivery [86].
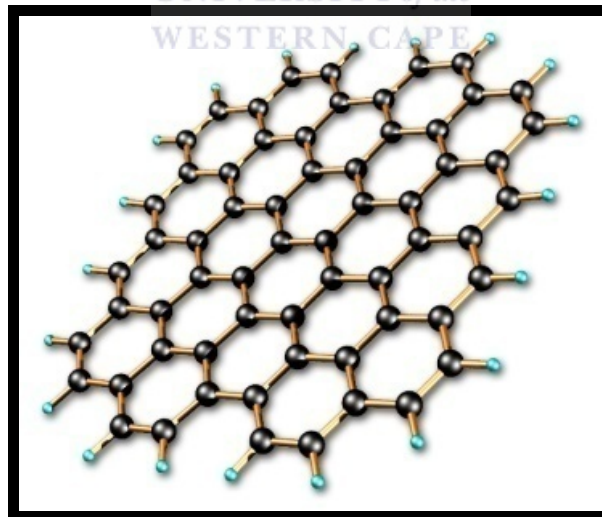
Figure 2.7: Structure of graphene [87].

2.8.2.1 Electronic Properties

The electronic properties of graphene are described in a series of publications. Electrons in graphene, obeying a linear dispersion relation, behave like massless relativistic particles or quantum billiard balls [79]. This results in a number of very peculiar electronic properties which are observed, from an anomalous quantum Hall effect to the absence of localization, in this, the first two-dimensional material [79]. Electrons in bilayer graphene possess an unusual property: they are chiral quasiparticles characterized by Berry phase 2π. Researchers at The University of Manchester have just found that electrons move more easily in graphene than all other materials, including gold, silicon, gallium arsenide and carbon nanotubes [88], and have singled graphene out as the "best possible" material for electronic applications. Graphene has a high electronic quality, measured at around 200,000 cm^2/Vs, which is a 100 times higher than for silicon, these researchers believe graphene has the potential to improve upon the capabilities of current semiconductors and open up exciting new possibilities [79].

2.8.2.2 Optical Properties

Due to graphene's interesting and unique electronic properties, it produces an unexpectedly high opacity for atomic monolayer. It absorbs $\pi\alpha$ 2.3 % white light, where α is the fine-structure constant [89]. This is " a consequence of the unusual low-energy electronic structure of monolayer graphene that features electron and hole conical bands meeting each other at the Dirac point…[which] is qualitatively different from more common quadratic massive bands" [90]. Recent publications shows that the bandgap of graphene can be turned from 0 to 25 eV by

applying voltage to a dual-gate bilayer graphene field-effect transistor (FET) at room temperature [91].
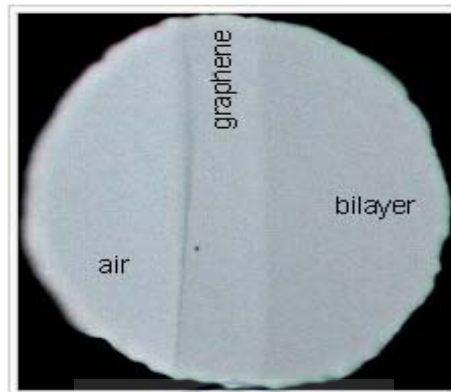
Figure 2.8: Photograph of graphene in transmitted light [92].
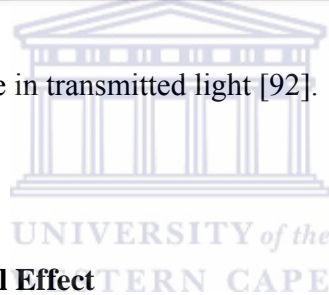
2.8.2.3 Anomalous Quantum Hall Effect

Klaus von Klitzing, Micheal Pepper and Gerhardt Dordda discovered the quantum Hall effect (QHE) in 1980. It is a phenomenon that occurs on a truly macroscopic scale and ever since its discovery it has been attracting intense interest. QHE is exclusively to two-dimensional (2-D) metals. This phenomenon concerns the dependence of a transverse conductivity on a magnetic field, which is perpendicular to a current carrying strip. The observation of the QHE usually occurs at very low temperature and at very high magnetic fields [93]. The QHE can be observed at room temperature [81]. This anomalous behavior is due to the highly unusual nature of charge carriers in graphene, which behave as massless relativistic particles (Dirac fermions) and move with little scattering under ambient conditions [94].

2.8.2.4 Mechanical Properties

Graphene is the brightest and still the rapidly rising star on the horizon of material science and condensed matter physics, revealing a wide variety of physical effects and potential applications [80]. As of 2009, graphene appears to be one of the strongest materials ever tested. Measurements have shown that graphene has a breaking strength 200 times greater than that of steel [95]. The spring constant of suspended graphene sheets has been measured using an atomic force microscope (AFM). An AFM tip was probed to test graphene's mechanical properties. The spring constant of graphene was in the range 1-5 N m^{-1} and the Young's modulus was 0.5 TPa, which differs from that of bulk graphite. These high values make graphene very strong and rigid. These intrinsic properties could lead to using graphene for NEMS applications such as pressure sensors and resonators [96].
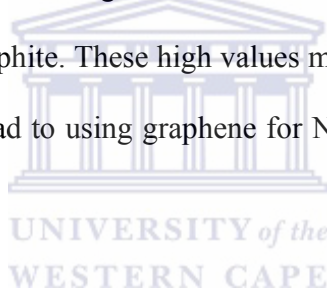
2.8.2.5 Thermal Properties

The near room temperature thermal conductivity of graphene was recently measured to be between $(4.84 \pm 0.44) \times 10^3$ to $(5.30 \pm 0.48) \times 103$ Wm^{-1} K^{-1}. The ballistic thermal conductance of graphene is isotropic [97]. Graphite, the 3-D version of graphene that has basal plane thermal conductivity is over a 1000 W/mK (comparable to diamond). In graphite, the c-axis (out of plane) thermal conductivity is over a factor of ~100 smaller due to the weak binding forces between basal plane as well as the larger lattice spacing [98]. Also, the ballistic thermal conductance of graphene is shown to give the lower limit of the ballistic thermal conductance, per unit circumference, length of carbon nanotubes [99].

2.8.3 Synthesis of Graphene

Graphene is synthesized in several different ways and new ways are also regularly proposed or studied to improve the quality of samples or to increase the cost-efficiency of the synthesis. Hereunder, details on these methods are given.

2.8.3.1 Exfoliated graphene

One of the very first and easiest methods for preparing graphene involved the use of Scotch tape. Take a piece of Scotch tape and lay it down on a flat surface, and place a piece of graphite on it. Fold the Scotch tape at the edges of the graphite flakes and peel it of gently. This is done repeatedly until a newly transparent region is observed on the Scotch tape. The Scotch tape graphene is then transferred to a clean silicon wafer and then Scotch tape is removed. The graphene layers can be seen under an optical microscope. The advantage of this method is that it is cheap and easy. No special equipment is necessary and you can find the thickness of the graphene layers based on the color of the silicon wafer. The disadvantage though is that it is very time consuming to find where the graphene is and it is also labor intensive which is not good for industry.

2.8.3.2 Epitaxial graphene

Take a SiC wafer and subject it to very high temperatures (> 1100 °C) to reduce it to graphene [100]. This method produces a sample size that is dependent upon the size of the SiC wafer used.

The advantage of the method is that it produces the most even films of any method and it doesn't require a lot of complicated steps. This method gives few-layer graphene (FLG). Also this method isn't very versatile since you can't really functionalize something you grow from thermal decomposition.

2.8.3.3 Graphite oxide

The most common route to graphene, involves the production of graphite oxide (GO) by extremely harsh oxidation chemistry [84]. Staudenmeier or Hummers methods are commonly used to produce GO a highly exfoliated material that is dispersed in water [101]. The structure of GO contains epoxide functional groups along the basal plane of the sheets as well as carbonyl and hydroxyl moieties along the edges (Fig 2-9).
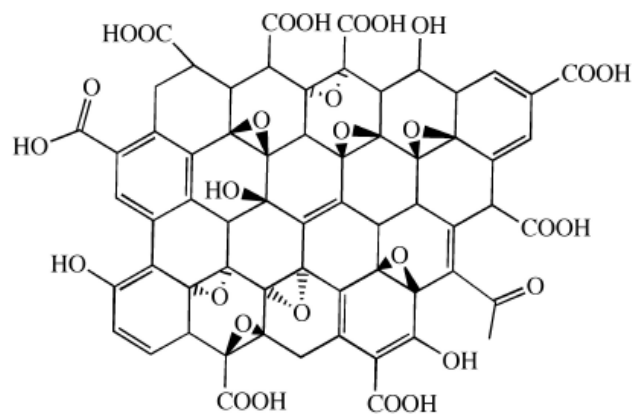
Figure 2.9: Idealized structure proposed for graphene oxide (GO). Adapted from C. E. Hamilton, PhD Thesis, Rice University (2009).

Graphite oxide is converted by chemical reduction into graphene because it is electrically insulating. The chemically converted graphene is reduced by either hydrazine or sodium borohydride. The properties of chemically converted graphene can never truly be the same as those of graphene because, the oxidation to GO introduces defects and also the chemical reduction does not fully restore the graphitic structure [84]. This method is more versatile then the epitaxial method, it's less time consuming and easier to scale up than exfoliation methods. The disadvantage though is the difficulty to keep the solution from re-aggregating into graphite, after reduction. The graphene layers are still partially oxidized, which could potentially change the electronic, optical and mechanical properties.
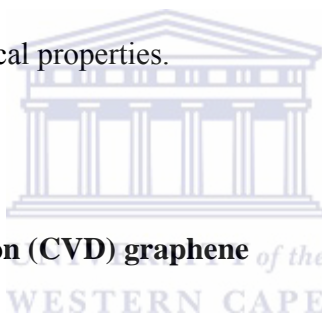
2.8.3.4 Chemical Vapor Deposition (CVD) graphene

Chemical vapor deposition is another method for producing graphene. Reina et al. [102], synthesized single- to few layer graphene film on evaporated polycrystalline nickel using ambient pressure CVD. Due to the use of ambient pressure and readily available nickel film, this method enables the inexpensive and high throughput growth of graphene over large areas with properties close to those found by micro-cleaving HOPG [102]. No further treatment of graphene films is necessary and it exhibits outstanding properties in terms of optical transparency and electrical conductivity. The growth of graphene monolayers on single crystalline transition metals such as Co [103], Pt [104], Ir [105], Ru [106] and Ni [107-109]. The method is great for making large amounts of film and it requires very little labor but it often makes unpredictably arranged multilayers, with defects being linked to the substrate being used. Another disadvantage

is the metal surfaces on which this method works best are not what graphene devices should be build on.

2.8.4 CHARACTERIZATION TECHNIQUES FOR GRAPHITE, GRAPHENE OXIDE AND GRAPHENE

Different characterization techniques can be used to characterize graphene, each providing complementary information. Hereunder, only the methods that have been used for this project i.e. Fourier transformed infrared spectroscopy (FT-IR), x-ray diffraction (XRD), Raman spectroscopy, atomic force microscopy (AFM) and solid state NMR are summarized.
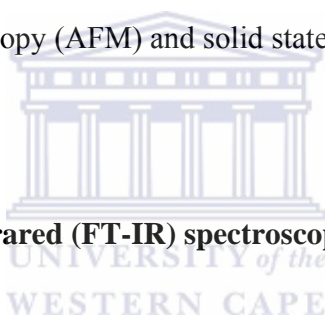
2.8.4.1 Fourier Transformed-Infrared (FT-IR) spectroscopy

Fourier transformed-infrared (FT-IR) spectroscopy is a molecular characterization technique that is used to identify the functional groups of the sample that is being studied. The FT-IR is a rapid mean of identifying substances, characterizing contaminants and comparing materials [110]. This technique is applicable to a wide variety of samples including polymer systems.

2.8.4.2 X-ray Diffraction (XRD)

X-ray diffraction (XRD) is a versatile, non-destructive technique that reveals detailed information about the chemical composition and crystallographic structure of natural and manufactured materials [111]. Based on the principle of XRD various structural, physical and chemical information about the material investigated can be observed.

2.8.4.3 Raman spectroscopy

Raman spectroscopy is a spectroscopic technique based on inelastic scattering of monochromic light, usually from a laser source. Photons of the laser light are absorbed by the sample and then re-emitted. Frequency of the re-emitted photons is shifted up or down in comparison with the original monochromic frequency. This shift provides information about vibrational, rotational and other low frequency transitions in molecules. Raman spectroscopy can be used to study liquid, solid and gaseous sample [112]. Raman spectroscopy has been successfully utilized as a convenient technique for identifying and counting graphene layers on the Si/SiO2 substrate [113, 114].

2.8.4.4 Atomic force microscopy (AFM)

Atomic force microscopy (AFM) is a very high-resolution type of scanning probe microscopy, with demonstrated resolution on the order of fraction of a nanometer. It does not rely on electromagnetic radiation such as photon or electron beams to create an image. An AFM is a mechanical imaging instrument and its purpose is to measure the three dimensional topography as well as physical properties of a surface with a sharpened probe. For the probe to interact with the force fields associated with the surface it needs to be positioned very close to the surface. The probe is scanned across the surface such that the forces between the probe remains constant. An image of the surface is then formed by monitoring the motion of the probe as it scanned over the surface [115].

2.8.4.5 Transmission electron microscopy (TEM)

Transmission electron microscopy (TEM) is a form of microscopy that uses a high energy electron beam rather than optical light. A beam of electrons are focused on a single spot or element on the sample being analyzed. The electrons interact with the sample and those that go past unobstructed hit the phosphor screen on the other side. The electrons are then converted to light and an image is formed. TEM is used to determine the difference between the mono-layer and bi-layer graphene.

2.8.4.6 Solid state nuclear magnetic resonance (ssNMR) spectroscopy

Solid state NMR spectroscopy is a kind of nuclear magnetic resonance (NMR) spectroscopy, characterized by the presence of anisotropic (directionally dependent) interactions. It does not require that the sample be soluble or form a crystal, and the approach can be used to study molecules larger than 100 kD [116].

2.9 APPLICATIONS OF GRAPHENE

2.9.1 Transparent conducting electrodes

Graphene is a very promising candidate for transparent conducting electrodes due to its high electrical conductivity and high optical transparency, which is required for applications such as touch screens, liquid crystal displays (LCD), organic photovoltaic cells and organic light-

emitting diode (OLED). Traditionally indium tin oxide is used in OLED devices, however, indium is rare, expensive and difficult to recycle [117]. Graphene on the other hand has a very good mechanical strength and flexibility which is advantageous compared to indium tin oxide [118, 119].

2.9.2 Ultracapacitors

Graphene has a very high surface area to mass ratio, which makes it a very good candidate for ultracapacitors. It is believed that graphene could be used to produce ultracapacitors with a great energy storage density than is currently available [120].
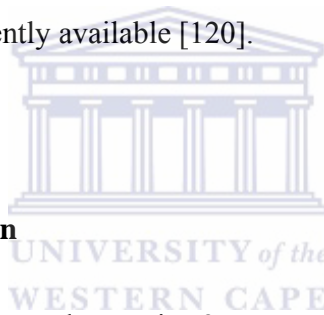
2.9.3 Single molecule gas detection

Graphene makes an excellent sensor due to its 2D structure. It detects adsorbed molecules efficiently due to the fact that its entire volume is exposed to its surrounding. Molecule detection is indirect: as a gas molecule adsorbed to the surface of graphene, the location of adsorbed experienced a local change in electrical resistance [121]. While this effect occurs in other materials, graphene is superior due to its high electrical conductivity and low noise which makes this change in resistance detectable [121].

2.9.4 Graphene Transistors

Graphene has excellent electronic properties, and has been attracting a lot of interest especially by technologist who see them as a way of constructing ballistic transistors. The first graphene field-effect transistors (FETs) have already been demonstrated by Georgia Technology researchers in 2006. They had successfully build an all graphene planar FET with side gates [122]. Due to the fact that the current graphene transistors show very poor-on-off ratio, researchers are trying to find ways for improvement. In 2009, the Massachusetts Institute of Technology researchers build an experimental graphene chip known as a frequency multiplier. This frequency multiplier is capable of taking an incoming electrical signal of a certain frequency and producing an output signal that is a multiple of that frequency [123]. These graphene chips may open up a range of new applications; however their practical use is limited by a very small voltage gain. None of these circuits was demonstrated to open at frequencies higher than 25 kHz. In February 2010 IBM researchers published a paper wherein they demonstrate a radio-frequency graphene transistor with the highest cut-off frequency achieved so far for any graphene device – 100 billion cycles/second (100 Gigahertz) [124].

3. EXPERIMENTAL

3.1 Reagents and Equipment

Chemicals	Source
1 wt. % Nafion	Aldrich
Isopropyl-alcohol	Sigma-Aldrich
Cadmium	Fluka
Lead	Fluka
Copper	Fluka
Zinc	Fluka
Bismuth	Fluka
Antimony	Fluka
Mercury	Fluka
Glacial Acetic Acid	Sigma-Aldrich
Sodium Acetate	Sigma
Double-distilled water	
96% Ethanol	Saarchem
37% Hydrochloric acid	Saarchem
65% Nitric acid	KIMIX

- The pH of the acetate buffer was measured using an 827 pH lab Metrohm pH meter. A pH of 4.6 was used.

- Buffer solutions : pH = 7.00 and pH = 4.00

3.2 Standard solutions

Standard solutions were prepared in polyethylene vials, by diluting the atomic absorption standard solution with 0.01 M HCl which was prepared by diluting HCl (37%) with high purity distilled water on a volume per volume basis.

3.2.1 Acetate buffer solution (Electrolyte solution)

0.1 M Acetate buffer solution was prepared by weighing out sodium acetate and mixing it with glacial acetic acid followed by diluting the solution with high purity water.
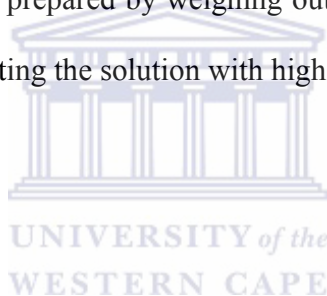
3.2.2 Nitric acid solution

6 M Nitric acid solution was used for cleaning glassware and it was prepared by diluting the Nitric acid (65%) with high purity distilled water on a volume per volume basis.

3.3 Instrumentation

Anodic stripping voltammetric measurements were performed using a 797 VA COMPUTRACE, interfaced with a personal computer. A glassy carbon electrode, first modified with a Nafion-G nanocomposite platform, followed by mercury, bismuth or antimony film, served as the working electrode, with the Ag/AgCl and platinum acting as the reference and counter electrode

respectively. All the experiments were carried out in a one compartment 20 mL volumetric cell. The sample solution was de-aerated prior to the voltammetric determination, by bubbling high purity nitrogen gas through the solution.

Figure 3.1: 797 VA Computrace Metrohm "Electrochemical Analyzer".
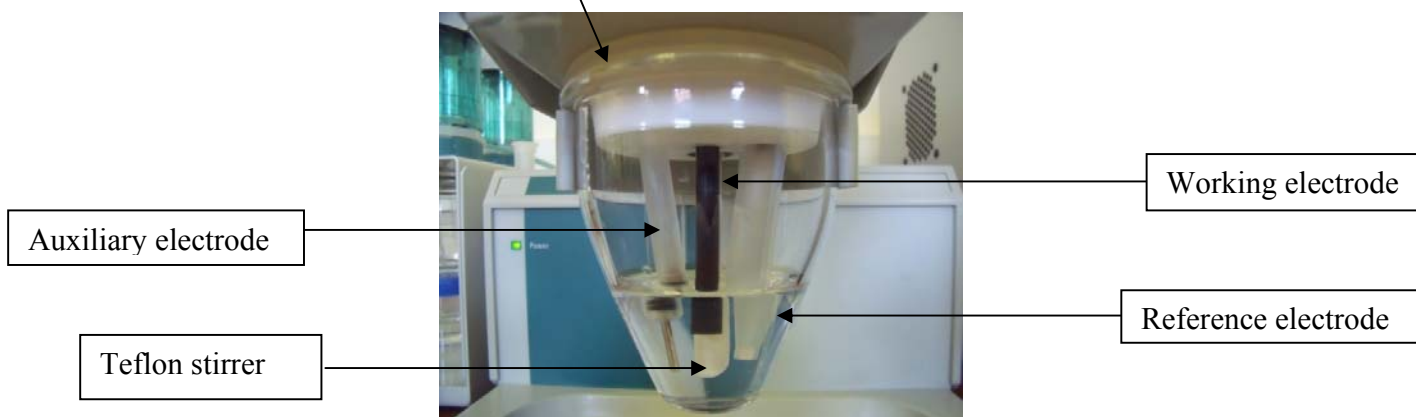
3.4 Instrumental parameters for SWASV analysis

Experimental parameter	Value
Initial purge	t = 900 s
Cleaning step	E = + 0.3 V t = 60 s
Preconcentration step (Deposition)	E = -1.3 V t = 120 s
Equilibrium time	t = 10 s
Potential scan	From -1.3 V to +0.1 V
Voltage step	0.005 V
Amplitude	0.025 V
Frequency	50 Hz
Stirring rate	1000 rpm

3.5 Preparation of graphene solution

The graphite oxide was synthesized from graphite powder according to the literature with little modification [101, 125]. 100 mg of graphite oxide was dispersed in 100 mL of water and sonicated for 1 h, followed by the addition of 200 mg of $NaBH_4$ to the dispersion. This mixture was stirred at 125 °C for 3 h. The black solid was isolated by centrifugation, washed with water and then dried.

3.6 Preparation of modified electrode

A 100 µL of 0.5 mg mL^{-1} graphene solution was mixed with equal volume of 1.0 wt % Nafion-isopropyl-alcohol solution by ultrasonication for ca. 30 or until fully dispersed. Then, an aliquot of 5µL of the mixture was coated on the glassy carbon electrode (GC) to obtain the Nafion-G modified electrode.

3.7 Procedure for SWASV analysis

The three electrodes were immersed into the electrochemical cell, containing 20 mL 0.1 M acetate buffer (pH 4.5), Hg^{2+} (Bi^{3+} or Sb^{3+}), and the target metal ions. The Nafion-G modified GCE with mercury film was plated *in situ* by spiking the sample with the required concentration of Hg^{2+} and simultaneously depositing Hg^{2+} and the target metals on the surface of the electrode at -1.3 V for 120 s. Following the conditioning step, the stirring was stopped and after a rest period the voltammogram was recorded by applying a continuously changing square-wave potential. The metals were quantified by the method of standard addition. To prevent carryover of metals from one sample to another the sample cell was rinsed with High purity water. A blank was then run, consisting of only the electrolyte solution and Hg^{2+} (Bi^{3+} or Sb^{3+}) to check for any spurious peaks before the next analysis was run.

3.8 Quantitation

The method of standard addition was used to determine the concentration of the analytes. For reproducibility purposes, each analysis was repeated four times. The concentration of the analyte was calculated using the Standard Addition Formula:

$$c(unknown) = \frac{c(standard) \times i \times v \times 1000}{(i' - i) \times (V + v)}$$

where,

c(unknown)	=	concentration of the final unknown solution.
c(standard)	=	concentration of the standard solution.
V	=	volume of the sample solution.
v	=	volume of the standard solution added.
i	=	peak height of the unknown solution.
i'	=	peak height of the unknown solution + standard.

54

3.9 Characterization techniques

3.9.1 Inductive Coupled Plasma Mass Spectrometry (ICP-MS)

The concentration of metals in water samples and in spiked electrolyte solution was measured by the inductively coupled plasma mass spectrometry (ICP-MS) technique. The purpose of this was to compare the results obtained from the ICP-MS with that from the results obtained by the Metrohm trace metal analyzer. Samples were prepared by weighing out the appropriate amount of metal to make up the metal standards. Trace elements were analyzed on an Agilent 7700 ICP-MS. The instrument is calibrated daily using NIST traceable standards. A quality control standard is analyzed prior to the samples to verify the accuracy of the calibration standards, while control standards are used throughout the analysis to monitor accuracy and instrument drift. Internal standards were used to correct for matrix effects and instrument drift. Data acquisition and processing is software controlled and exported in Excel format.

3.9.2 X-ray Diffraction (XRD)

The structural properties of graphite, graphite oxide and graphene were evaluated through X-ray diffraction (BRUKER AXS X-ray diffractometer) with Cu-Kα radiation. The instrument operating conditions were as given in Table 3-1.

Table 3-1: XRD operating parameters.

Radiation source	Cu-Kα
Radiation wavelength (λ)	1.506 Å
Tube Voltage	40 kV
Tube Current	40 mA
Variable Slits	0.28 mm

3.9.3 Fourier Transformed Infrared (FT-IR) Spectroscopy

Fourier transformed infrared (FT-IR) spectroscopy was done to confirm whether the product synthesized was actually graphite oxide and graphene. FT-IR requires no sample preparation so in this case 15 mg of graphite, graphite oxide and graphene was placed on the Attenuated Total Reflectance (ATR) sample holder of the Perkin Elmer spectrum 100 FT-IR spectrometer and the spectrum was recorded.

3.9.4 Raman Spectroscopy

Raman spectroscopy was performed on a Dilor XY Raman spectrometer with a Coherent Innova 300 Argon laser with a 514.5 nm laser excitation.

3.9.5 Solid State NMR (ssNMR) Spectroscopy

Solid state NMR spectra were recorded on a Varian VNMRS 500 MHz two-channel spectrometer using 4 mm zirconia rotors and 4 mm Chemagnetics™ T3 HX MAS probe. The rotors were packed with a mixture of either GO and kaolinite or graphene and kaolinite, since both GO and graphene are conductive material. All direct polarization (DP/SPE) spectra were recorded at ambient temperature with proton decoupling. A 2.75 μm 90 ° pulse and a recycle delay of 4 s. The free induction decay had 1339 complex points, Fourier transformed with 50 Hz line broadening. Magnetic-angle-spinning (MAS) was performed at 12 Hz and Ademantane was used as an external chemical shift, where the download peak was references to 38.3 ppm.
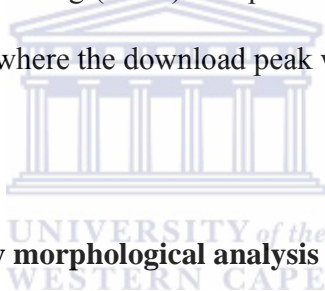
3.9.6 Physical characterization by morphological analysis

3.9.6.1 Atomic Force Microscopy (AFM)

The tapping-mode atomic force microscope (Veeco Nanoman V) was employed to evaluate the morphology of graphite oxide and graphene, with special emphasis on estimating its thickness. The silicon tip (Antimony (n) doped) had a curvature radius of 2.5-3.5 μm, a force constant of 1-5 N m^{-1} and a resonance frequency of 60-100 kHz. The samples for AFM were prepared by drop coating the graphene/water and graphene oxide/water (5 μL) dispersion onto a silicon wafer.

3.9.6.2 Transmission Electron Microscopy (TEM)

Samples were prepared by diluting the graphite; graphite oxide and graphene in ethanol, ultrasonicating and depositing a drop onto S147-4 Holey carbon film 400 mesh Cu grids. Field Emission gunlens 1 was used with spotsize 3, at 200 kV using Tecnai G2 F20 X-Twin MAT 200 kV Field Emission Gun Transmission Electron Microscope.

4. RESULTS AND DISCUSSION

4.1 PART A: Morphology and Structural Characterization of Graphene

4.1.1 Fourier Transformed Infrared Spectroscopy (FT-IR)

Figure 4.1 shows the Fourier transformed infrared (FT-IR) image of graphite, graphite oxide (GO) and graphene. For graphite, no distinct peaks are detected. GO however, showed a rich collection of transmission bands corresponding to C=O (1719 cm^{-1}), aromatic C=O (1597 cm^{-1}), carboxy C-O (1411 cm^{-1}, epoxy (1283 cm^{-1}) and O-H (3400 cm^{-1}). After reduction with NaBH$_4$ most of the functional groups were eliminated. These results also concur with those reported by [126].
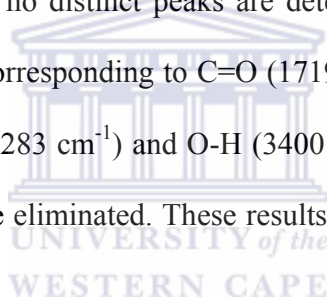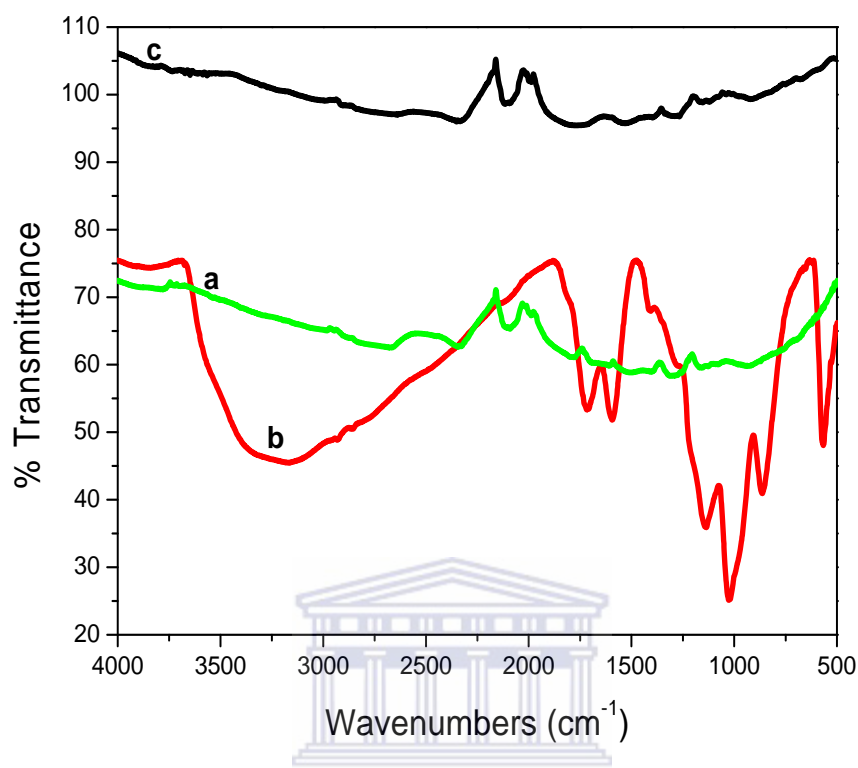
Figure 4.1: FT-IR spectra of (a) graphite, (b) GO and (c) graphene.

4.1.2 X-ray Diffraction (XRD)

The XRD patterns of graphite, graphite oxide (GO) and graphene are shown in Figure 4.2. Graphite showed a very strong 002 peak at 26. 37°, GO a 001 peak at 9.88° and graphene, 002 peak at 24.88°. The GO peak shift is due to the formation of hydroxyl, epoxy and carboxyl groups. After reduction to graphene some of the oxygen-containing functional groups are removed and this causes the graphene peak to shift to 24.88°. This suggests the conjugated graphene network (sp^2 carbon) is reestablished during the reduction process, which is associated with the ring-opening of the epoxides [23].
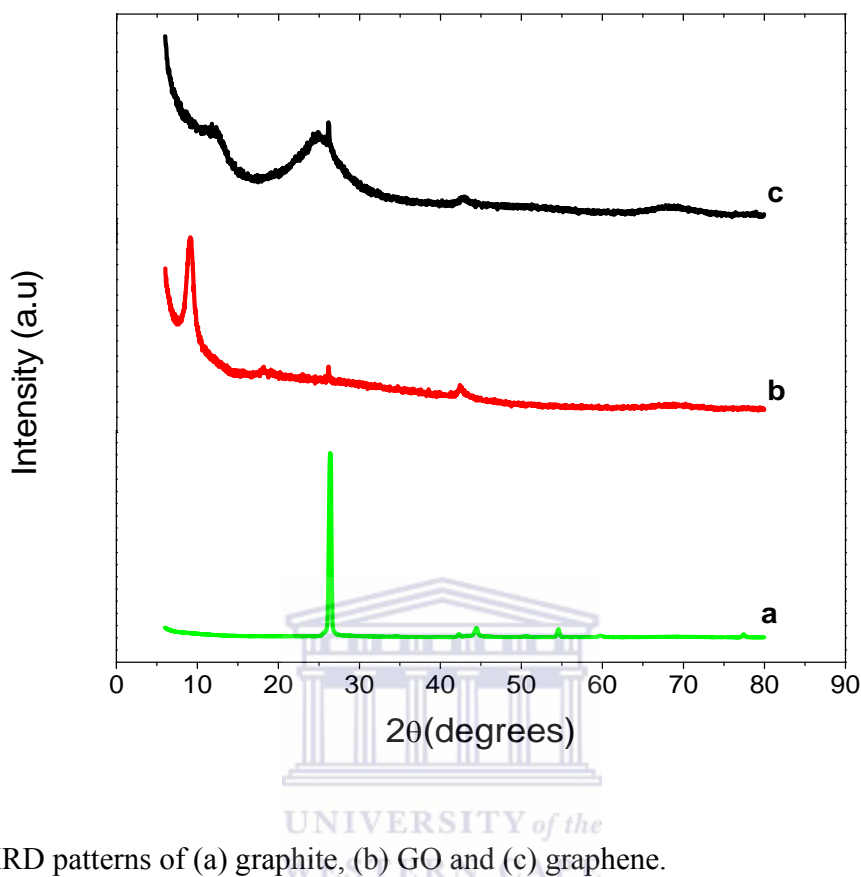
Figure 4.2: XRD patterns of (a) graphite, (b) GO and (c) graphene.

4.1.3 Raman Spectroscopy

The Raman spectrum of graphite, GO and graphene is shown in Fig. 4.3. The Raman spectra of the materials just confirm the observations of the XRD patterns i.e., the changes of structure during the reduction process from GO to graphene. Graphite as expected displayed a prominent G band at 1581 cm^{-1} and a 2-D band at 2721 cm^{-1}. For GO the G band is broadened and shifted to 1600 cm^{-1}. In addition the D band at 1360 cm^{-1} becomes prominent, indicating the reduction in size of the in-plane sp^{2} domains, possibly due to the extensive oxidation. Graphene contains both D and G bands, with an increased D/G intensity ratio. This suggests a decrease in the average

size of the sp^2 domains upon reduction of the exfoliated GO. The intensity ratio (I_D/I_G) of D band and G band of GO is about 0.952, while the I_D/I_G of graphene is 1.14 due to the presence of unrepaired defects that remained after the removal of large amounts of oxygen-containing functional groups. This I_D/I_G ratio value is consistent with most chemical reduction reports [127, 128].
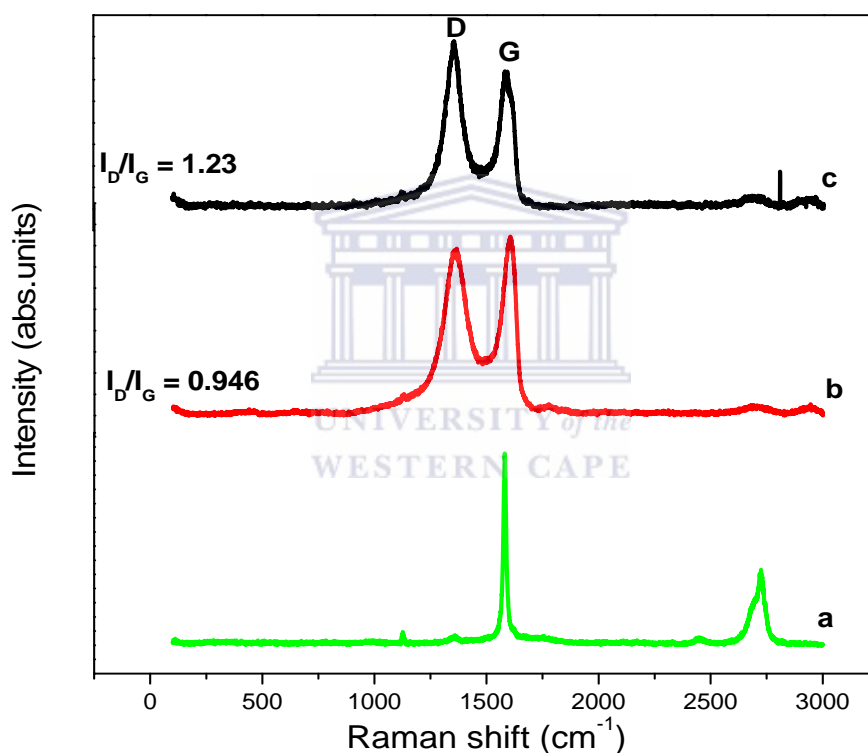
Figure 4.3: Raman spectra of (a) graphite, (b) GO and (c) graphene.

4.1.4 Transmission electron microscopy (TEM)

TEM samples were prepared by pipetting the graphene dispersion onto a holey mesh grid. The TEM image of graphite (Fig. 4.4a) shows its graphitic structure as large thick dark flakes.

Graphite cannot be exfoliated even when sonicated under the same conditions as GO. For GO (Fig. 4.4b) large sheets were observed to be situated on top of the grid, resembling wavy silk veils. The sheets are transparent and entangled with one another. The structure of graphene is different from that of GO (Fig. 4.4c). At low magnification the structure of graphene looks flat, with transparent layers on top of one another. Wrinkles and folding are observed on the surface as well as the edges of the structure. When graphene was further studied at higher magnification (Fig. 4.4d) it revealed the actual layers of graphene.
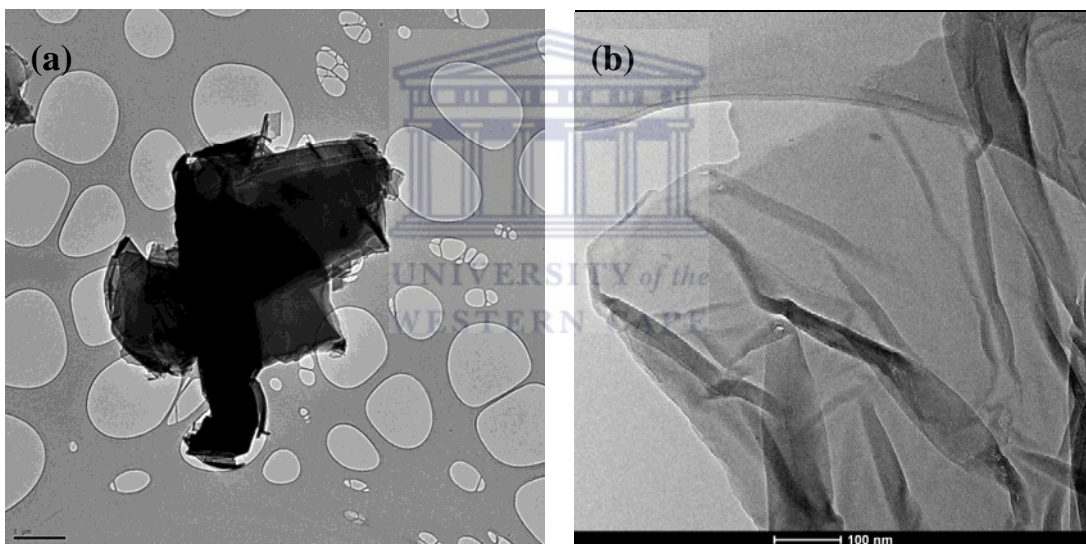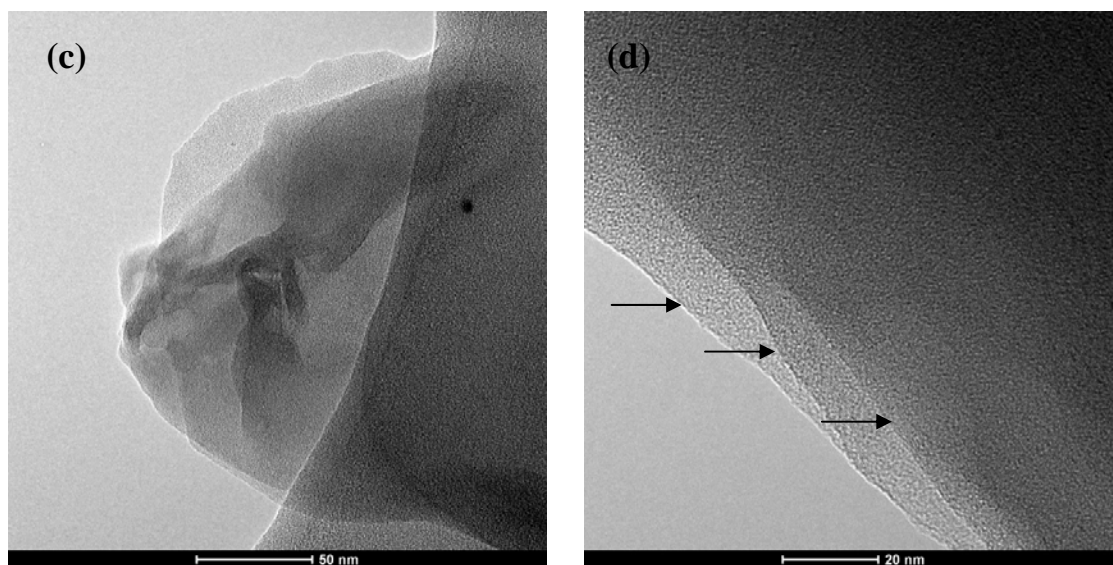
Figure 4.4: TEM images of (a) graphite, (b) GO, (c) graphene and (d) HRTEM of graphene.

4.1.5 Atomic Force Microscopy (AFM)

Atomic force microscopy (AFM) was also performed on graphene oxide and graphene, to characterize the degree of exfoliation. From Fig. 4.5a the GO appears to be well dispersed with wrinkles being observed as well as transparent sheets, stacked together or on top of one another. For further analysis a certain part of GO images was enlarged and then investigated using the three-dimensional (3-D) view (Fig. 4.5b). The surface of the GO was a bit rough but layers could still be seen from this image. The cross sectional view of the GO indicated that the average thickness of GO sheets is ~ 1.4 nm (Fig. 4.5c).

Figure 4.5d represents the AFM topography image of graphene, wherein several graphene sheets were randomly deposited on the silicon substrate. A flat graphene sheet was selected for further investigation using the 3-D view (Fig. 4.5e). The graphene surface was slightly rough and this could be due to the existence of some functional groups. The cross sectional view across the plain area of the sheet gave an average thickness of 1.3 nm (Fig. 4.5f).

64

150.0 nm

(a)

0.0   1: Height   3.0 μm

(b)

79.6 nm

0.0   1: Height   1.0 μm

(c)
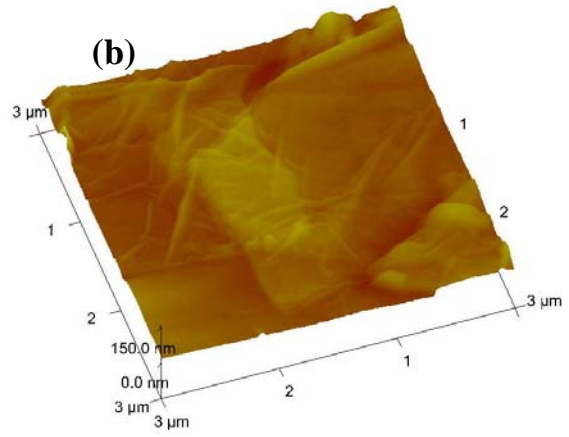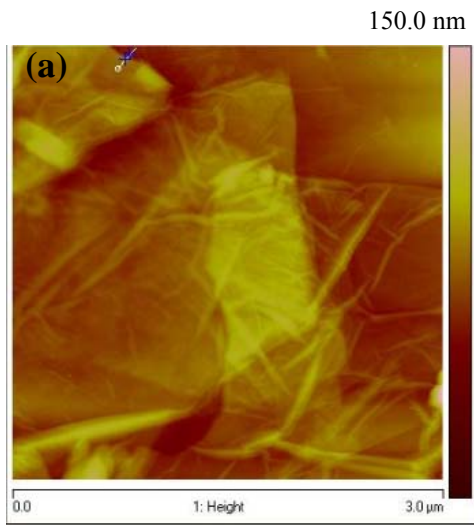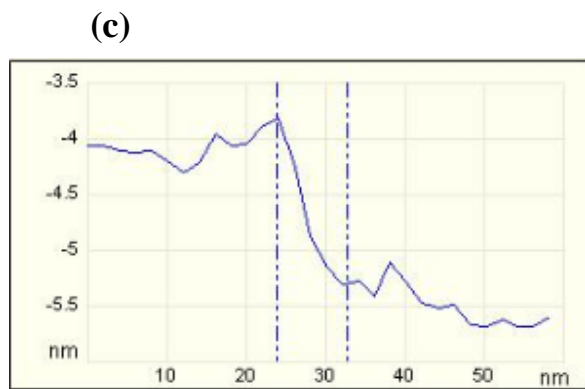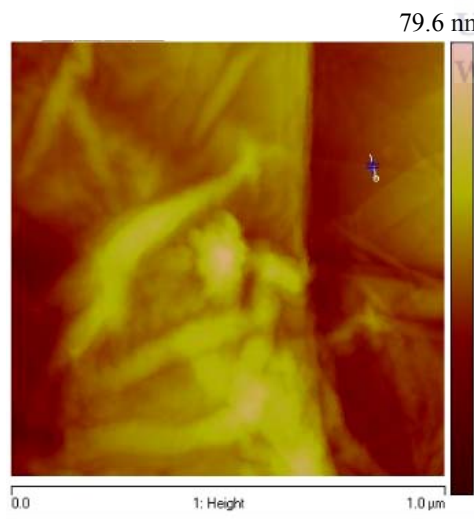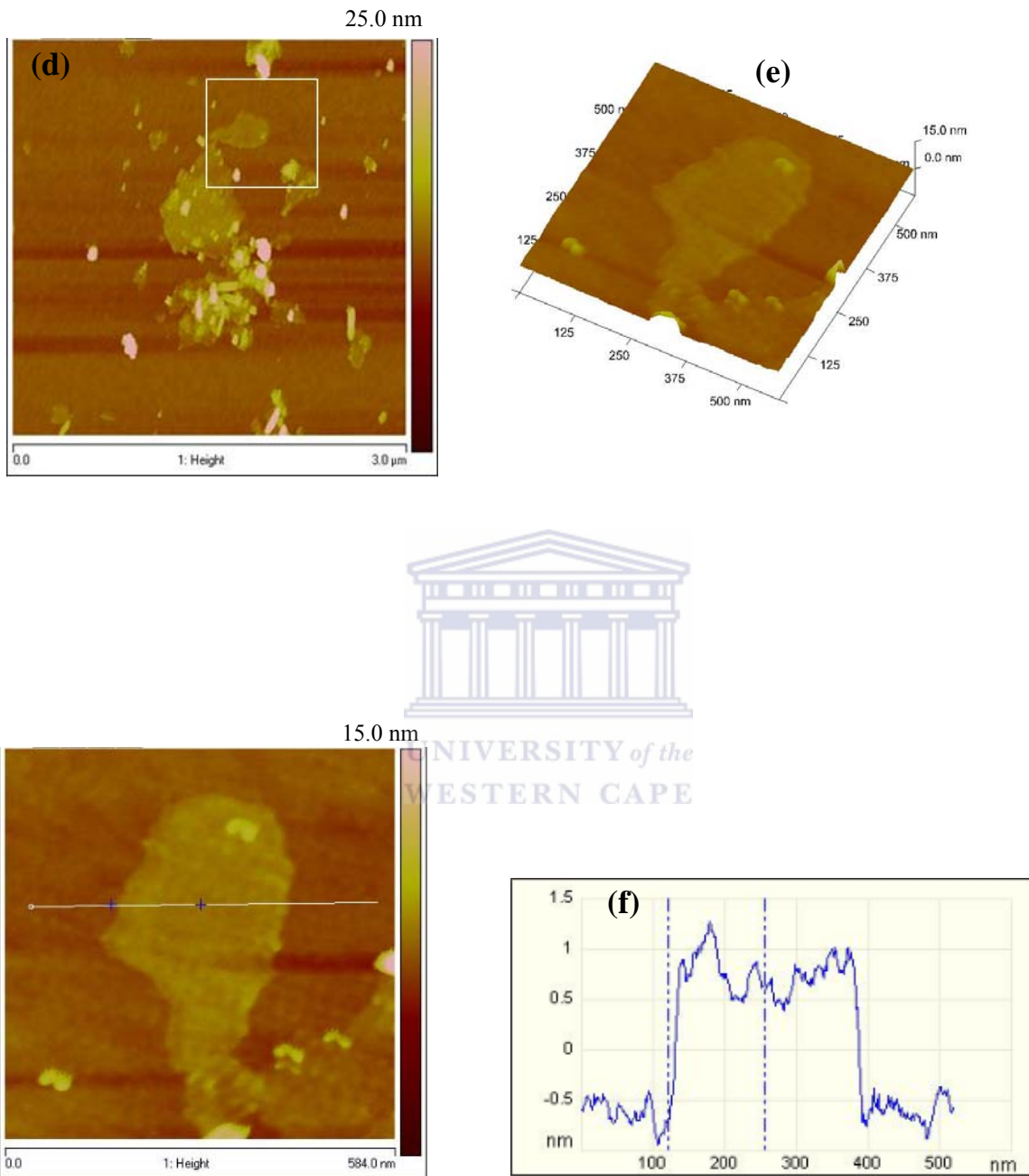
Figure 4.5: (a) AFM topography image of graphene oxide, (b), 3-D representation, (c) cross sectional analysis graphene oxide, (d) topography image of graphene, (e) 3-D representation of the selected area in (d) and (e) cross sectional analysis of the selected individual graphene.

4.1.6 Solid state nuclear magnetic (ssNMR) spectroscopy

The ^{13}C MAS NMR spectra of GO and graphene are shown in Figure 4.6. The spectra of GO consists of three lines at ca. 65, 72 and 135 ppm. The first two peaks represent ^{13}C nuclei in the epoxide and hydroxyl groups respectively [129]. The resonance at 135 ppm belongs to the un-oxidized sp^2 carbons of the graphene network. In the ^{13}C spectrum of graphene, the peaks from the oxygenated and the carbonyl carbons are no longer present. The remaining prominent feature is the resonance at 119 ppm that is broadened by the chemical shift distribution and corresponds to variation of carbon atom environments [130].
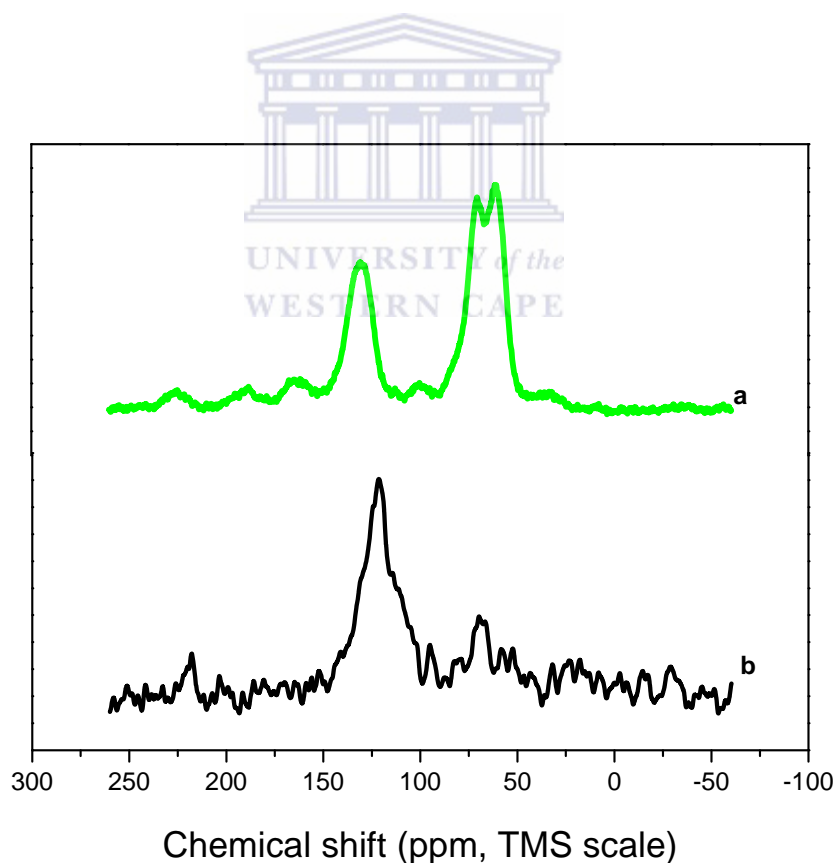
Figure 4.6: Solid state ^{13}C MAS NMR spectra of (a) GO and (b) graphene.

4.2 PART B: Nafion-Graphene Mercury film electrode

In the following section the optimum conditions such as deposition potential, deposition time, rotation speed, frequency and amplitude which were analyzed are discussed with regards to the Nafion-G-HgFE. As well as the sensitivity and detection limits of the Nafion-G-HgFE obtained for each metal (i.e. Zn, Cd, Pb, and Cu) analyzed individually and simultaneously.

4.2.1 Electrochemical characterization of the Nafion-G nanocomposite film

4.2.1.1 Electrode current response of different Nafion-G HgFE platforms

The sensitivity of different electrode platforms (GCE, Nafion-G, Nafion, Graphene, and mercury film) was compared by SWASV (Fig. 4.7). Each platform contained 30 μg L^{-1} of Zn^{2+}, Cd^{2+} and Pb^{2+} in 0.1 M acetate buffer solution (pH 4.6). This figure clearly shows that the Nafion-G-HgFE indicates the sharpest and highest peak current. The sensitivity then decreases in the following order Graphene-HgFE, Nafion-HgFE, HgFE and GCE. So even though analysis can be done on just a Graphene-HgFE, adding the Nafion and the graphene together not only enhances the sensitivity but the Nafion also stabilizes the graphene and functions as a very good proton exchanger. Each peak appearing at a certain peak potential in Fig. 4.7, represents the point at which a particular metal strips out of the amalgam (stripping step) or re-oxidized back into solution. The stripping potentials for Zn^{2+}, Cd^{2+} and Pb^{2+} appear at approximately -1.1 V, -0.7 V and -0.5 V respectively; the redox reaction involved during stripping analysis is given by equation (1).

$$Mn^{n+} + n\acute{e} + Hg \rightarrow M (Hg) \qquad \text{Deposition step (reduction reaction)}$$

$$M (Hg) \rightarrow M^{n+} + n\acute{e} + Hg \qquad \text{Stripping step (oxidation reaction)}$$
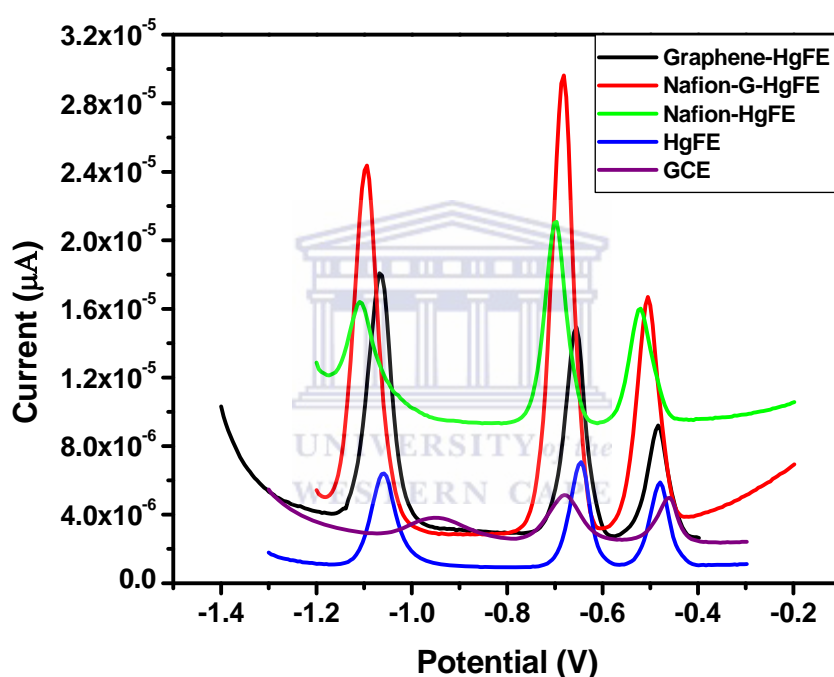
Figure 4.7: SWASV of 30µg L^{-1} of Zn^{2+}, Cd^{2+} and Pb^{2+} on different metal platforms. Supporting electrolyte: 0.1 M acetate buffer (pH 4.6); deposition potential: -1.3 V; deposition time: 120 s; frequency: 50 Hz; amplitude: 0.025 V and voltage step: 0.005 V.

For the determination of Zn^{2+}, Cd^{2+}, Pb^{2+} and Cu^{2+} on a Nafion-G HgFE, 0.1 M acetate buffer with a pH of 4.6 was used as the electrolyte solution. Using acid would have eliminated any adsorption problems; however the Nafion-G nanocomposite does not perform well in acidic

solutions as it does in buffer. That is, the modified electrode gets saturated much quicker and when sensitivities are compared between acid and buffer electrolytes, the buffer has the better sensitivity as can be seen from Fig. 4.8. Graphene only has a certain number of active sites available, so when HCl is used as an electrolyte, there are large chlorine molecules which occupies some of these sites on the graphene, leaving only a limited amount of active sites for the metal ions, which then have to compete with each other for those available active sites, resulting in a loss of metals. However metal standard were prepared in 0.1 M HCl or 0.5 M HNO_3 in poly-ethylene containers, to avoid adsorption of metals onto the wall of the containers.
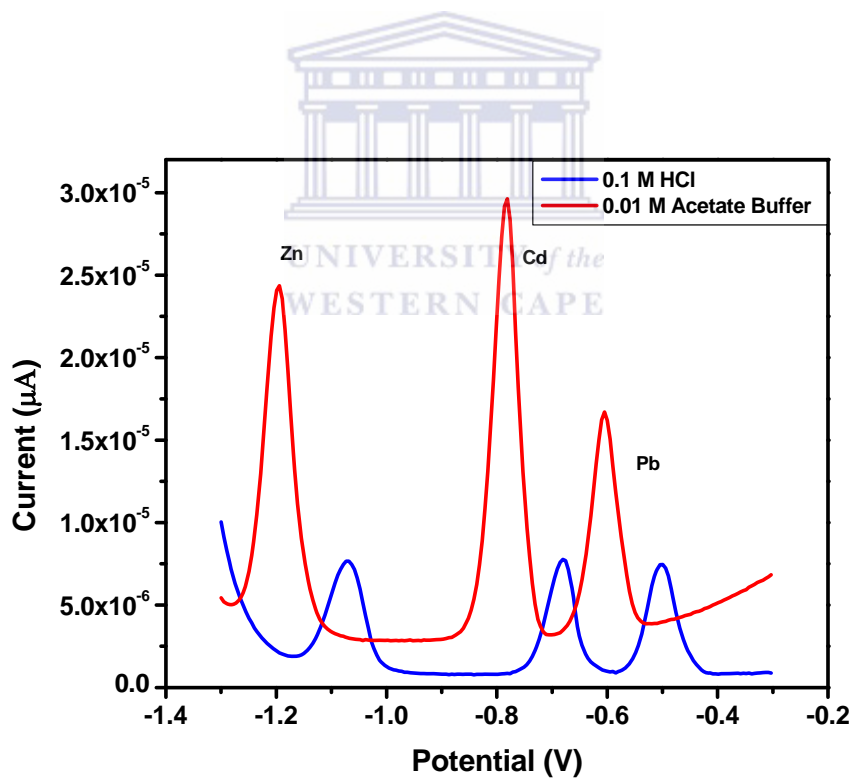
Figure 4.8: SWASV of 30 µg L^{-1} Zn^{2+}, Cd^{2+} and Pb^{2+} on Nafion-G-HgFE in 0.1 M acetate buffer (pH 4.6) and 0.1 M HCl. Other conditions as in Fig. 4-7.

4.2.2 Effect of experimental parameters on the stripping peak currents of Zn^{2+}, Cd^{2+} and Pb^{2+} on Nafion-G HgFE.

4.2.2.1 Deposition potential

As shown in Fig. 4.9a, the stripping peak current of Cd^{2+} and Zn^{2+} were found to occur at potentials more negative than -0.6 V and -1.1 V, respectively. As the deposition potential became more negative, the peak currents increased up to -1.1 V and -1.3 V for Cd^{2+} and Zn^{2+} respectively. The Pb^{2+} peak current did not increase significantly and it was unaffected by the deposition potential due to its more positive reduction potential. A potential of -1.3 V was chosen as the optimum deposition potential.
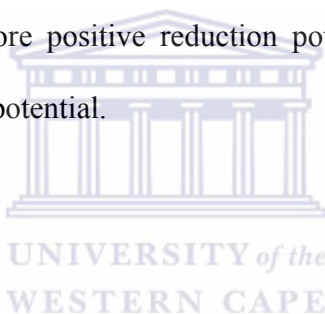
4.2.2.2 Deposition time

Figure 4.9b illustrates the deposition time on the peak currents of Zn^{2+}, Cd^{2+} and Pb^{2+}. All three metals increase linearly with deposition time meaning that the longer the deposition time the more metals get deposited, the higher the peak current. To avoid the electrode from getting saturated 120 s was chosen as the optimum deposition time for further experiments.

4.2.2.3 Rotation speed

The effect of rotation speed on the metals peak current was also investigated as shown in Fig. 4.9c. The peak currents of all three metals i.e. Zn^{2+}, Cd^{2+} and Pb^{2+} increased continuously.

Establishing the optimum rotation speed facilitates the convective transport of the metal ions in solution to the working electrode surface and hence contributes towards the sensitivity of stripping analysis. The faster the square-root of rotation speed, the more metals reach the electrode surface, but to avoid electrode saturation a rotation speed of 1000 rpm was chosen.

4.2.2.4 Frequency

To validate whether the correct frequency was being used, the frequency was varied as shown in Fig. 4.9d. Zn^{2+}, Cd^{2+} and Pb^{2+} increased linearly with an increase in frequency. A frequency of 50 Hz was used to perform the experiments, and it fell within the linear range.

4.2.2.5 Amplitude

Optimization of the amplitude is shown in Fig 4.9e. The amplitude for Cd^{2+} and Pb^{2+} increased linearly up to 0.04 V, and then the peak currents started to deviate. After 0.04 V the stripping peak current of Cd^{2+} started to develop a shoulder and the Pb^{2+} peak got broader with the increase in amplitude. Zn^{2+} increases linearly with an increase in amplitude. Amplitude of 0.025 V was selected for further experiments.
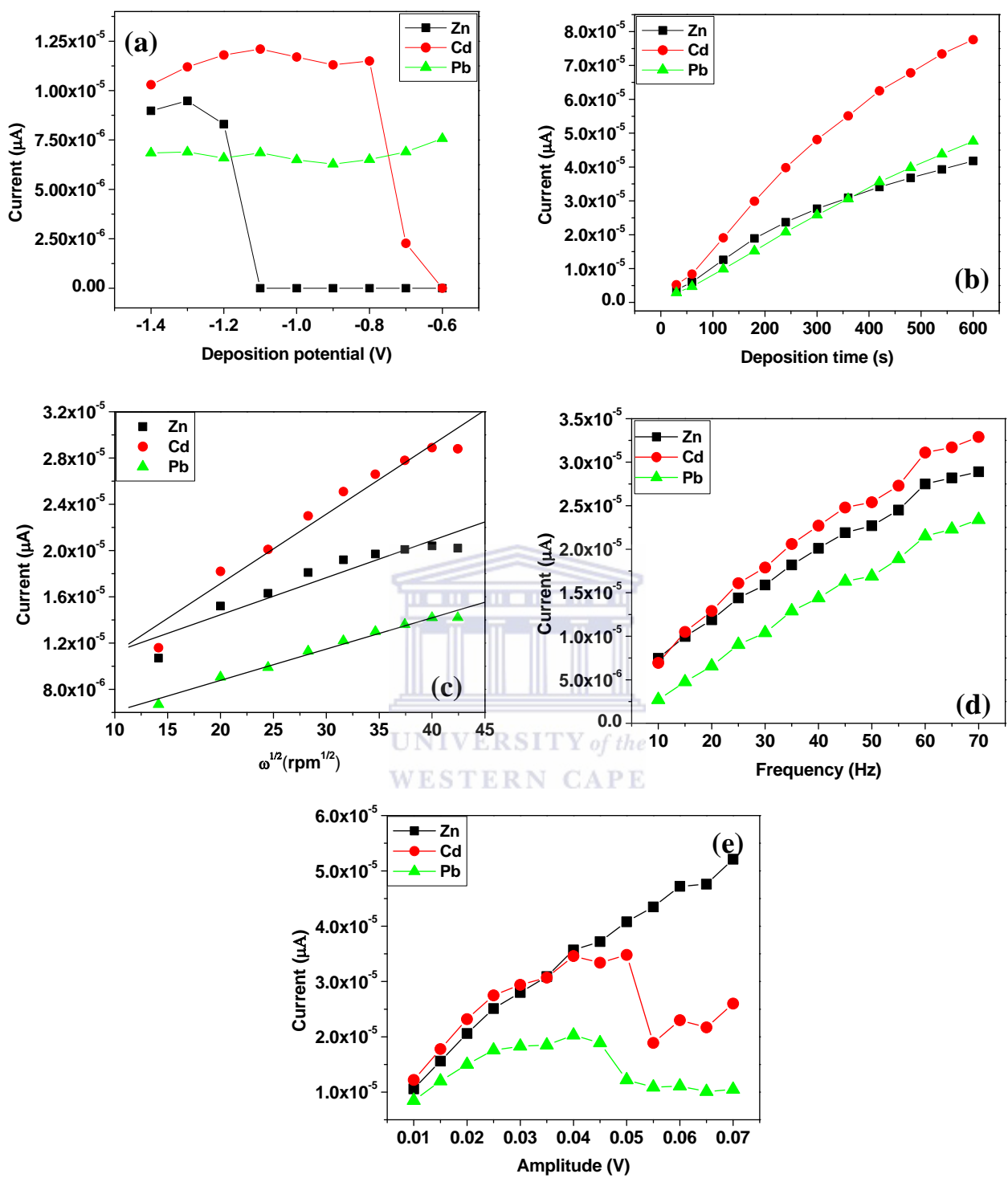
Figure 4.9: Effect of (a) deposition potential, (b) deposition time, (c) rotation speed, (d) frequency and (e) amplitude on the stripping peak current of Zn^{2+}, Cd^{2+} and Pb^{2+} on Nafion-G-HgFE. Other conditions as in Fig 4.7.

4.2.3 Film stability and reproducibility

There was no problem with the Nafion-G nanocomposite film, it was stable when drop coated onto the GCE surface and when dried after an hour was ready to use. To check the reproducibility of the Nafion-G nanocomposite film, metal peak currents were compared, to make sure a similar coating was placed on the GCE surface. However mercury had to be electrochemically plated onto the Nafion-G modified electrode surface to form the Nafion-G HgFE. Forming a mercury film which is stable and reproducible can be some what tricky [131]. The first signal of an analysis was always smaller in comparison to the second signal (Fig. 4.10). This could be due to the instability of the mercury film, but even if the electrode is cycled for a longer period or left in electrolyte for 10 min prior to use, the first signal was still smaller. It is as if the electrode does not respond to the first run of an analysis, or all of the metal does not strip out with the first run but with the second. Running a blank was then eliminated (i.e. acetate buffer and mercury), and the metal ions and mercury were added to the acetate buffer simultaneously and a potential was then applied for 120 s during which the metal ions and mercury co-deposited forming an *in situ* film onto the Nafion-G platform. This eliminated the very small peaks that were observed after the first run. When a blank is run at the beginning of an experiment the mercury deposits onto the Nafion-G nanocomposite film. The electrode is then electrochemically cleaned and all of the metal ions are stripped out, however it may not be clean sufficiently, some of the mercury ions may still be left behind, occupying the active sites on the electrode surface causing; only a certain amount of metals to be deposited onto the electrode surface. When the metals are added they need to compete for the remaining active sites causing the drop in the sensitivity and leading to the small signal being observed. Also note the shift in

the peak potentials of the metals. This could also be attributed to the film being unstable. The Nafion-G-HgFE could also be used for several analyses.
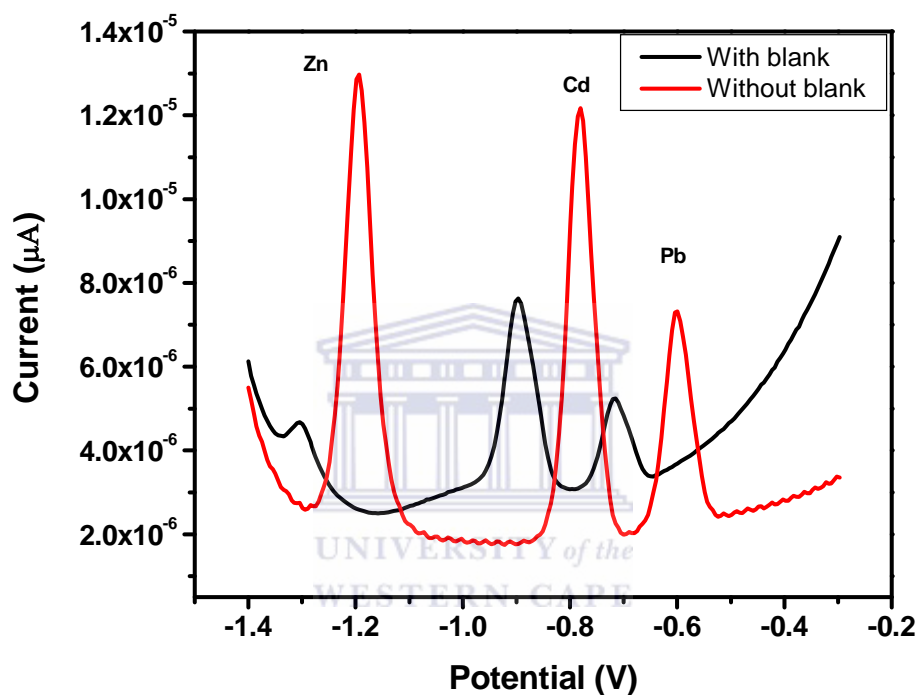
Figure 4.10: SWASV of Zn^{2+}, Cd^{2+} and Pb^{2+} determined with running a blank first and without running a blank. Other conditions as in Fig. 4.7.

4.2.4 Interferences

Like with many analytical techniques intermetallic interference is a concern when analyzing more than one trace metal. Intermetallic interferences usually occur when there is a large change

75

in concentration, which takes place on deposition of the metals into the film, in this case the Nafion-G mercury film. Copper-zinc is the most common type of intermetallic interference which is shown in Fig.4.11. This interference occurred, while trying to analyze all four metal i.e. Zn^{2+}, Cd^{2+}, Pb^{2+} and Cu^{2+} simultaneously. Figure 4.11 shows a split peak for Cu^{2+} as well as a bump between Zn^{2+} and Cd^{2+}. This type of interference can be overcome by the addition of an excess of gallium ions to the sample solution. A larger formation constant exists between Ga-Cu than Cu-Zn, therefore gallium preferentially combines with Cu leaving Zn to be determined without interference [4]. Another method of alleviating this interference is by adjusting the deposition time to reduce the concentration of metals in the amalgam or by setting the deposition potential to a value where only the metals of interest is deposited and detected [52]. For this study however, to avoid the copper-zinc intermetallic interference, these two metals were never determined simultaneously, thus for analysis purposes, Zn^{2+}, Cd^{2+} and Pb^{2+} were determined simultaneously and Cu^{2+} individually. However when analyzing real samples, all four meals (i.e. Zn^{2+}, Cd^{2+}, Pb^{2+} and Cu^{2+}), are usually present, so in this experiment, Zn^{2+} was analyzed separately in a fresh sample, the reason being that very low recoveries were obtained when analyzed in the same sample as well as simultaneously. The remaining three metals (i.e. Cd^{2+}, Pb^{2+} and Cu^{2+}) are then determined, depending on which metal ions are present in solution.
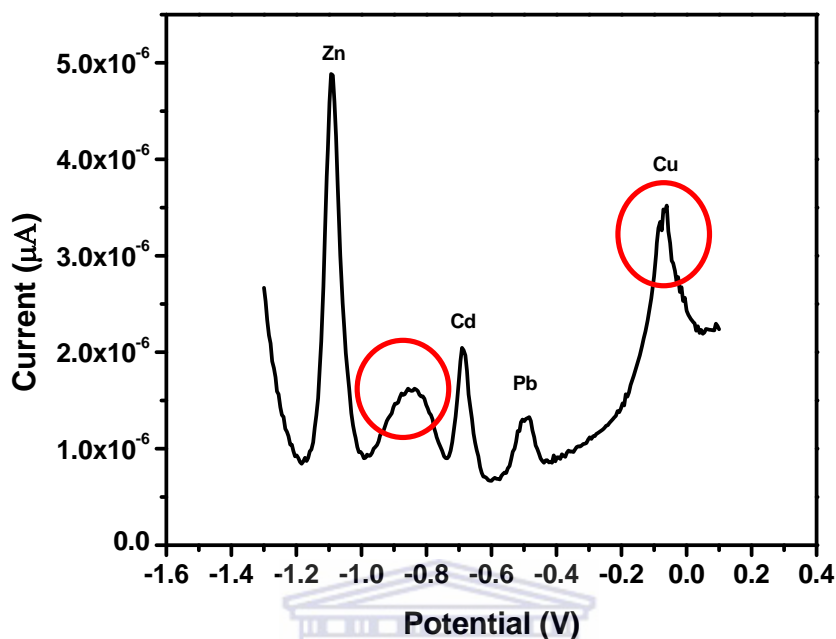
Figure 4.11: Intermetallic interferences observed for simultaneous analysis of Zn^{2+}, Cd^{2+}, Pb^{2+} and Cu^{2+}

4.2.5 Analytical Performance of Nafion-G HgFE

4.2.5.1 Individual and simultaneous determination of Zn^{2+}, Cd^{2+}, Pb^{2+} and Cu^{2+}.

All four metals i.e. Zn^{2+}, Cd^{2+}, Pb^{2+} and Cu^{2+} were determined individually as well as simultaneously with Nafion-G-HgFE in 0.1 M acetate buffer containing 10 mg L^{-1} Hg^{2+} solution using SWASV. Calibration plots (Figure 4.12a-d), for individual metal solutions ranging from 1-7 µg L^{-1} gave correlation coefficients, sensitivities and detection limits shown in Table 4.1. A slight shift in the peak potentials of the metals with increasing metal ion concentration towards positive potential was observed and suggests an IR-drop effect.
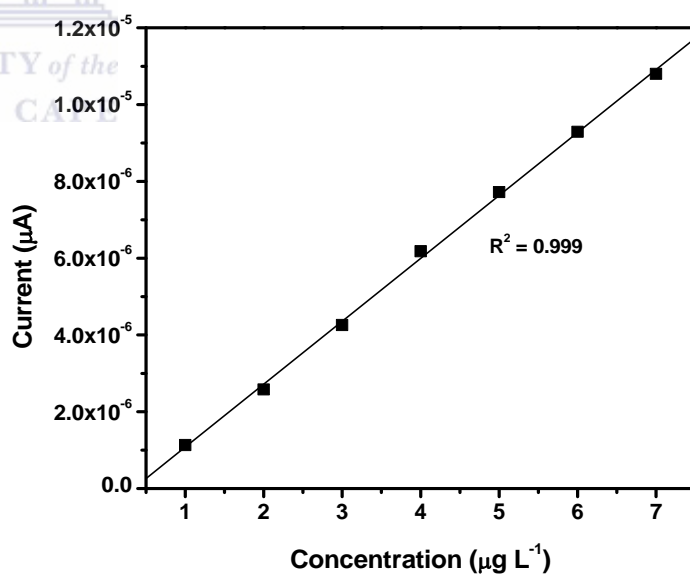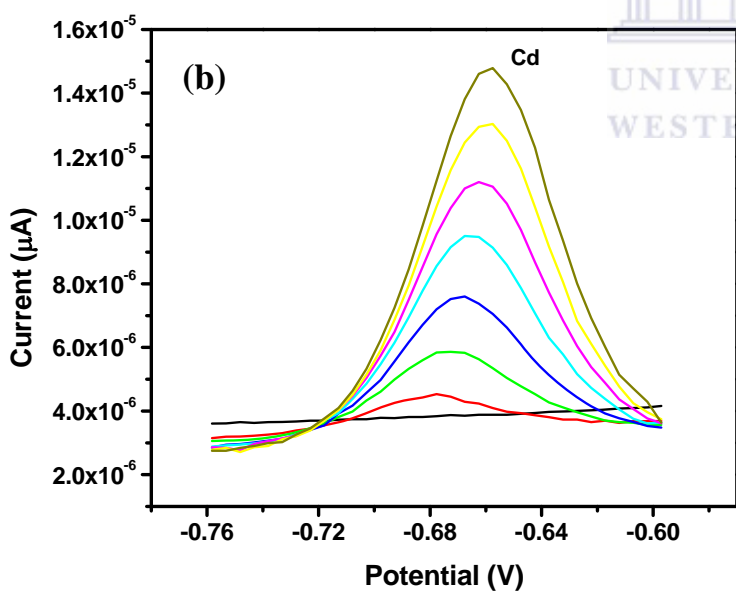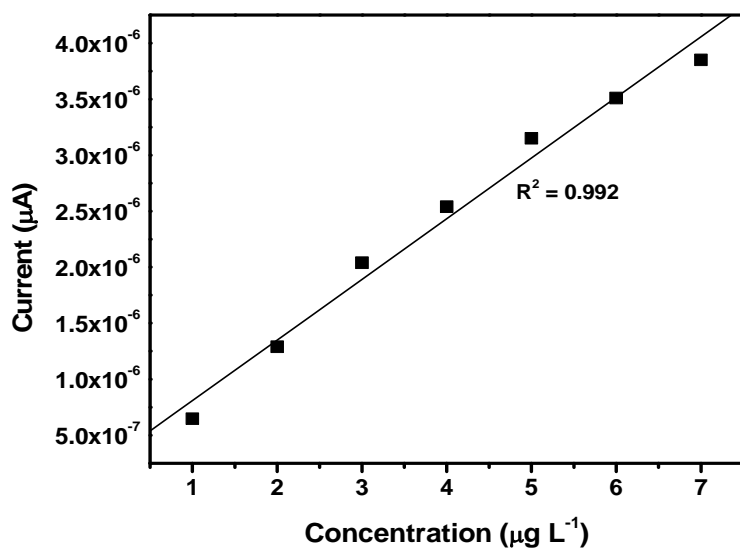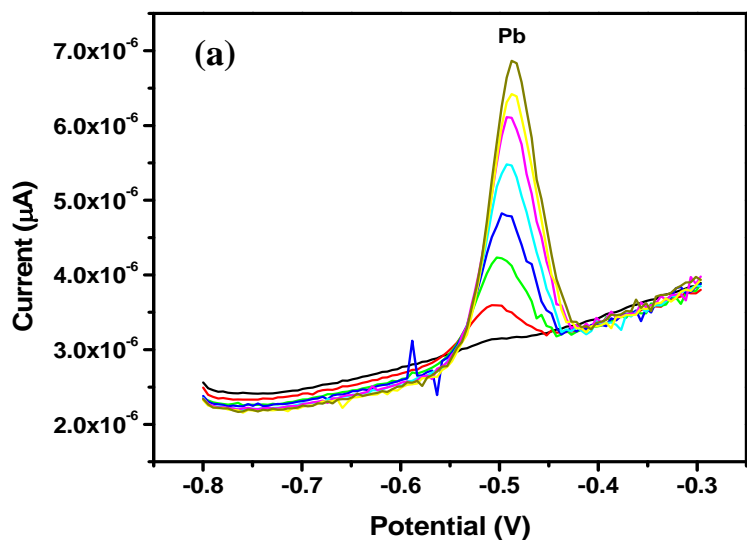
Figure 4.12: Voltammograms for increasing concentration of (a) Pb^{2+}, (b) Cd^{2+} obtained with Nafion-G-HgFE. Other conditions as in Fig. 4.7.
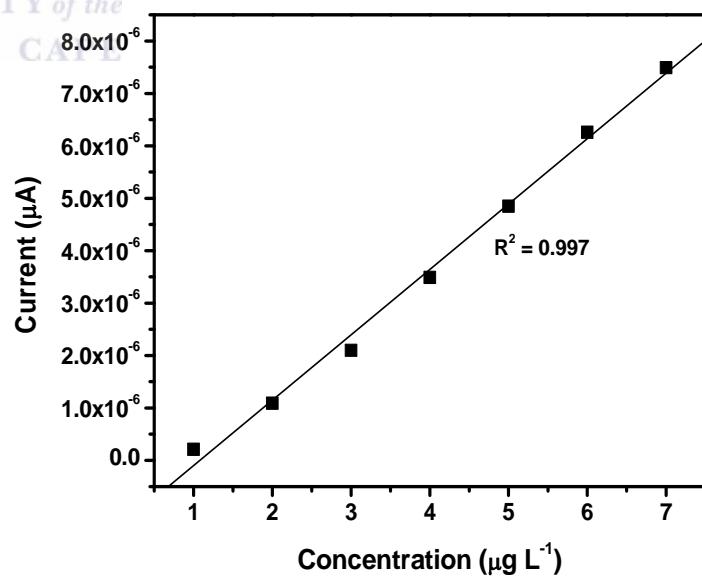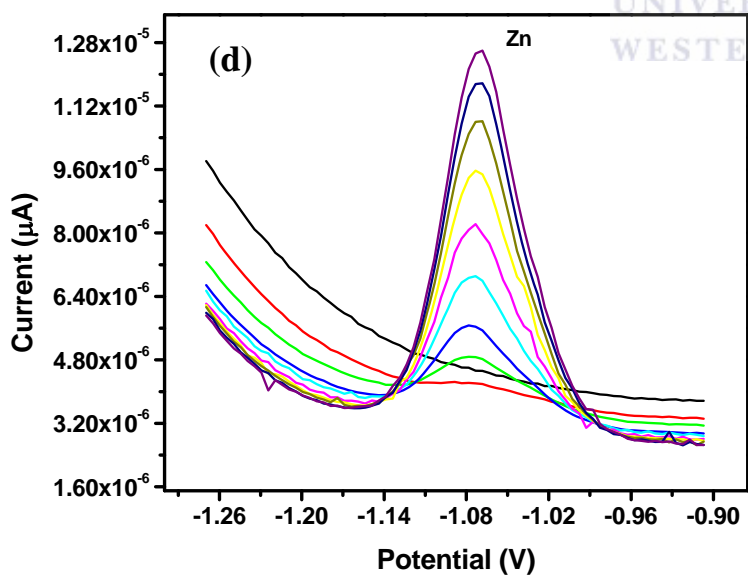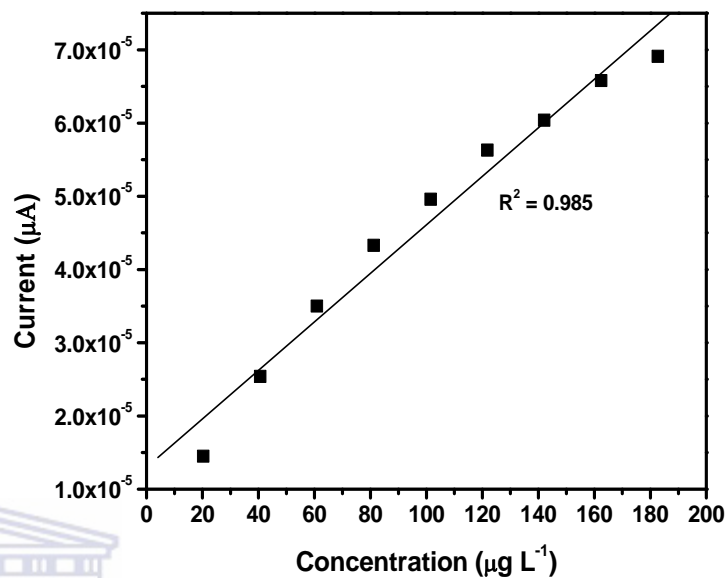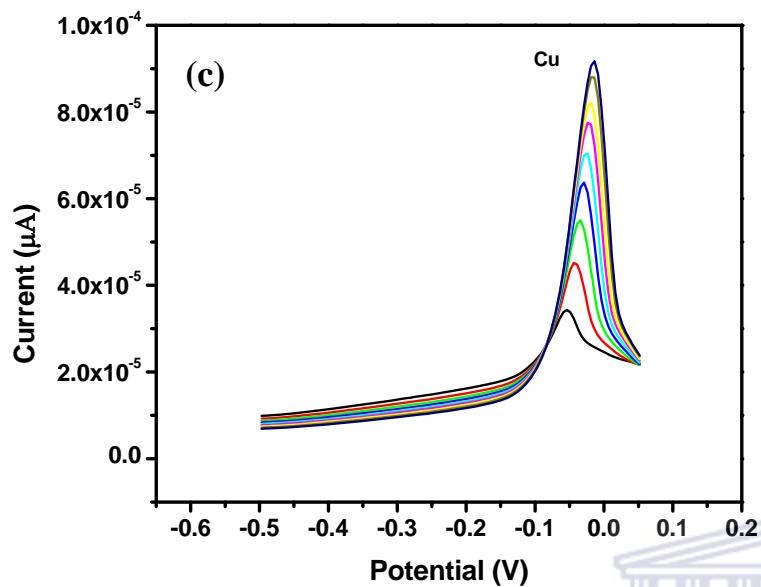
Figure 4.12: Voltammograms for increasing concentration of (c) Cu^{2+} and (d) Zn^{2+} obtained with Nafion-G-HgFE. Other conditions as in Fig. 4.7.

Table 4.1: Correlation coefficient (R^2), sensitivity and detection limits of Pb^{2+}, Cd^{2+}, Zn^{2+} and Cu^{2+} for individual determination at the Nafion-G HgFE.

Individual	R^2	Sensitivity ($\mu A\ L\ \mu g^{-1}$)	Detection limits ($\mu g\ L^{-1}$)
Pb^{2+}	0.992	0.541 ± 0.06	0.07
Cd^{2+}	0.999	1.64 ± 0.13	0.08
Zn^{2+}	0.997	1.25 ± 0.22	0.07
Cu^{2+}	0.985	12.95 ± 1.13	0.13

Simultaneous analyses of metals were also performed according to the same parameters as that of the individual analysis. A series of stripping voltammograms for Cd^{2+} and Pb^{2+} (1-10 $\mu g\ L^{-1}$) are shown in Fig. 4.13a and Zn^{2+}, Cd^{2+} and Pb^{2+} (0.5-5 $\mu g\ L^{-1}$) in Fig. 4.13b. Calibration plots for the simultaneous analysis of metals gave correlation coefficients (R^2), sensitivities and detection limits in Table 4.2. When the Cd^{2+} and Pb^{2+} are determined simultaneously (Fig 4.13a) the calibration curves are very linear ($R^2 = 0.999$), however as soon as Zn^{2+} is determined simultaneously (Fig. 4.13b) with the other two metals the electrode reaches saturation much quicker and the linear regression is low. This is due to the competition between the metal for the active site at the electrode surface.
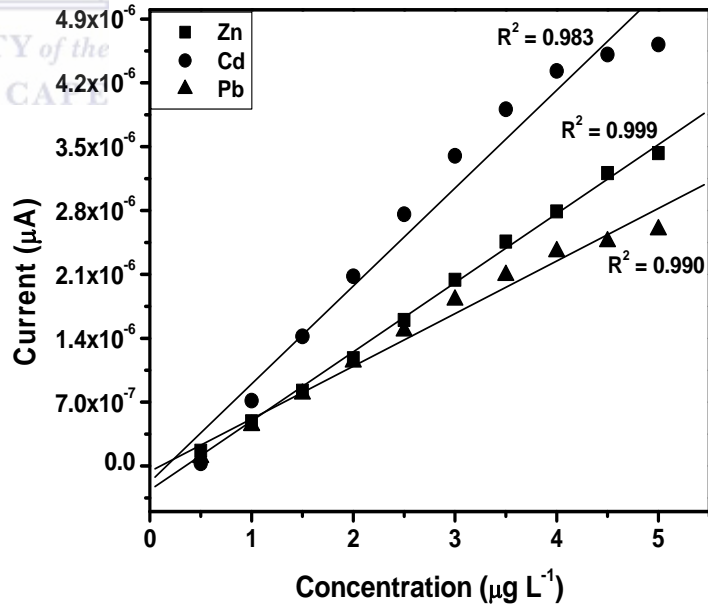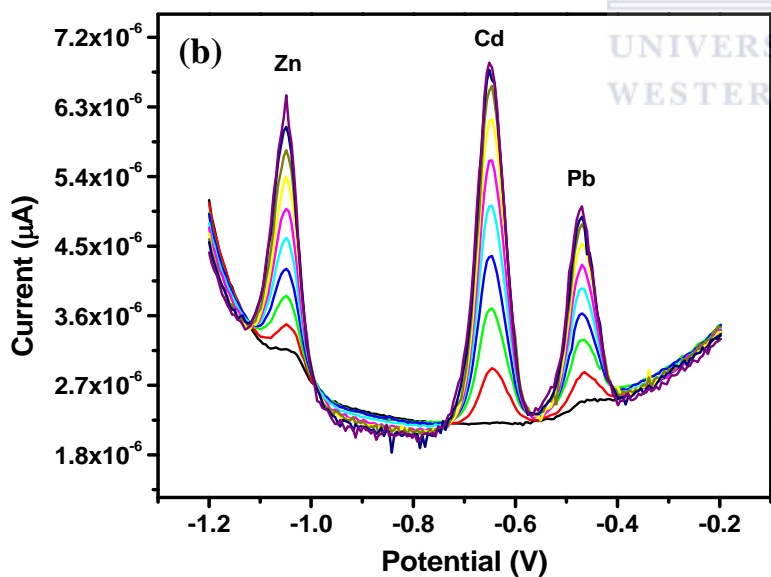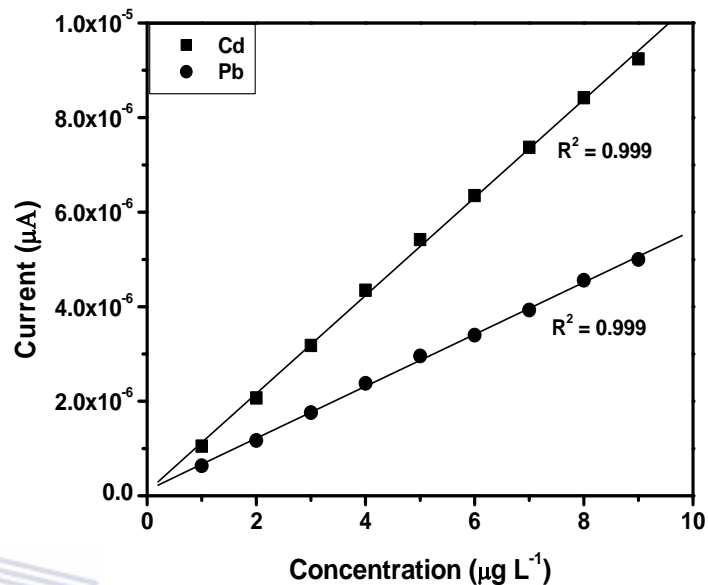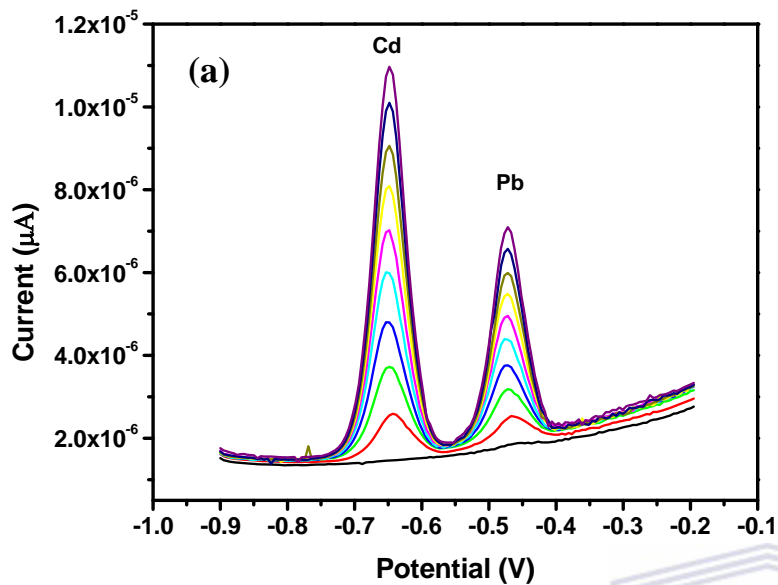
Figure 4.13: Voltammograms for simultaneous determination of (a) Cd^{2+} and Pb^{2+} (1-10 µg L^{-1}) and (b) Zn^{2+}, Cd^{2+} and Pb^{2+} (0.5-5 µg L^{-1}) obtained with Nafion-G-HgFE. Other conditions as in Fig. 4.7.

Table 4.2: Correlation coefficient (R^2), sensitivity and detection limits of Pb^{2+}, Cd^{2+} and Zn^{2+} determined simultaneously at the Nafion-G HgFE.

Simultaneous	R^2	Sensitivity ($\mu A\ L\ \mu g^{-1}$)	Detection limits ($\mu g\ L^{-1}$)
Pb^{2+}	0.990	0.577 ± 0.04	0.07
Cd^{2+}	0.983	1.070 ± 0.10	0.13
Zn^{2+}	0.999	0.758 ± 0.07	0.14

4.2.5.2 Comparison between individual and simultaneous determination of metals

The sensitivities of metals determined individually, differed from those determined simultaneously. Metals such as Cd^{2+} and Zn^{2+} experienced a significant decrease in sensitivity when analyzed simultaneously. Cadmium went from 1.64 $\mu A\ L\ \mu g^{-1}$ (individually) to 1.04 $\mu A\ L\ \mu g^{-1}$ and 1.07 $\mu A\ L\ \mu g^{-1}$ (simultaneously). In general, higher sensitivities were obtained for individual analysis, since only one of the metals binds to the limited number of active sites at the modified electrode surface and is involved in forming the amalgam film during the deposition step. However, during simultaneous analysis all metals present in solution compete for the limited number of active sites and are all co-deposited during the formation of the amalgam film. In addition, differences in sensitivities between individual and simultaneous determinations can also be attributed to the formation of intermetallic compounds between heavy metals when present together in the same solution. For Pb^{2+} however the sensitivity remains relatively the same. Zn^{2+} also shows a decrease in sensitivity (from 1.25 $\mu A\ L\ \mu g^{-1}$ to 0.758 $\mu A\ L\ \mu g^{-1}$). This could be due to adsorption of metals onto the wall of the glass cell, causing a smaller amount of metal to be deposited and stripped out [132]. The interaction among heavy metal, when placed in a solution could also account for the difference in sensitivity.

4.3 PART C: Nafion-Graphene Bismuth Film Electrode

The following section follows on the same principle as discussed in part B; the only difference is that the discussion is based on the Nafion-G bismuth film electrode.

4.3.1 Electrochemical characterization of Nafion-G Bismuth film electrode

4.3.1.1 Electrode current response of different Nafion-G BiFE platforms

The sensitivities of the different electrode platforms (GCE, Nafion-BiFE, Graphene-BiFE, Nafion-G-BiFE or BiFE) were compared. Figure 4.14 shows the stripping voltammograms of 30 μg L^{-1} Zn^{2+}, Cd^{2+} and Pb^{2+} in 0.1 M acetate buffer (pH 4.6) at different electrode surfaces. The figure shows that Nafion-G-BiFE has the highest and sharpest peak current and is therefore the most sensitive in terms of electrode current response. This is followed by Graphene-BiFE, Nafion-BiFE, BiFE and lastly the bare GCE which is the least sensitive platform for metal determination.
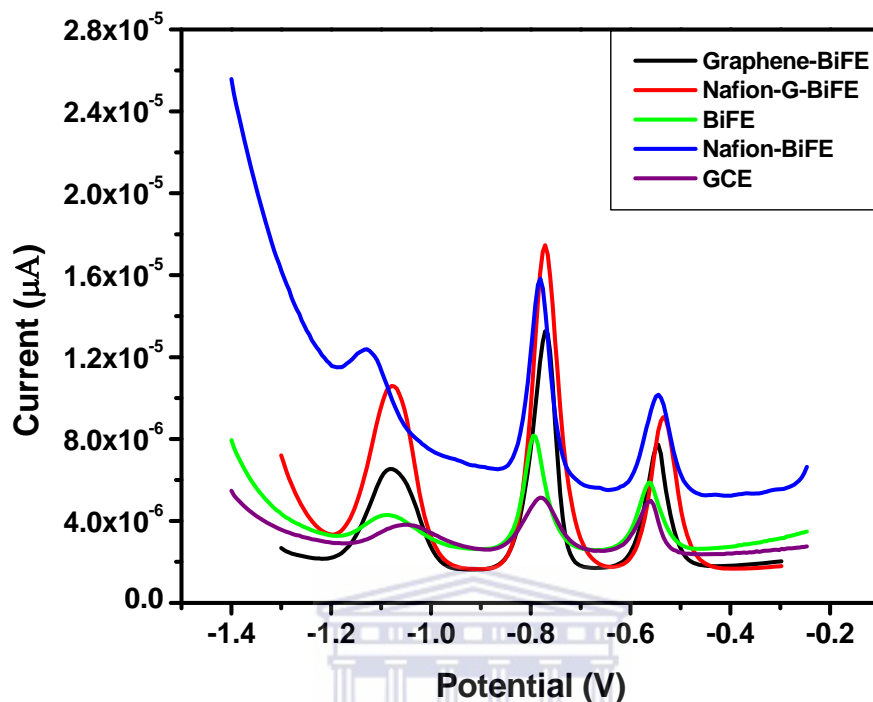
Figure 4.14: SWASV of 30 μg L^{-1} Zn^{2+}, Cd^{2+} and Pb^{2+} on different metal platforms. Other conditions as in Fig. 4.7.

4.3.2 Effect of experimental parameters on the stripping peak currents of Zn^{2+}, Cd^{2+} and Pb^{2+} on Nafion-G-BiFE.

4.3.2.1 Deposition potential

The effect of deposition potential on the peak current of Zn^{2+}, Cd^{2+} and Pb^{2+} after 120 s deposition time was studied in the potential range -1.5 V to -0.7 V as shown in Fig. 4.15a. As the deposition potential became more negative the peak current of Cd^{2+} and Pb^{2+} increased up to -1.2 V and -1.3 V respectively. The peak current of Zn^{2+} was found to occur at potentials more negative than -1.2 V. A deposition of -1.3 V was chosen as the optimum deposition potential.

4.3.2.2 Deposition time

The sensitivity of the analysis was further improved by the deposition time. As the deposition time increased, so does the peak current of Zn^{2+}, Cd^{2+} and Pb^{2+} as shown in Fig. 4.15b. This occurs due to the increased amount of analyte on the Nafion-G-BiFE. The peak current of Zn^{2+} did not change significantly with increased deposition time. However to avoid electrode saturation at higher deposition time, 120 s was chosen as the optimum for the subsequent analysis.

4.3.2.3 Rotation speed

Rotation speed was varied in the range 200-200 rpm (Fig. 4.15c). As the rotation speed increased so did the peak current of Cd^{2+} and Pb^{2+}. The stripping peak current of Zn^{2+} did increase significantly with the increase in rotation speed. To avoid saturation or the Nafion-G-BiFE from being damaged, deposition was performed at 1000 rpm.

4.3.2.4 Frequency

The frequency was varied in the range 10-70 Hz to validate whether the frequency being used was still in the linear range as shown in Fig. 4.15d. The peak current of the metals increased with the increase in frequency. Zn^{2+} and Cd^{2+} increased linearly. The frequency was kept at 50 Hz since it was used initially and fell within the linear range for each metal.

4.3.2.5 Amplitude

Figure 4.15e shows the effect of increased amplitude on the peak current of Zn^{2+}, Cd^{2+} and Pb^{2+}. The peak current of Zn^{2+} increases up to 0.04 V then starts to level off, the same can be said of Cd^{2+}. The peak current of Pb^{2+} increases continuously. The amplitude was also kept at 0.025 V because it fell within the linear range.
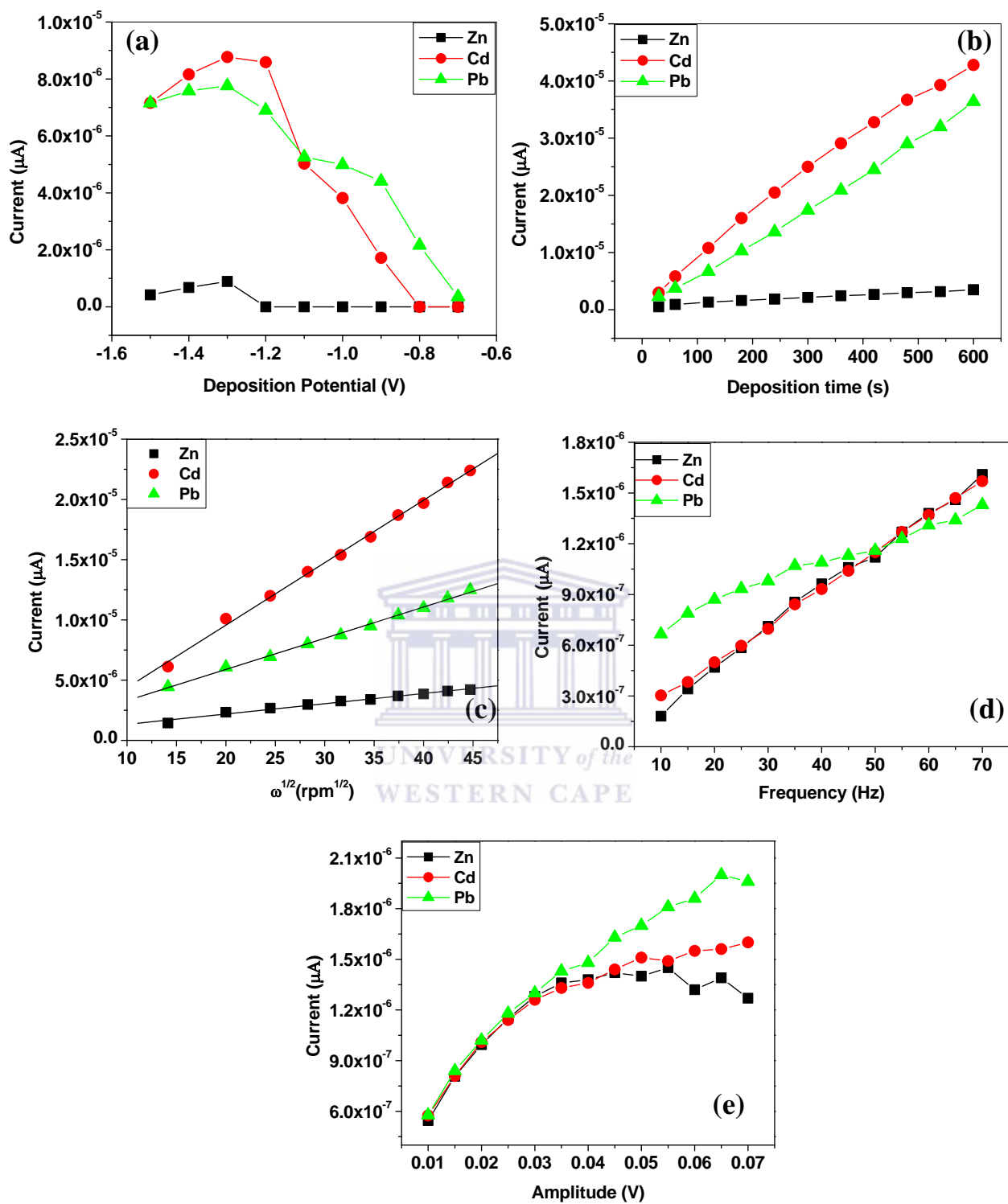
Figure 4.15: Effect of (a) deposition potential, (b) deposition time, (c) rotation speed, (d) frequency and (e) amplitude on the stripping peak current of Zn^{2+}, Cd^{2+} and Pb^{2+} on Nafion-G-BiFE. Other conditions as in Fig 4.7.

4.3.3 Film stability and reproducibility

The Nafion-G-BiFE was stable and could be used at least three times, i.e. for three analyses. To ensure the modified electrode had no carry over metal on it, it was first cycled in 0.1 M acetate buffer. If no metal stripping peaks were observed then the electrode was ready to be used again. Stripping peaks were also very reproducible.

4.3.4 Intermetallic interference

An intermetallic interference exists between copper and bismuth due to the competition between bismuth and copper ions at the active sites of the electrode surface [7]. When Cu^{2+}, Cd^{2+} and Pb^{2+} were determined simultaneously on the Nafion-G-BiFE, the stripping peak current of Cd^{2+} and Pb^{2+} decreased dramatically (Fig. 4.16). However in this study three metals were determined simultaneously to see what detection limits would be obtained, and how copper influences the peak currents of the other two metals (i.e. Cd^{2+} and Pb^{2+}) if a Nafion-G-BiFE were to be used. Notice the decrease of the bismuth peak, from Fig 4.16 as well as when copper was determined individually on the Nafion-G-BiFE (Fig.4.17d). This also reflects the competition between the two metals (Bi-Cu) for surface active sites.
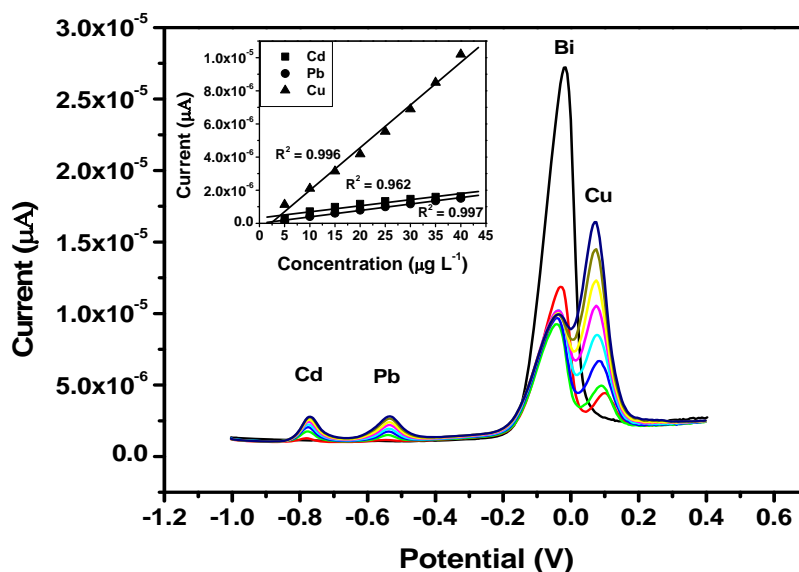
Figure 4.16: SWASV of Cu^{2+}, Cd^{2+} and Pb^{2+} determined simultaneously in 0.1 M acetate buffer (pH 4.6) and 2 mg L^{-1} Bi^{3+} on Nafion-G-BiFE. Other conditions as in Fig. 4.7.
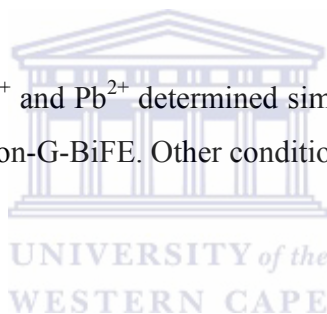
4.3.3 Analytical Performance

4.3.3.1 Individual and simultaneous analysis of Zn^{2+}, Cd^{2+}, Pb^{2+} and Cu^{2+}.

Individual as well as simultaneous analysis of Zn^{2+}, Cd^{2+}, Pb^{2+} and Cu^{2+} were done in 0.1 M acetate buffer (pH 4.6) and 2 mg L^{-1} Bi^{3+} on the Nafion-G-BiFE. Figure 4.17a-d shows the stripping voltammograms for 5-45 µg L^{-1} of metals determined individually at a deposition time of 120 s. The insets show the calibration plot of each metal. Correlation coefficients, sensitivities and detection limits are shown in Table 4.3. For Cd^{2+} and Pb^{2+} there appears to be a peak potential dependence on concentration. As the metal concentration increases the peak potential of these two metals shift in a positive direction (cathodic direction). This result suggests that the shift is due to an IR-drop effect.

89
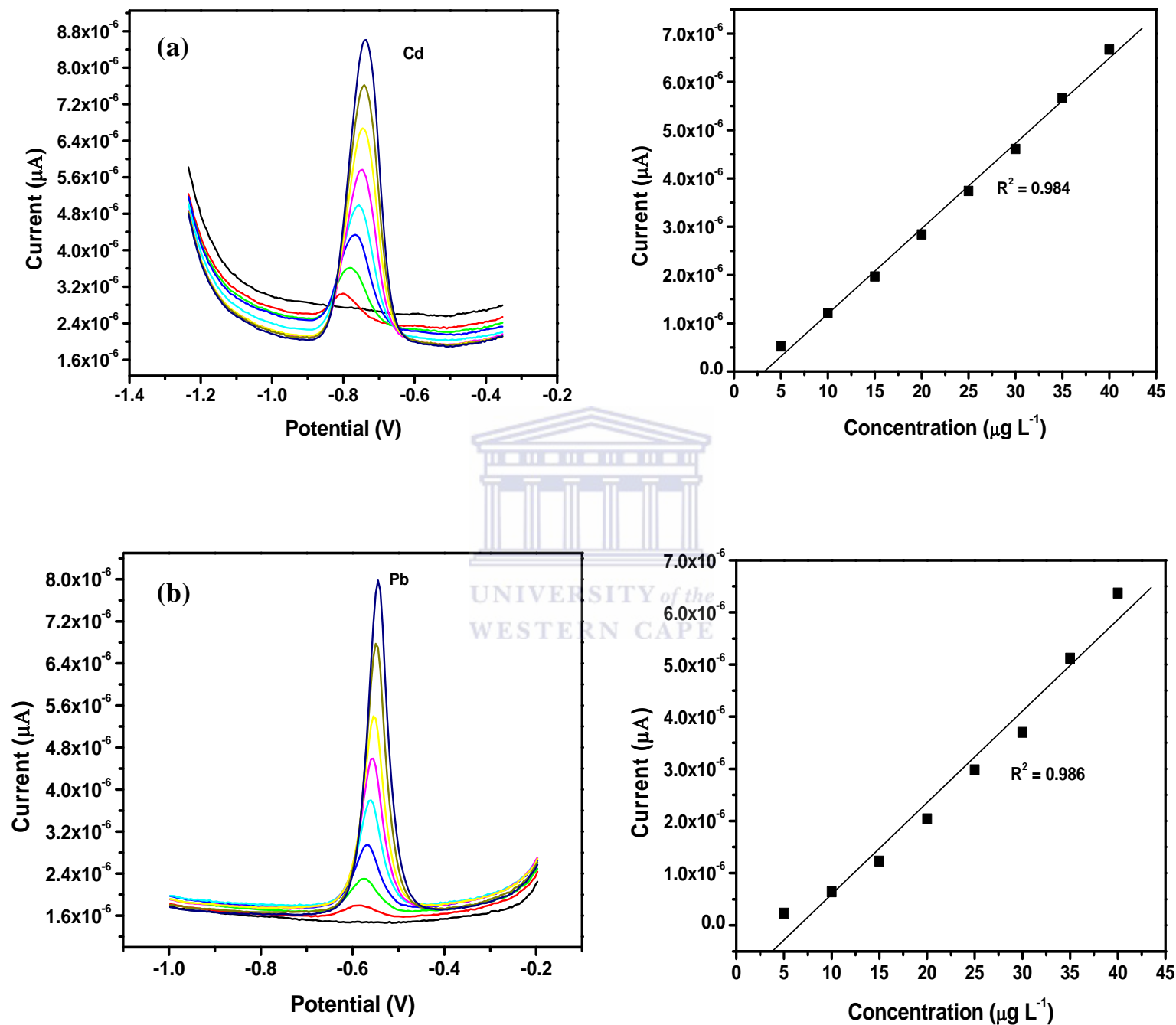
Figure 4.17: Voltammograms for the individual determination of (a) Cd^{2+}, (b) Pb^{2+} (5-45 µg L^{-1}) obtained with Nafion-G-BiFE. Other conditions as in Fig. 4.7.
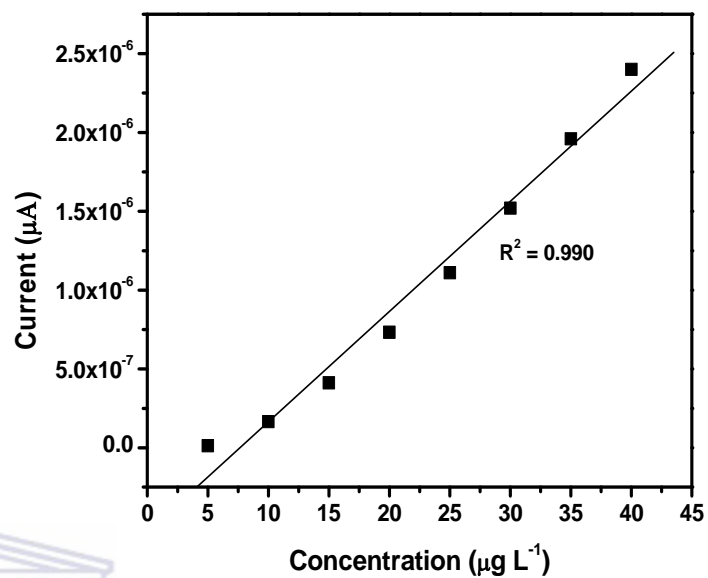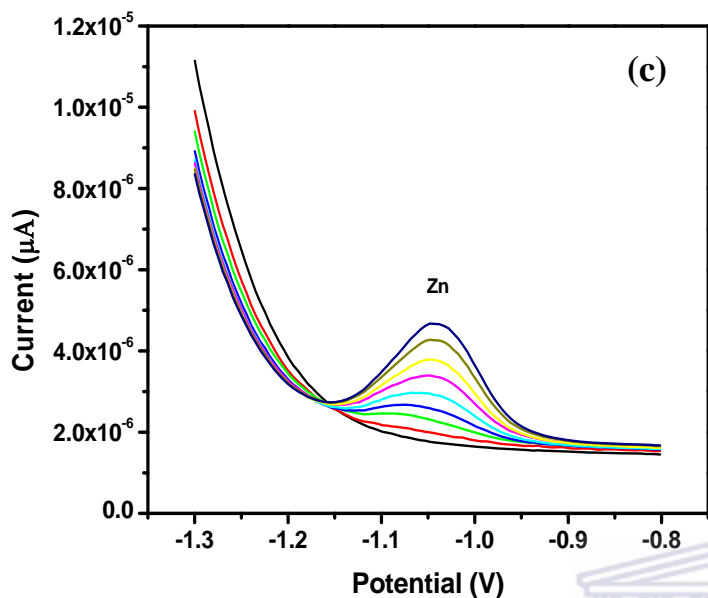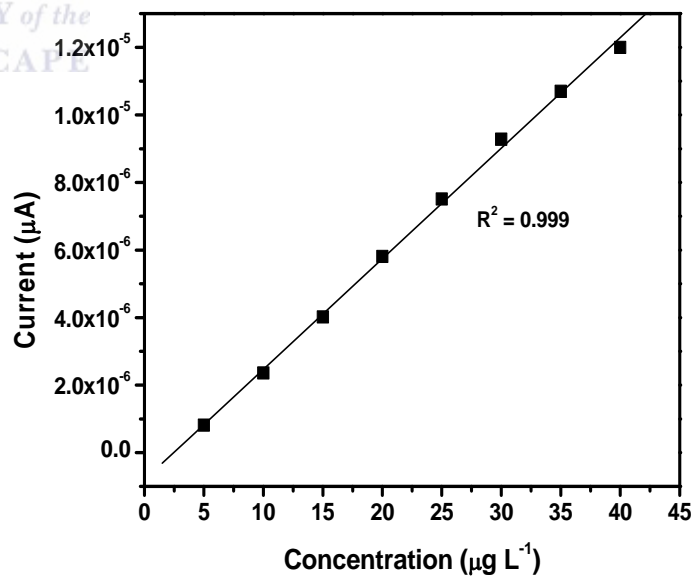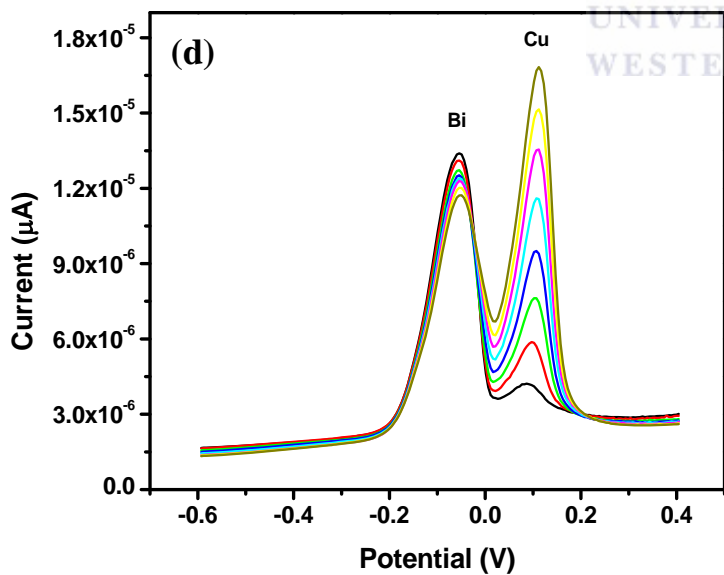
Figure 4.17: Voltammograms for the individual determination of (c) Zn^{2+} and (d) Cu^{2+} (5-45 µg L^{-1}) obtained with Nafion-G-BiFE. Other conditions as in Fig. 4.7.

Table 4.3: Correlation coefficient (R^2), sensitivity and detection limits of Pb^{2+}, Cd^{2+}, Zn^{2+} and Cu^{2+} determined individually at the Nafion-G BiFE.

Individual	R^2	Sensitivity ($\mu A\ L\ \mu g^{-1}$)	Detection limit ($\mu g\ L^{-1}$)
Pb^{2+}	0.986	0.176 ± 0.23	0.13
Cd^{2+}	0.984	0.177 ± 0.83	0.18
Zn^{2+}	0.990	0.0699 ± 0.09	0.33
Cu^{2+}	0.999	0.327 ± 0.13	0.17

Simultaneous analyses of Zn^{2+}, Cd^{2+}, and Pb^{2+} were performed in accordance with the experimental conditions of individual analyses. Figure 4.18a-b shows the stripping voltammograms for 5-45 $\mu g\ L^{-1}$ of metal determined simultaneously at 120 s deposition time with the insets showing the calibration plots. Sensitivity, correlation coefficient R^2 and detection limits are indicated in Table 4.4. The peaks for each metal whether determined individually or simultaneously are well resolved and increase linearly with the metal concentration.

Table 4.4: Correlation coefficient (R^2), sensitivity and detection limits of Pb^{2+}, Cd^{2+} and Zn^{2+} determined simultaneously at the Nafion-G BiFE.

Simultaneous	R^2	Sensitivity ($\mu A\ L\ \mu g^{-1}$)	Detection limit ($\mu g\ L^{-1}$)
Pb^{2+}	0.999	0.120 ± 0.07	0.12
Cd^{2+}	0.999	0.428 ± 0.16	0.08
Zn^{2+}	0.997	0.237 ± 0.17	0.85

4.3.3.2 Comparison between individual and simultaneous determination of metals.

When comparing individual to simultaneous analyses, it is worth noting the difference in sensitivities being observed. A significant change in sensitivity is observed for certain metals. The sensitivity of Pb^{2+} decreased when determined simultaneous with Cd^{2+} and Zn^{2+}. However for Zn^{2+} and Cd^{2+} the sensitivity increased, when in a mixture. The drop in sensitivity could be attributed to the fact that in a mixture containing Zn^{2+}, Cd^{2+} and Pb^{2+},all three metal are deposited simultaneously however, Pb^{2+} is stripped last leaving only a limited amount of active sites left, sine most of it have already been taken up by the other two metals.
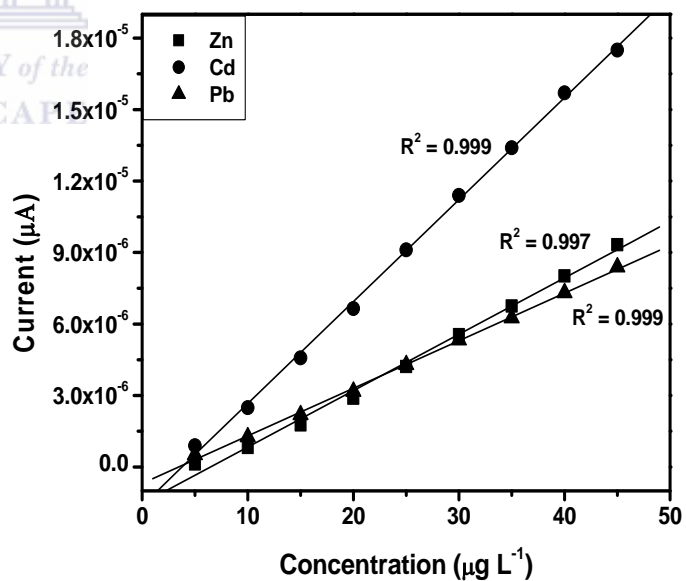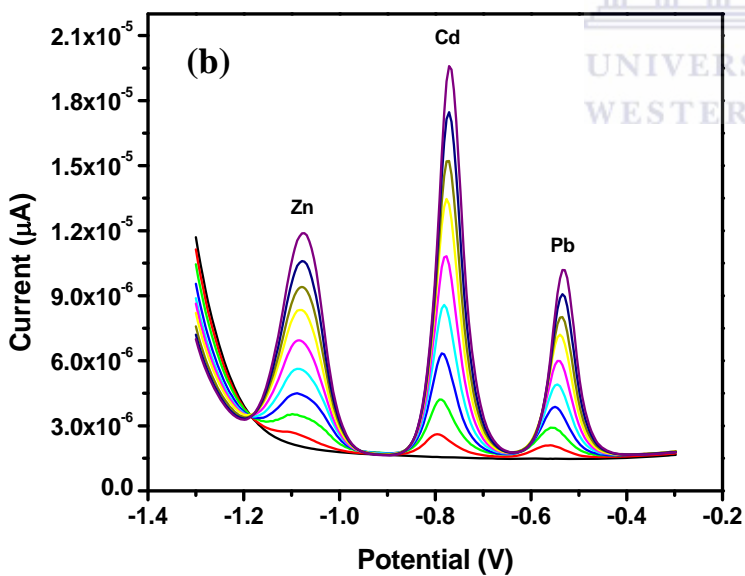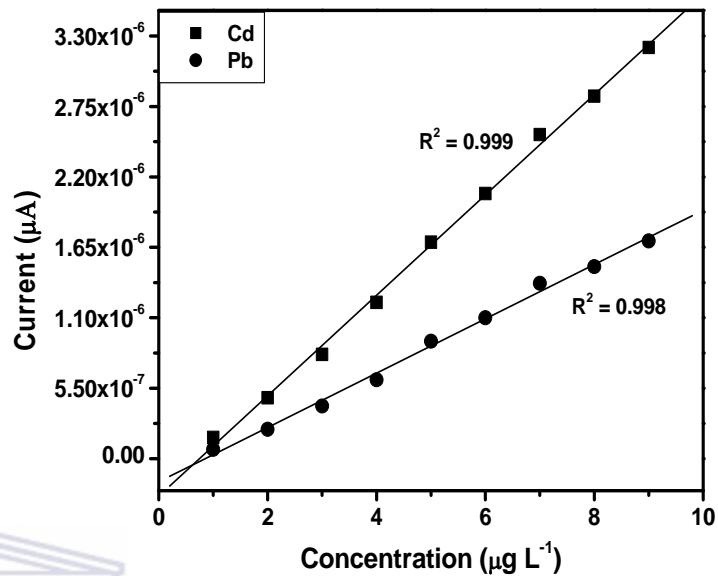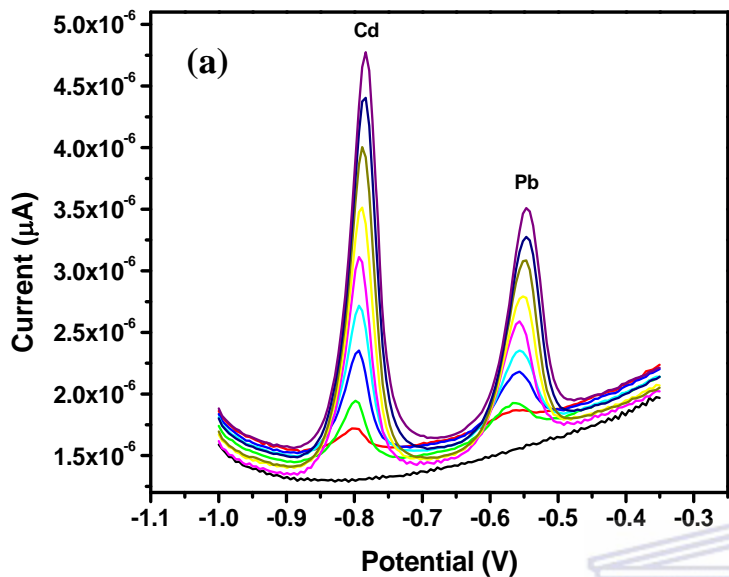
Figure 4.18: Voltammograms for simultaneous determination of (a) Cd^{2+} and Pb^{2+} and (b) Zn^{2+}, Cd^{2+} and Pb^{2+} obtained with Nafion-G-BiFE. Other conditions as in Fig. 4.7.

4.4 PART D: Nafion-Graphene Antimony Film Electrode

In this section the effect of different parameters on the stripping peak currents of the metals are discussed as well as the sensitivity of the Nafion-G antimony film electrode and detection limits much the same as in the previous section. The main focus here is the Nafion-G-SbFE.

4.4.1 Electrochemical characterization of Nafion-G-SbFE

4.4.1.1 Electrode current response of different Nafion-G SbFE platforms

The sensitivities of different electrode platforms (GCE, Nafion-G SbFE, Nafion-SbFE, Graphene-SbFE and SbFE) were compared by SWASV in 0.1 M acetate buffer (pH 4.6). The stripping voltammogram of 30 µg L^{-1} Zn^{2+}, Cd^{2+} and Pb^{2+} on different platforms are shown in Fig. 4.19. This figure clearly shows that the Nafion-G-SbFE has the greatest sensitivity, i.e. it has the highest peak current of metals. This figure shows the same trend as that observed in Fig 4.8 and 4.13.
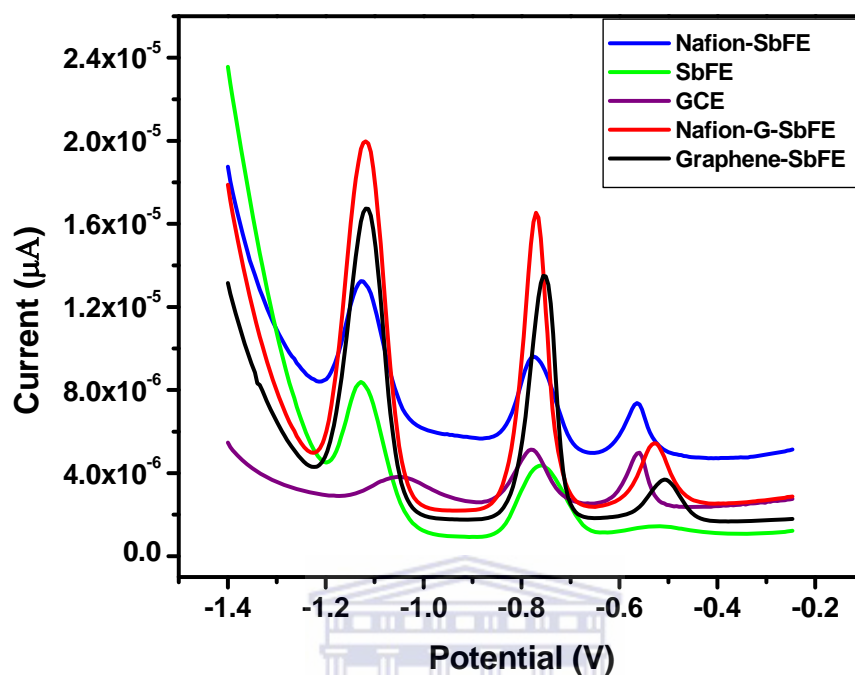
Figure 4.19: SWASV of 30 μg L^{-1} Zn^{2+}, Cd^{2+} and Pb^{2+} on different metal platforms. Other conditions as in Fig. 4.7.

4.4.2 Effect of experimental parameters on the stripping peak currents of Zn^{2+}, Cd^{2+} and Pb^{2+} on Nafion-G-SbFE.

4.4.2.1 Deposition potential

As shown in Fig. 4.20a, the stripping peak responses of Pb^{2+} and Cd^{2+} were found to occur at potentials more negative than -1.1 V and for Zn^{2+} at -1.2 V. As the deposition potential became more negative, the peak currents of Zn^{2+} and Pb^{2+} increased up to -1.3 V and that of Cd^{2+} up to -1.2 V. A potential of -1.3 V was chosen as optimum deposition potential.

4.4.2.2 Deposition time

Figure 4.20b illustrates the effect of deposition time on the stripping peak current of each metal. As the deposition time increases, so does the peak current of Zn^{2+}, Cd^{2+} and Pb^{2+}. A deposition time of 120 s was chosen as the optimum to avoid saturation of the electrode. Even though when using a longer deposition time, more metal gets deposited, only a certain amount of additions may be done whereas at a shorter deposition time more additions may be made. But this pattern allows one the use of prolonged deposition time aimed at obtaining lower detection limits when needed.

4.4.2.3 Rotation speed

Rotation speed was varied in the range 200-2000 rpm as shown in Fig. 4.20c. The stripping peak currents of all three metals increased continuously with an increase in rotation speed. This pattern also shows that faster rotation can be used but to avoid destroying the antimony film on the modified electrode 1000 rpm was chosen as the optimum rotation speed for further analysis.

4.4.2.4 Frequency

Figure 4.20d shows the effect of frequency on the stripping peak current of Zn^{2+}, Cd^{2+} and Pb^{2+} in the range 10-70 Hz. The frequency increases linearly and continuously for all three metals however, the peak current of Pb^{2+} does not increase significantly with the increase of frequency.

The frequency of 50 Hz which was used initially was not changed since it fell within the linear range.

4.4.2.5 Amplitude

Amplitude was also varied in the range 0.01-0.07 V as shown in Fig. 4.20e to validate whether the amplitude being used was within a linear range. The peak currents of the metals increased continuously with the increase in amplitude, however Pb^{2+} was not affect by the change in amplitude since its peak current did not increase significantly. The amplitude was kept at 0.025 V. Higher amplitude may cause peak broadening and the developments of shoulders on the metals stripping peaks.
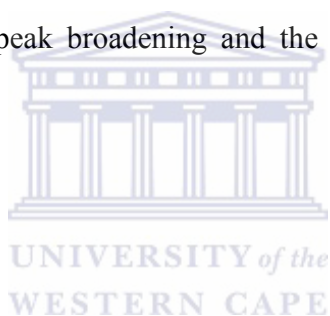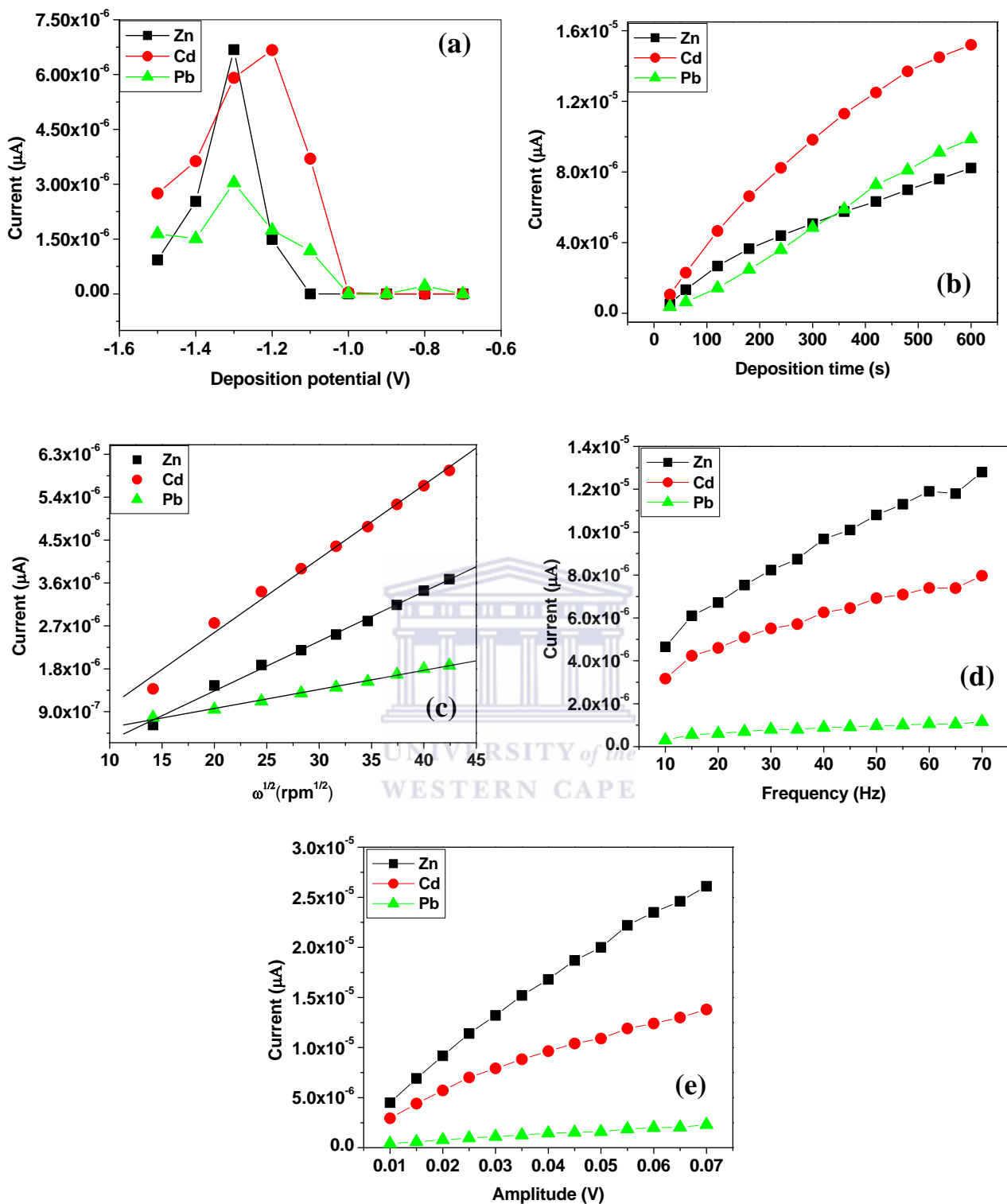
Figure 4.20: Effect of (a) deposition potential, (b) deposition time, (c) rotation speed, (d) frequency and (e) amplitude on the stripping peak currents of Zn^{2+}, Cd^{2+} and Pb^{2+} on Nafion-G-SbFE. Other conditions in Fig. 4.7.

4.4.3 Film stability and reproducibility

The Nafion-G-SbFE was stable and could be used three times depending on whether all the metal ions had been removed from the modified electrode surface. This was usually confirmed by cycling the modified electrode in 0.1 M acetate buffer and if no spurious peaks were observed the electrode was reused. Each signal obtained was reproducible.

4.4.4 Analytical Performance

4.4.4.1 Individual and simultaneous analysis of Zn^{2+}, Cd^{2+} and Pb^{2+}.

To demonstrate the electroanalytical performance of the Nafion-G-SbFE, individual as well as simultaneous analysis of metals were done in 0.1 M acetate buffer (pH 4.6) and 0.5 mg L^{-1} Sb^{3+} ions. Figure 4.21a-c illustrates favorable linear response of the Nafion-G-SbFE while simultaneously increasing the concentration of Cd^{2+}, Pb^{2+} and Zn^{2+} from 5-40 μg L^{-1}. The insets show the corresponding calibration plots for each metal and correlation coefficients, sensitivities and detection limits of each metal determined individually are shown in Table 4.5.
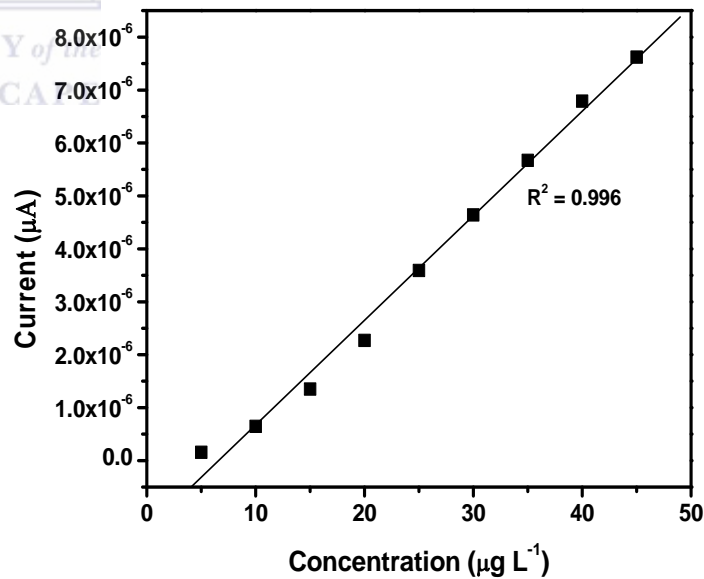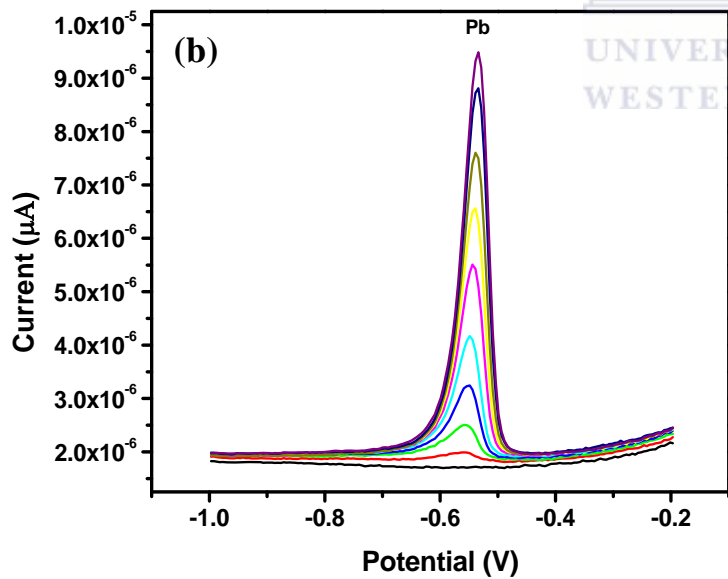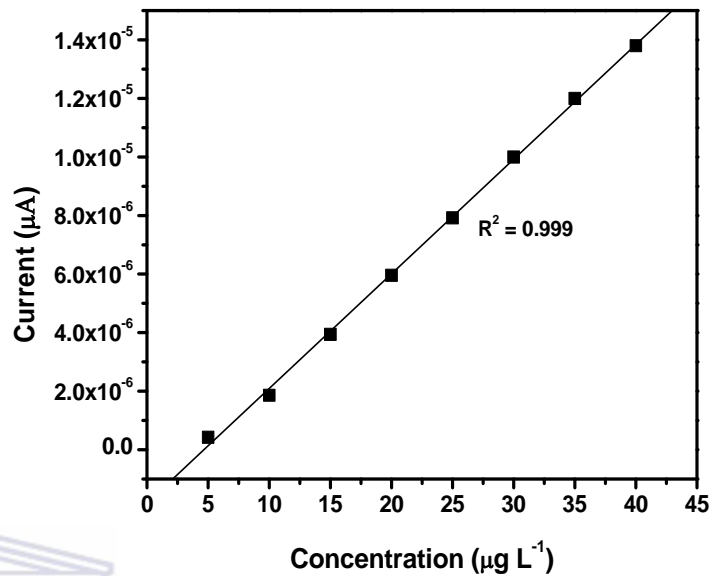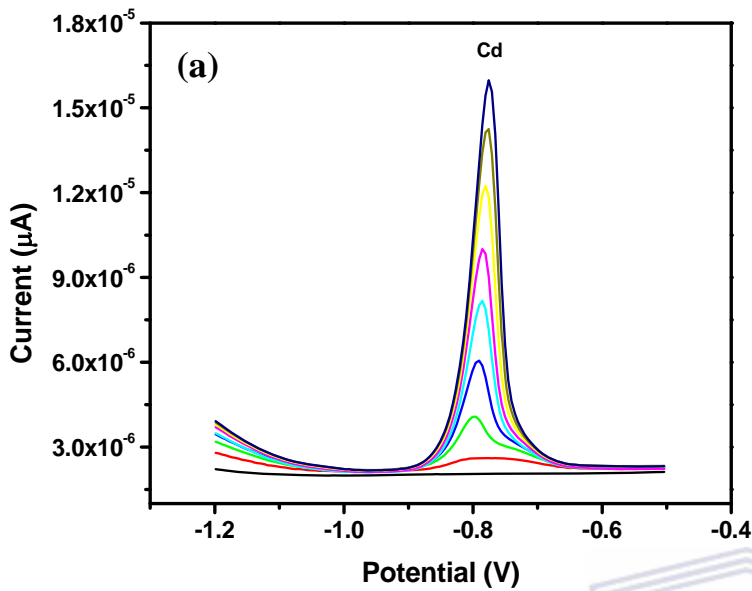
Figure 4.21: Voltammograms for individual determination of (a) Cd^{2+} and (b) Pb^{2+} obtained with Nafion-G-SbFE. Other conditions as in Fig. 4.7.
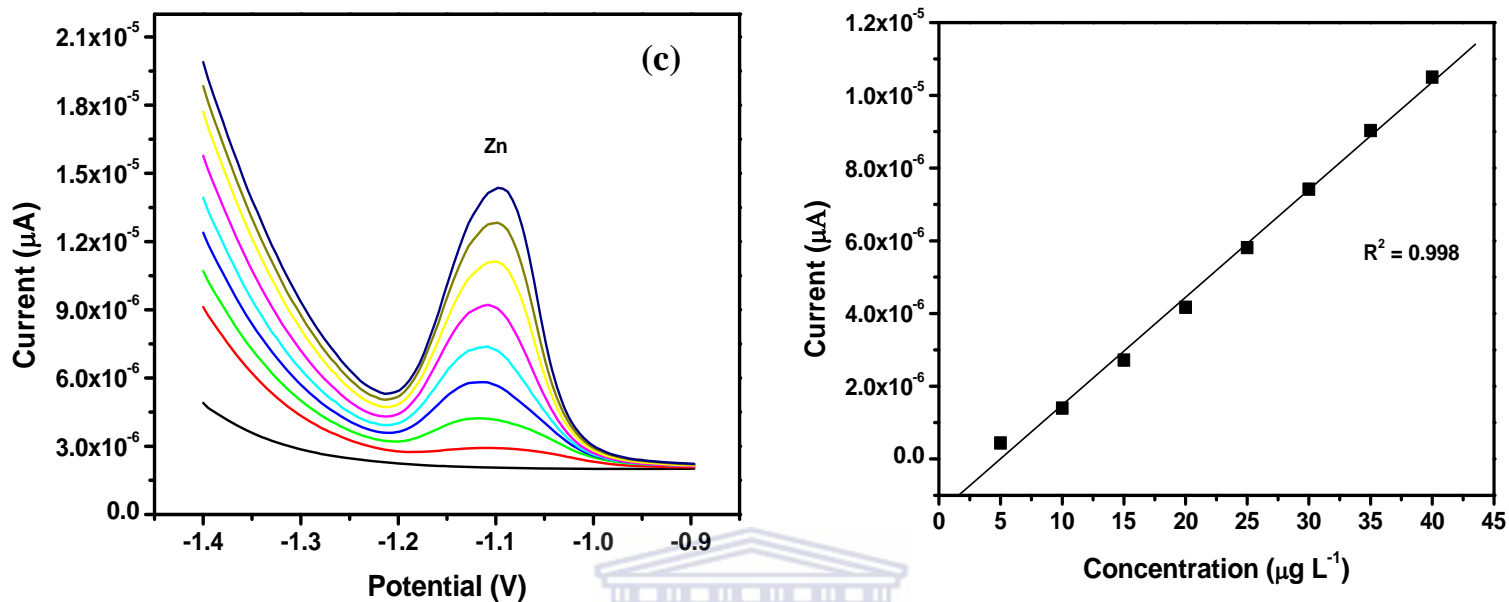
Figure 4.21: Voltammograms for individual determination of (c) Zn^{2+} obtained with Nafion-G-SbFE. Other conditions as in Fig. 4.7.

Table 4.5: Correlation coefficient (R^2), sensitivity and detection limits of Pb^{2+}, Cd^{2+} and Zn^{2+} determined individually at the Nafion-G SbFE.

Individual	R^2	Sensitivity (μA L μg^{-1})	Detection limit (μg L^{-1})
Pb^{2+}	0.998	0.198 ± 0.18	0.03
Cd^{2+}	0.999	0.392 ± 0.12	0.07
Zn^{2+}	0.998	0.296 ± 0.18	0.32

For the simultaneous analyses the same procedure was followed as that of individual analyses. Figure 4.22a are the stripping voltammograms for Pb^{2+} and Cd^{2+} (2-18 μg L^{-1}) and Fig. 4.22b for Pb^{2+}, Cd^{2+} and Zn^{2+} (5-45 μg L^{-1}) in 0.1 M acetate buffer (pH 4.6) and 0.5 mg L^{-1} Sb^{3+}. For the simultaneous analysis of Cd^{2+} and Pb^{2+} the inset showing the calibration plots which is not very linear for Cd^{2+} but a favorable response is obtained for Pb^{2+}. When all three metal are determined simultaneously i.e. Zn^{2+}, Cd^{2+} and Pb^{2+}, good correlation coefficients are obtained as can be seen from Table 4.6.
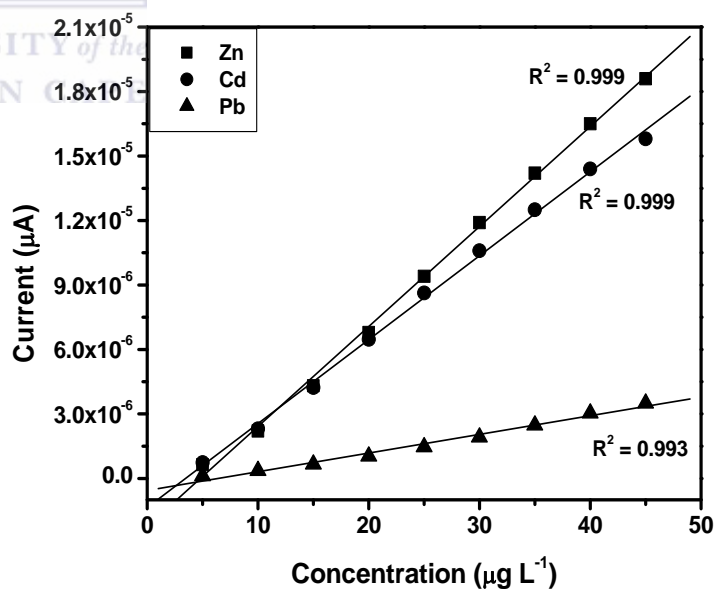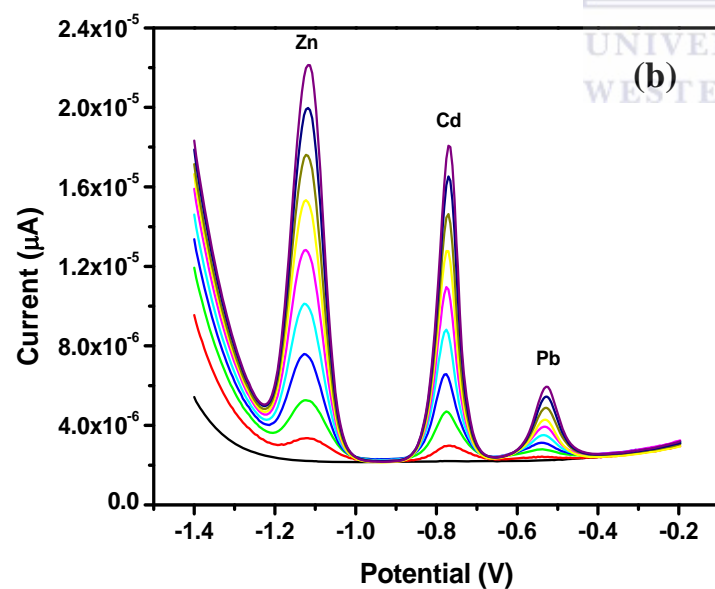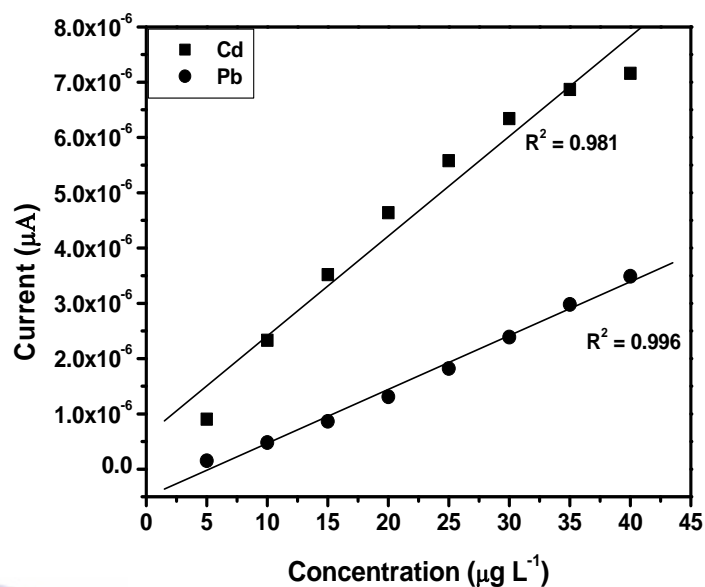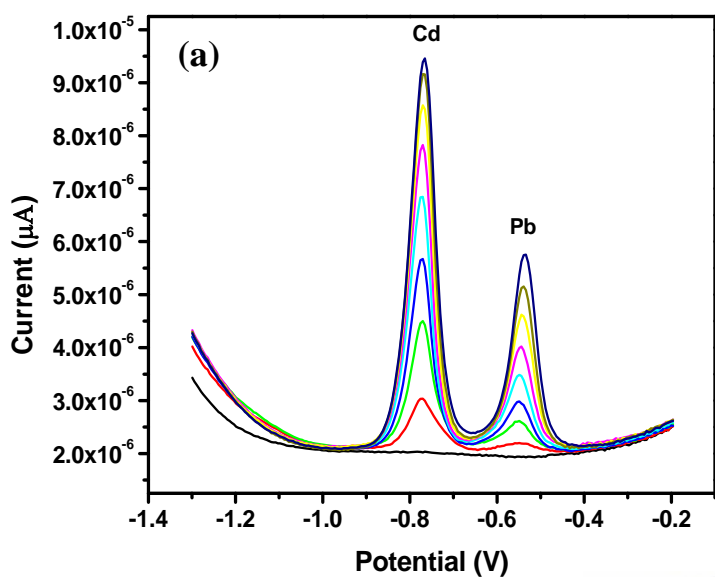
Figure 4.22: Voltammograms for simultaneous determination of (a) Cd^{2+} and Pb^{2+} and (b) Zn^{2+}, Cd^{2+} and Pb^{2+} obtained with Nafion-G-SbFE. Other conditions as in Fig. 4.7.

Table 4.6: Correlation coefficient (R^2), sensitivity and detection limits of Pb^{2+}, Cd^{2+}, Zn^{2+} and Cu^{2+} determined simultaneously at the SbFE.

Simultaneously	R^2	Sensitivity ($\mu A\ L\ \mu g^{-1}$)	Detection limit ($\mu g\ L^{-1}$)
Pb^{2+}	0.993	0.0869 ± 0.10	0.07
Cd^{2+}	0.999	0.391 ± 0.18	0.07
Zn^{2+}	0.999	0.465 ± 0.21	0.20

4.4.4.2 Comparison between individual and simultaneous determination of metals

The sensitivity of certain metals determined individually differed when analyzed simultaneously. The sensitivity of Cd^{2+} stayed relatively the same when determined individually versus simultaneous. Pb^{2+} however had a decrease in sensitivity from 0.19 $\mu A\ L\ \mu g^{-1}$ to 0.0869 $\mu A\ L$ μg^{-1}. In this solution where all three metals are present Pb^{2+} is stripped last, thus it is left with the remaining active sites since most of it has already been taken up by Zn^{2+} and Cd^{2+}. The low sensitivity of Pb^{2+}, could also be attributed to a possible Sb-Pb intermetallic interference which was reported by Tesarova et al. [9].

4.5 Comparison of metal platforms

The sensitivity of the three different Nafion-G metal platforms (Nafion-G HgFE, Nafion-G BiFE, and Nafion-G SbFE) were compared by SWASV to see which of the platforms being used in this analysis is the most sensitive. The stripping voltammograms are illustrated in Fig. 4.23 and were obtained in 30 µg L^{-1} of Zn^{2+}, Cd^{2+} and Pb^{2+} in 0.1M acetate buffer (pH 4.6) solution. The Nafion-G-HgFE exhibited the sharpest and highest peak current and the therefore is the most sensitive in terms of electrode peak current. The sensitivity decreased in the order of Nafion-G BiFE > Nafion-G-SbFE. The peak height of Zn^{2+} on the Nafion-G HgFE is four times greater than on the Nafion-G BiFE and Nafion-G SbFE, for Cd^{2+} it two times and five times respectively and for Pb^{2+} roughly 1.5 times and six times respectively. The differences in peak height of the metals on the different Nafion-G metal platforms are tremendous. This is one of the major reasons why industries are still using mercury as a platform, whether it is a HMDE, DME or thin film electrode. Even if it is extremely toxic, it still gives the better sensitivity.
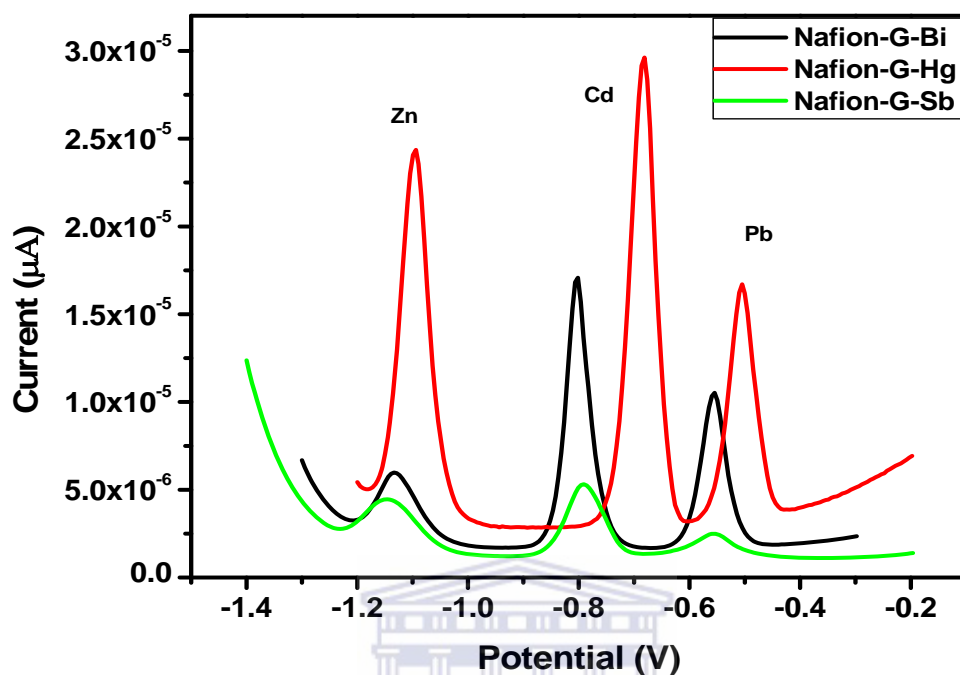
Figure 4.23: SWASV of 30 μg L^{-1} Zn^{2+}, Cd^{2+} and Pb^{2+} at a Nafion-G-HgFE, Nafion-G-BiFE and Nafion-G-SbFE. Supporting electrolyte: 0.1 M acetate buffer (pH 4.6); deposition potential: -1.3 V; deposition time: 120 s; frequency: 50 Hz; amplitude: 0.025 V and voltage step: 0.005 V.

4.6 Summary of tables with detection limits of metals on the different Nafion-G metal platforms

Low detection limits were obtained for each metal on the different Nafion-G metal platforms. Individual analysis gave lower sensitivities that simultaneous, which is attributed to the fact that during simultaneous analysis, all three metals are placed in the same solution and each metal is competing for the same active sites on the electrode surface. On the Nafion-G BiFE Pb^{2+} and Cd^{2+}, gave lower detection limits when determined simultaneously as well as Zn^{2+} on the Nafion-

G SbFE. This is due to the solubility of the metals in the bismuth and antimony. As described previously in the literature review, the formation of an amalgam depends on the solubility of the metal in the mercury; these films follow the same principle. The detection limits from this work was also compared to those from previously reported work (Table 4.9) and compared favorably. The Nafion-G HgFE gave better detection limits than those from previously reported work.

Table 4.7: Correlation coefficient (R^2), sensitivities and detection limit values for the individual determination of Pb^{2+}, Cd^{2+}, Zn^{2+} and Cu^{2+} at the different Nafion-G modified electrode platforms.

Electrode type	Individual	R^2	Sensitivity ($\mu A\ L\ \mu g^{-1}$)	Detection limits ($\mu g\ L^{-1}$)
Nafion-G-Hg film	Pb^{2+}	0.992	0.54	0.07
	Cd^{2+}	0.999	1.64	0.08
	Zn^{2+}	0.997	1.25	0.07
	Cu^{2+}	0.985	12.98	0.07
Nafion-G-Bi film	Pb^{2+}	0.986	0.176	0.13
	Cd^{2+}	0.984	0.177	0.18
	Zn^{2+}	0.990	0.0699	0.33
	Cu^{2+}	0.999	0.327	0.17
Nafion-G-Sb film	Pb^{2+}	0.998	0.198	0.03
	Cd^{2+}	0.999	0.392	0.07
	Zn^{2+}	0.998	0.296	0.32

Table 4.8: Correlation coefficient (R^2), sensitivities and detection limits for the simultaneous analysis of Pb^{2+}, Cd^{2+} and Zn^{2+} at the different Nafion-G modified electrode platforms.

Electrode type	Simultaneous	R^2	Sensitivity ($\mu A\ L\ \mu g^{-1}$)	Detection limits ($\mu g\ L^{-1}$)
Nafion-G-Hg film	Pb^{2+}	0.990	0.577	0.07
	Cd^{2+}	0.983	1.07	0.13
	Zn^{2+}	0.999	0.758	0.14
Nafion-G-Bi film	Pb^{2+}	0.999	0.120	0.12
	Cd^{2+}	0.999	0.428	0.08
	Zn^{2+}	0.997	0.237	0.85
Nafion-G-Sb film	Pb^{2+}	0.993	0.0869	0.07
	Cd^{2+}	0.999	0.391	0.07
	Zn^{2+}	0.999	0.465	0.20

Table 4.9: Detection limits found from previous studies of Zn^{2+}, Cd^{2+} and Pb^{2+} at various electrodes.

Metal Detected	Electrode Type	Deposition time (s)	Electrochemical stripping technique	Detection limit (µg L)	References
Pb^{2+}, Cd^{2+}	Sb film C-paste	120	SWASV	Pb^{2+} = 0.8 Cd^{2+} = 0.2	[9]
Pb^{2+}, Cd^{2+} Zn^{2+}	Bi-C-nanotubes	300	SWASV	Pb^{2+} = 1.3 Cd^{2+} = 0.7 Zn^{2+} = 12	[7]
Pb^{2+}, Cd^{2+}	Bi film C-paste	120	SWASV	Pb^{2+} = 0.8 Cd^{2+} = 1.0	[133]
Pb^{2+}, Cd^{2+}	Bi nanopowder on carbon	180	SWASV	Pb^{2+} = 0.15 Cd^{2+} = 0.07	[134]
Pb^{2+}, Cd^{2+} Zn^{2+}	Bi/poly (p-ABSA)	240	DPASV	Pb^{2+} = 0.80 Cd^{2+} = 0.63 Zn^{2+} = 0.62	[135]
Pb^{2+}, Cd^{2+} Zn^{2+}	Bi-nanoparticles on screen printed-C	120	SWASV	Pb^{2+} = 0.9 Cd^{2+} = 1.3 Zn^{2+} = 2.6	[136]

Pb^{2+}, Cd^{2+} Zn^{2+}, Cu^{2+}	Boron-doped diamond	60	DPASV	Pb^{2+} = 1.15 Cd^{2+} = 0.36 Zn^{2+} = 1.6	[137]
Pb^{2+}, Cd^{2+} Zn^{2+}	Disc-graphite BiFE	120	SWASV	Pb^{2+} = 0.497 Cd^{2+} = 0.325 Zn^{2+} = 0.785	[138]
Pb^{2+}, Cd^{2+} Zn^{2+}, Cu^{2+} Ag^+	Boron-doped diamond		DPASV	Pb^{2+} = 5.0 Cd^{2+} = 1.0 Zn^{2+} = 50	[139]
Pb^{2+}, Cd^{2+} Zn^{2+}, Cu^{2+} Ag^+	Mercury film electrode		DPASV	Pb^{2+} = 5.0 Cd^{2+} = 1.0 Zn^{2+} = 10	[139]
Pb^{2+}, Cd^{2+}	Bismuth film electrode	90	SWASV	Pb^{2+} = 6.9 Cd^{2+} = 1.4	[140]
Pb^{2+}, Cd^{2+} Zn^{2+}	NC (Bpy) BiFE	120	SWASV	Pb^{2+} = 0.077 Cd^{2+} = 0.12 Zn^{2+} = 0.56	[141]
Pb^{2+}, Cd^{2+} Zn^{2+}	NC BiFE		SWASV	Pb^{2+} = 2 Cd^{2+} = 2 Zn^{2+} = 6	[142]
Cd^{2+}	Nafion-graphene HgFE	500	DPASV	Cd^{2+} = 0.005	[29]

Pb^{2+}, Cd^{2+}	Nafion-G-BiFE	300	DPASV	$Pb^{2+} = 0.02$ $Cd^{2+} = 0.02$	[16]
Pb^{2+}, Cd^{2+}, Zn^{2+}, Cu^{2+}	Nafion-G-HgFE	120	SWASV	$Cd^{2+} = 0.08$ $Pb^{2+} = 0.07$ $Zn^{2+} = 0.07$ $Cu^{2+} = 0.07$	In this work
Pb^{2+}, Cd^{2+}, Zn^{2+}, Cu^{2+}	Nafion-G-BiFE	120	SWASV	$Cd^{2+} = 0.18$ $Pb^{2+} = 0.13$ $Zn^{2+} = 0.33$ $Cu^{2+} = 0.17$	In this work
Pb^{2+}, Cd^{2+}, Zn^{2+}	Nafion-G-SbFE	120	SWASV	$Cd^{2+} = 0.07$ $Pb^{2+} = 0.03$ $Zn^{2+} = 0.32$	In this work

4.5 PART E: Application of Nafion-G modified electrodes

4.5.1 Recovery from spiked electrolyte solution

The accuracy of the analyses at the different Nafion-G metal platforms was evaluated through recovery studies. The electrolyte solution (0.1 M acetate buffer) was spiked with 10 μg L^{-1} of metal ions and analyzed by SWASV. Four replicates for each sample was run and the concentration determined using the Standard Addition Calculation. The results obtained were compared to ICP-MS. The recovery results of each metal on the different platforms are shown in Table 4.10.
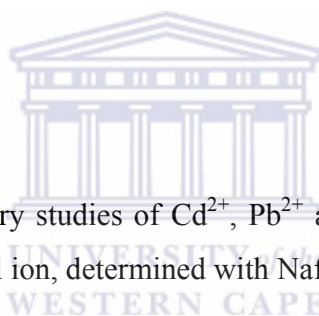
Table 4.10: Comparison of recovery studies of Cd^{2+}, Pb^{2+} and Zn^{2+} from 0.1 M acetate buffer spiked with 10 μg L^{-1} of each metal ion, determined with Nafion-G metal platforms and ICP-MS.

Metals	Nafion-G Mercury film electrode (μg L^{-1})	Nafion-G Bismuth film electrode (μg L^{-1})	Nafion-G Antimony film electrode (μg L^{-1})	ICP-MS (μg L^{-1})
Cd^{2+}	11.34 ± 0.10	6.48 ± 0.321	6.10 ± 0.28	7.12
Pb^{2+}	14.23 ± 0.40	8.27 ± 0.28	2.67 ± 0.27	7.20
Zn^{2+}	8.56 ± 1.00	4.40 ± 0.24	7.28 ± 0.32	9.42

From Table 4.10 one notices the difference in the results obtained from SWASV versus that of the ICP-MS. The low ICP-MS results can be attributed to sodium present in the acetate buffer solution. Sodium is a very strong reducing agent and thus when the standards were prepared and

113

analyzed it caused the peak suppression resulting in the low recovery [143]. When the metal ions were analyzed in HCl nearly 100 % recovery was obtained (Table 4.11) and this was because HCl has the tendency to stabilize the metal ions in a solution. A comparison was run just to prove that samples made up in acidic media behave better than those made up in buffer media. For the results obtained using SWASV, the high recoveries obtained for Cd^{2+} and Pb^{2+} on the Nafion-G HgFE can be attributed to metal carryover. The low recovery obtained for Zn^{2+} on the Nafion-G BiFE can be attributed to the difficulty of determining Zn^{2+} simultaneous with Cd^{2+} and Pb^{2+} due to the competition of these metals [7]. A low recovery for Pb^{2+} was also obtained on the Nafion-G SbFE, this can be attributed to a possible Sb-Pb intermetallic interference where the stripping signal of Pb^{2+} is dependent on the Sb^{3+} concentration [9].
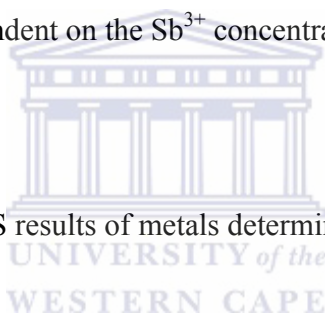
Table 4.11: Comparison of ICP-MS results of metals determined in 0.1 M HCl and 0.1 M acetate buffer.

Metals	ICP-MS (0.1 M HCl) (%)	ICP-MS (0.1 M acetate buffer) (%)
Cd^{2+}	94.3	71.2
Pb^{2+}	94.1	72.0
Zn^{2+}	102.3	94.2

4.5.2 Recovery from lake water sample

For the purpose of practical applicability, a real water sample was collected from Edith Stephens Wetlands Park and the Nafion-G HgFE was employed for the determination of Zn^{2+}, Cd^{2+} and Pb^{2+} metal ions. The lake water was adjusted to pH 4.6 using sodium acetate buffer and a deposition time of 600 s was used for the analysis. In lake water the total metal concentration consists of free metal ions as well as metal bound or which form complexes with other organic acids e.g. humic acids, hence since stripping analysis measurements are based on the available free metal ions in solution a longer deposition time is required to pre-concentrate the free ions. The deposition time of 120 s was used for a test solution which consists mainly of free metal ions and 600 s for the lake water. On the other hand the ICP-MS technique measures the total metal concentration (free metal ion + bound metal) since the sample matrix is completely destroyed in the plasma leaving the metal exposed for measurement.

The results obtained were compared with ICP-MS. The Nafion-G HgFE was sensitive enough to be able to detect Zn^{2+}, Cd^{2+} and Pb^{2+} as shown in Table 4.12. From Table 4.12, Zn^{2+} and Pb^{2+} compares favorably with ICP-MS, however for Cd^{2+}, a very high result was obtained with SWASV compared to ICP MS. This can be attributed to intermetallic interferences which exist between Cu-Cd [6]; even though SWASV could not detect the Cu^{2+} it may still be present in the lake water. For ICP-MS a variation in the result for Cd^{2+} was obtained, which tells us that the concentration of Cd^{2+} changed continuously which is understandable since the amount Cd^{2+} was so low it is difficult to obtain the same result constantly.

These metals (i.e. Zn^{2+}, Cd^{2+}, Pb^{2+}) were below the detection limit for the Nafion-G BiFE and Nafion-G SbFE since it could not be detected, thus to determine Cd^{2+} and Pb^{2+} on theses two Nafion-G metal platforms, the lake water was spiked with 10 µg L^{-1} of Cd^{2+} and Pb^{2+} and then determined using the Standard Addition Calculation with a deposition time of 120 s. Results are found in Table 4.13 and are compared with ICP-MS results.

Table 4.12: Comparison of recovery studies of Cd^{2+}, Pb^{2+} and Zn^{2+} from Edith Stephens Wetlands lake water, determined with Nafion-G HgFE and ICP-MS.

Metal	Nafion-G Mercury film electrode (µg L^{-1})	ICP-MS (µg L^{-1})
Cu^{2+}	N/D	5.780
Cd^{2+}	0.1403 ± 0.00513	$<0.009 - 0.65$
Pb^{2+}	0.534 ± 0.0419	0.520
Zn^{2+}	1.817 ± 0.4992	2.310

Table 4.13: Comparison of recovery studies of Cd^{2+} and Pb^{2+} from Edith Stephens Wetlands lake water spiked with 10 μg L^{-1} of Cd^{2+} and 10 μg L^{-1} of Pb^{2+} determined with Nafion-G BiFE, Nafion-G SbFE and ICP-MS.

Metal	Nafion-G Bismuth film electrode (μg L^{-1})	Nafion-G Antimony film electrode (μg L^{-1})	ICP-MS (μg L^{-1})
Pb^{2+}	8.016 ± 0.660	8.705 ± 0.251	10.090
Cd^{2+}	7.273 ± 1.281	6.553 ± 0.500	9.820

The recoveries obtained from the lake water on the Nafion-G BiFE and Nafion-G SbFE did not compare very favorably. The ICP-MS behaves better than SWASV technique for these two platforms. This may be due to different interferences which operate at specific techniques and which influence the final result.

5. CONCLUSION and FUTURE WORK

5.1 Conclusion

A highly enhanced sensing platform based on the Nafion-graphene nanocomposite film was established for the individual as well as simultaneous determination of Zn^{2+}, Cd^{2+}, Pb^{2+} and Cu^{2+} by square-wave anodic stripping voltammetry. The nanocomposite film combining the advantages of graphene and the cation exchange capacity of Nafion enhanced the sensitivity of the target metal ions. In this project the cation exchange capacity of the Nafion and the enhanced electron conduction of graphene are combined and this yields a sensing platform with enhanced sensitivity towards the selected metal ions. The Nafion not only acts as an effective solubilizing agent for the graphene nanocomposite but also as an antifouling coating to reduce the influence of surface-active macromolecules. The electrochemical sensing interface exhibited excellent stripping performances for trace analysis of Zn, Cd and Pb combining the advantages of graphene nanosheets together with the unique features of the *in situ* plating mercury film, bismuth film as well as antimony film. To our knowledge Nafion-G SbFE has never been used for metal detection as well as the simultaneous analysis of Zn^{2+}, Cd^{2+} and Pb^{2+} on Nafion-G HgFE using SWASV. The analytical application of the Nafion-G modified electrode was assessed by doing recovery studies and the result for the Nafion-G mercury film electrode (Nafion-G BiFE, Nafion-G SbFE) was compared with the results obtained by ICP-MS. By analyzing lake water, the capability of the Nafion-G nanocomposite metal film electrodes for use in environmental analysis was demonstrated. Even though the Nafion-G BiFE and the Nafion-G-

SbFE is more environmentally friendly than the Nafion-G HgFE, the combination of the mercury with the Nafion-G nanocomposite film is still the more sensitive out of the three electrodes and was the only one which detected trace metals in the lake water. For the Nafion-G BiFE and SbFE the lake water was spiked because it was below the detection limit. The detection limits obtained for each metal clearly shows that this technique is capable of detecting metals below the detection requirements of the Environmental Protective Agency (EPA).

5.2 Future Work

Future work includes trying to find a way of analyzing zinc and copper simultaneously without the use of gallium ions on the Nafion-G HgFE. Focus more on the application part of the analysis and finding explanations to why low recoveries are obtained for certain metals on certain instrumentations, and whether adsorption or intermetallic interferences are actually occurring. Develop more mercury free electrodes which give superior sensitivity.

REFERENCES

1. http://www.lenntech.com/heavymetals.htm, *Heavy Metals.* Water Treatment Solutions LENNTECH, 03:11:2010.

2. Ala, A.Walker.; A. P.; Ashkan, K.; Dooley, J. S.; Schilsky, M. L. *Wilson's Disease.* The Lancet, 2007. **369**: p. 397-408.

3. http://www.epa.gov/safewater/contaminants/index.html. *<<Environmental Protective Agency>>*. 16:06:2010.

4. Wang, J., *Stripping Analysis: Principles, Instrumentation, and Application*. 1985, Deerfield Beach, Florida: VCH Publishers, Inc.

5. Achterberg, E. P.; Braungardt., C. *Stripping voltammetry for the determination of trace metal speciation and in-situ measurements of trace metal distributions in marine waters.* Analytica Chimica Acta, 1999. **400**: p. 381.

6. Batley, G.E., *Electroanalytical techniques for the determination of heavy metals in seawater.* Marine Chemistry., 1983. **12**: p. 107.

7. Hwang, G, H.; Han., W. K.; Park, J. S.; Kang, S. G. *Determination of trace metals by anodic stripping voltammetry using a bismuth-modified carbon nanotube electrode.* Talanta, 2008. **76**: p. 301-308.

8. Baldrianova, L.; Svancara, I.; Vlcek, M.; Economou, A.; Sotiropoulos, S. *Effect of Bi(III) concentration on the stripping voltammetric response of in situ bismuth-coated carbon paste and gold electrodes.* Electrochimica Acta, 2006. **52**: p. 481-490.

9.   Tesarova, E.; Baldrianova., L.; Hocevar, S. B.; Svancara, I.; Vytras, K.; Ogorevc, B. *Anodic stripping voltammetric measurement of trace heavy metals at antimony film carbon paste electrode.* Electrochimica Acta, 2009. **54**: p. 1506-1510.

10.   Novoselov, K. S.; Jiang., Z.; Zhang, Y.; Morozov, S.V.; Stormer, H.L.; Zeitler; U.; Maan, J.C.; Boebinger, G.S.; Kim., P.; Geim, A.K. *Room-temperature quantum Hall effect in graphene.* Science, 2007. **315**: p. 1379.

11.   Abanin, D. A.; Levitov., L. S. *Quantized Transport in Graphene p-n Junctions in a magnetic field.* Science, 2007. **317**: p. 641.

12.   Zhang, Y. B.; Tan., Y. W.; Stormer, H. L.; Kim, P. *Experimental observation of the quantum Hall effect and Berry's phase in graphene.* Nature, 2005. **438**: p. 201.

13.   Balandin, A. A.; Ghosh., S.; Bao, W. Z.; Calizo, I.; Tewelderbrhan, D.; Miao, F.; Lau, C. N. *Superior Thermal Conductivity of Single-Layer Graphene.* Nano Letters, 2008. **8**: p. 902.

14.   Lee, C.; Wei., X. D.; Kysar, J. W.; Hone, J. *Measurement of the Elastic Properties and Intrinsic Strength of Monolayer Graphene.* Science, 2008. **321**: p. 385.

15.   Gomez-Navarro, C.; Burghard., M.; Kern, K. *Elastic Properties of Chemically Derived Single Graphene Sheets.* Nano Letters, 2008. **8**: p. 2045.

16.   Li, J.; Guo, S.; Zhai., Y. Wanga, E, *High-sensitivity determination of lead and cadmium based on the Nafion-graphene composite film.* Analytica Chimica Acta 2009. **649**: p. 196-201.

17.   Novoselov, K. S.; Geim., A.K.; Morozov, S.V.; Jiang., D.; Zhang, Y.; Dubonos, S.V.; Grigorieva, I.V, Firsov, A.A. *Electric field effect in atomically thin carbon films.* Science, 2004. **306**: p. 666.

18.   Paredes, J.I.; Villar-Rodil., S.; Mart_inez-Alonso, A.; Tasc_on, J.M.D. *Graphene Oxide Dispersions in Organic Solvents.* Langmuir, 2008. **24**: p. 10560-10564.

19.   Novoselov, K.S.; Jiang., D.; Schedin, F.; Booth, T.J.; Khotkevich, V.V.; Morozov, Geim, A.K. *Proceedings of the National Academy of Science* USA, 2005. **102**: p. 10451-10453.

20.   Hernandez, Y.; Nicolosi., V.; Lotya, M.; Blighe, F.M.; Sun, Z.Y.; De, S.; Mcgovern, I.T.; Holland, B.; Byrne, M.; Gun'Ko, Y.K.; Boland, J.J.; Niraj, P.; Duesberg, G.; Krishnamurthy, S.; Goodhue, R.; Hutchison, J.; Scardaci, V.; Ferrari, A.C.; Coleman, J.N. *High-yield production of graphene by liquid-phase exfoliation of graphite.* Nature Nanotechnology, 2008. **3**: p. 563-568.

21.   Somani, P.R.; Somani., S.P.; Umeno, M. , *Planer nano-graphenes from camphor by CVD.* Chemical Physics Letters, 2006. **430**: p. 56-59.

22.   Subrahmanyam, K.S.; Vivekchand., S.R.C.; Govindaraj, A.; Rao, C.N.R. *A study of graphenes prepared by different methods: characterization, properties and solubilization.* Journal of Material Chemistry, 2008. **18**: p. 1517-1523.

23.   Shen, J.; Hue., Y.; Li, C.; Qin, C.; Shi, M.; Ye, M. *Layer-by-Layer Self-Assembly of Graphene Nanoplatelets.* Langmiur, 2009. **25**: p. 6122-6128.

24.   Si, Y.C.; Samulski., E.T., *Synthesis of Water Soluble Graphene.* Nano Letters, 2008. **8**: p. 1679-1682.

25.   Gilje, S.; Han., S.; Wang, M.S.; Wang, K.L.; Kaner, R.B. *A Chemical Route to Graphene for Device Applications.* Nano Letters, 2007. **7**: p. 3394-3398.

26.   Wang, Y.; Li., Y.M.; Tang, L.H.; Lu, J.; Li, J.H. *Application of graphene-modified electrode for selective detection of dopamine.* . Electrochemistry Communications, 2009. **11**: p. 889.

27.   Lu, J.; Drzal., L.T.; Worden, R.M.; Lee, I. *Simple Fabrication of a Highly Sensitive Glucose Biosensor Using Enzymes Immobilized in Exfoliated Graphite Nanoplatelets Nafion Membrane.* Chemistry of Materials 2007. **19**: p. 6240.

28.   Frenzel, W. *Mercury films on a glassy carbon support: attributes and problems.* Analytica Chimica Acta, 1992. **273**: p. 123-137.

29.   Li, J.; Guo., S.; Zhai, Y.; Wang, E. *Nafion–graphene nanocomposite film as enhanced sensing platform for ultrasensitive determination of cadmium.* Electrochemistry Communications, 2009. **11**: p. 1085-1088.

30.   Kissinger, P., Heineman, W. R. *Laboratory Techniques in Electroanalytical Chemistry*. 2nd ed. 1996.

31.   Zoski, C.G. *Handbook of Electrochemistry* 2007.

32.   Bard, A.J.; Faulkner, L. R. *Electrochemical Methods: Fundamentals and Applications*. 2nd ed. 2000: Wiley.

33.   Protti, P. *Introduction to Modern Voltammetric and Polarographic Analisys Techniques* 4th ed. AMEL Electrochemistry. 2001.

34.   Beaty, R. D.; Kerber., J. D. *Concepts, Instrumentation and Techniques in Atomic Absorption Spectrophotometry*. 2nd ed. 1993, USA: THE PERKIN-ELMER CORPORATION.

35.   Boss, C. B.; Fredeen., K. J. *Concepts, Instrumentation and Techniques in Inductively Coupled Plasma Optical Emission Spectrometry*. 2nd ed. 1997, USA: THE PERKIN ELMER CORPORATION.

36.   Merkoci., A. S. ed. *Electrochemical Sensor Analysis*. Comprehensive Analytical Chemistry, ed. D. Barcelo. Vol. 49. 2007, Elsevier: UK.

37. http://www.basinc.com/mans/EC/epsilon/Techniques/Pulse/pulse.html,*PulseVoltammetricTechniques* 01:11:2010.

38.   Barker, G.C., *Square wave polarography and some related techniques.* Analytica Chimica Acta, 1958. **18**: p. 118.

39.   Florence, T.M. *Cathodic stripping voltammetry: Part I. Determination of organic sulfur compounds, flavins and porphyrins at the sub-micromolar level.* Journal of Electroanalytical Chemistry, 1979. **97**: p. 219.

40.   Economou, A.; Fielden., P. R. *Mercury film electrodes: developments, trends and potentialities for electroanalysis.* Analyst, 2003. **128**: p. 205.

41.   http://people.clarkson.edu/~ekatz/scientists/kemula_small.jpg,*WiktorKemula.*09:09:2010.

42.   Florence, T.M., *Anodic Stripping Voltammetry With A Glassy Carbon Electrode Mercury-Plated in situ.* Journal of Electroanalytical Chemistry, 1970. **27**: p. 273.

43.   Wang, J.; Lu., J.; Hocevar, S. B.; Farias, P. A. M.; Ogorevc, B. *Bismuth-coated carbon electrodes for anodic stripping voltammetry.* Analytical Chemistry, 2007. **72**(14): p. 3218-3222.

44.   Long G. G.; Freedman., L. D.; Doak, G. O. *Bismuth and bismuth alloys, in: Encyclopedia of Chemical Technology.* 1978 New York: Wiley.

45.   Hocevar, S.B.; Ogorevc., B.; Wang, J.; Pihlar, B. *A study on operational parameters for advanced use of bismuth film electrode in anodic stripping voltammetry.* Electroanalysis 2002. **14**: p. 1707.

46.   G. Kefala, A.; Economou., A. Voulgaropoulos and M. Sofoniou. *A study of bismuth-film electrodes for the determination of trace metals by anodic stripping voltammetry and their application to the determination of Pb and Zn in tapwater and human hair.* Talanta, 2003. **61**: p. 603.

47.   Krolicka, A.; Pauliukaite., R.; Svancara, I.; Metelka, R.; Bobrowski, A.; Norkus, E.;. Kalcher., K.; Vytras, K. *Bismuth-film-plated carbon plated electrodes.* Electrochemistry Communication, 2002. **4** p. 193.

48.   Wang, J.; Lu., J. M Kirgoz, U. A.; Hocevar., A. B.; Ogorevc, B. *Insight into the anodic stripping voltammetric behaviour of bismuth film electrodes.* Analytica Chimica Acta, 2001. **434**: p. 29.

49.   Batley, G.E.; Florence., T. M, *Determination of copper in sea water by anodic stripping voltammetry.* Journal of Electroanalytical Chemistry, 1974. **55**: p. 23.

50.   Florence, T.M. *Determination of trace metals in marine samples by anodic stripping voltammetry.* Journal of Electroanalytical Chemistry, 1972. **35**: p. 237.

51.   Copeland, T.R.; Osteryoung., R. A.; Skogerboe, R. K. *Elimination of copper-zinc intermetallic interferences in anodic stripping voltammetry.* Analytical Chemistry, 1974. **46**: p. 2093.

52.   Farghaly, O.A. *Direct and simultaneous voltammetric analysis of heavy metals in tapwater samples ar Assiut city: an approach the analysis time for nickel and cobalt determination at mercury film electrode.* Microchemical Journal, 2003. **75**: p. 119.

53.   Carvalho, L.M.; Nascimento., P. C.; Koschinsky, A.; Bau, M.; Stefanello, R. F.; Spengler, C.; Bohrer, D.; Jost, C., *Simultaneous determination of cadmium, lead, copper and thallium in highly saline samples by anodic stripping voltammetry (ASV) using mercury film and bismuth film electrode.* Electroanalysis, 2007. **19**: p. 1719.

54.   Baldo, M.A.; Danielle., S., *Anodic stripping voltammetry at bismuth-coated and uncoated carbon microdisk electrodes: application to trace metals analysis in food samples.* Analytical Letters, 2005. **37**: p. 995.

55.   Pacheco, W.F.; Miguel., E. M.; Ramos, G. V.; Cardoso, C. E.; Farias, P. A. M.; Aucelio, R. Q., *Use of hydrogen peroxide to achieve interference-free stripping voltammetry determination of copper at the bismuth film electrode.* Analytica Chimica Acta, 2008. **625**: p. 22-27.

56.   Brezonik, P.L.; Brauner., P. A.; Stumm, W., *Trace metal analysis by anodic stripping voltammetry: effect of sorption by natural and model organic compounds.* Water Resources, 1976. **10**: p. 605.

57.   Sagberg, P.; Lund., W. *Trace metal analysis by anodic stripping voltammetry: Effect of surface-active substances.* Talanta, 1982. **29**: p. 457.

58.   Abdullah, M.I.; Reusch.B., B.; Klimek, R. *The determination of zinc, cadmium, lead and copper in a single sea-water sample by differential pulse anodic stripping voltammetry.* Analytica Chimica Acta, 1976. **84**: p. 307.

59.   Wang, J.D., Dewald, H. *Dual coulometric-volummetric cells for on-line stripping voltammetry.* Analytical Chemistry, 1983. **55**: p. 933.

60.   Gerlach, R.W.; Kowalski., B. R. *The generalized standard addition method: intermetallic interferences in anodic stripping voltammetry.* Analytica Chimica Acta, 1982. **134**: p. 119.

61.   Bonneli, J.E.; Taylor., H. E.; Skogerboe, R. K. *A direct differential pulse anodic stripping voltammetric method for the determination of thallium in natural waters.* Analytica Chimica Acta, 1980. **118**: p. 243.

62.   Neeb, R.W., G.; Kiehnast, J. Z, Analytical Chemistry, 1970. **249**: p. 86.

63.   Desimoni, E.; Palmisano., F.; Sabbatini, L. *Simultaneous determination of tin and lead at the parts-per-billion level by coupling differential pulse anodic stripping voltammetry with a matrix exchange method.* Analytical Chemistry, 1980. **52**: p. 1889.

64.   Brown, T.F.; Brown., S. D. *Resolution of overlapped electrochemical peaks with the use of the Kalman filter.* Analytical Chemistry, 1981. **53**: p. 1410.

65.   Bond, A.M.; Grabaric., B. S. *Simple approach to the problem of overlapping waves using a micro-processor controlled polarograph.* Analytical Chemistry, 1976. **48**: p. 1624.

66.   Lui, J.H. *A new approach to the quantitative analysis of overlapping anodic stripping voltammograms.* Analyst, 1980. **105**: p. 939.

67.   Batley, G.E.F., Y. J, *Irradiation techniques for the release of bound heavy metals in natural waters and blood.* Analytica Chimica Acta, 1978. **99**: p. 283.

68.   Brihaye, C.D., G, *Determination of traces of metals by anodic stripping voltammetry at a rotating glassy carbon ring-disk electrode: Part 2 Comparison between linear anodic stripping voltammetry with ring collection and various other stripping techniques.* Analytica Chimica Acta, 1983. **146**: p. 37.

69.   Riley, J.P.G., H, *A physically-coated mercury film electrode for anodic stripping voltammetry.* Analytica Chimica Acta, 1981. **130**: p. 199.

70.   Khandekar, R.N.D., R. G.; Palrecha, M. M.; Zarapkar, L. R. Z, *Simultaneous determination of lead, cadmium and zinc in aerosols by anodic stripping voltammetry.* Analytical Chemistry, 1981. **307**: p. 365.

71.   Tietz, N.W., *Fundamentals of Clinical Chemistry.* 1976, Philadelphia: Saunders.

72.   Geim, A.K., Novoselov, K. S, *The rise of graphene.* Nature Materials 2007. **6**: p. 183-191.

73.   *October 22, 2004: Discovery of Graphene*, in *APS News*. 2009.

74.   *Discovery of Graphene*, in *American Physical Society*. October 22, 2004.

75.   Kroto, H.W., Heath, J. R., O'Brien, S., Curl, R. F. and Smalley, R. F, *C_{60}: Buckminsterfullerenes.* Nature 1985. **318**: p. 162-163.

76.   Iijima, S., Nature 1991. **354**: p. 56-58.

77.   Srinivasan, C., *Graphene – Mother of all graphitic materials*, in *RESEARCH NEWS*. 2007. p. 1338-1339.

78.   http://acigjapan.com/graphite.html, *Characteristics of graphite.* 01:11:2010.

79. Kharisov, O.V.K.a.B.I., *Graphenes, One of the Hottest Areas in the Nanotechnology: Attention of Chemists is Needed.* The Open Inorganic Chemistry Journal, 2008. **2**: p. 39-49.

80. Ernie W. Hill , A.K.G., *The remarkable electronic and mechanical properties of graphene.*

81. Novoselov, K. S.; Jiang., Z.; Zhang, Y.; Morozov, S.; Stormer, H. L.; Zeitler, U.; Maan, J. C.; Boebinger, G. S.; Kim, P.; Geim, A.K. *Room-Temperature Quantum Hall Effect in Graphene.* Science, 2007. **315**(5817): p. 1379.

82. Li, D., Kaner, R. B, *Graphene-based materials.* Science, 2008. **320**: p. 1170.

83. Lemme, M.C., Echtermeyer, T. J., Baus, M., Kurz, H. A, *A graphene field effect device.* IEEE Electron Device Lett., 2007. **28**: p. 282.

84. http://cnx.org/content/m29187/latest, Graphene, 23:03:2010.

85. Bunch, J.S., van der Zande, A. M., Verbridge, S. S., Frank, I. W., Tanenbaum, D. M., Parpia, J. M., Craighead, H. G., Mceuen. P.L, *Electromechanical resonators from graphene sheets.* Science, 2007. **315**: p. 490.

86. Liu, Z., Robinson, J, T., Sun, X. M., Dai. H. J, *PEGylated nanographene oxide for delivery pf water soluble cancer drugs.* J. Am. Chem. Soc. , 2008. **130**: p. 10876.

87. http://mxp.physics.umn.edu/s07/Projects/s07_Graphene/intro.htm, *Structure of graphene.* 18:10:2010.

88. http://www.physorg.com/news119030362.html. *Graphene makes movement easy for electrons*. 19:10:2010.

89.   Kuzmenko, A.B.; van.Heumen., E.; Carbone, F.; van der Marel, D, *Universal infrared conductance of graphite.* Phys Rev Lett 2008. **100**(11): p. 117401.

90.   Nair, R. R.et al., *Fine Structure Constant Defines Visual Transparency of Graphene.* Science, 2008. **320** (5881): p. 1308.

91.   Zhang, Y.et al., *Direct observation of a widely tunable bandgap in bilayer graphene.* Nature, 2009. **459** (7248): p. 820-823.

92.   www.enotes.com/topic/Graphene, Graphene, 18:09:2010.

93.   Das Sarma, S.; Pinczuk, A. *Perspectives in Quantum Hall Effects*. 1997, New York: Wiley.

94.   Novoselov, K.S., Geim, A. K., Morozov, S. V., Jiang, D., Katnelson, M. I., Grignorieva, I. V., Dubonos, S. V., Firsov, A. A., *Two-dimensional gas of massless Dirac fermions in graphene.* Nature, 2005. **438**: p. 197-200.

95.   Lee, C.et al., *"Measurement of the Elastic Properties and Intrinsic Strength of Monolayer Graphene".* Science, 2008. **321** (5887): p. 385.

96.   Frank, I.W., Tanenbaum, D. M., Van Der Zande, A.M., and McEuen, P. L. , *"Mechanical properties of suspended graphene sheets"* J. Vac. Sci. Technol. , 2007. **25**: p. 2558–2561.

97.   Saito, K., Nakamura, J., and Natori, A, *Ballistic thermal conductance of a graphene sheet* Physical Review, 2007. **B 76**: p. 115409.

98.   Delhaes, P., *Graphite and Precursors*. 2001: CRC Press.

99.   Mingo N.; Broido., D.A. , *Carbon Nanotube Ballistic Thermal Conductance and Its Limits.* Physical Review Letters 2005. **95**: p. 096105.

100.   Sutter, P., *Epitaxial graphene: How silicon leaves the scene.* Nature Materials, 2009. **8**(3): p. 171.

101.   Hummers, W.S.; Offeman., R. E, *Preparation of graphitic oxide.* Journal of American Chemical Society, 1958. **80**: p. 1339.

102.   Alfonso Reina, X.J., John Ho, Daniel Nezich, Hyungbin Son, Vladimir Bulovic, Mildred S. Dresselhaus, and Jing Kong, *Large Area, Few-Layer Graphene Films on Arbitrary Substrates by Chemical Vapor Deposition.* NANO LETTERS, 2008. **9**(1): p. 30-35.

103.   Vaari, J.L., J.; Hautoja¨rvi, P. , *The adsorption and decomposition of acetylene on clean and K-covered Co(0001).* Catal. Lett., 1997. **44**(1): p. 43-49.

104.   Ueta, H.S., M.; Nakai, C.; Yamada, Y.; Sasaki, M.; Yamamoto, S. , *Highly oriented monolayer graphite formation on Pt(111) by a supersonic methane beam.* Surf. Sci, 2004. **560**(1-3): p. 183-190.

105.   Gall′, N.; Rut'.kov., E.; Tontegode, A . *Interaction of silver atoms with iridium and with a two-dimensional graphite film on iridium: Adsorption, desorption, and dissolution.* Phys. Solid State, 2004. **46** (2): p. 371-377.

106.   de Parga, A.L.V.; Calleja., F.; Borca, B.; Passeggi, J. M. C. G.; Hinarejos, J. J.; Guinea, F.; Miranda. R. *Periodically Rippled Graphene: Growth and Spatially Resolved Electronic Structure.* Phys. ReV. Lett., 2008. **100**(5): p. 056807-4.

107.   Goodman, D.W.; Yates., J. T. *CO isotopic mixing measurements on nickel: Evidence for irreversibility of CO dissociation.* J. Catal., 1983. **82**(2): p. 255-260.

108.   Madden, H.H.K., J.; Ertl, G. *Interaction of carbon monoxide with (110) nickel surfaces.* J. Chem. Phys., 1973. **58**(8): p. 3401–3410.

109. Gamo, Y.N., A.; Wakabayashi, M.; Terai, M.; Oshima, C., *Atomic structure of monolayer graphite formed on Ni(111). .* Surf. Sci., 1997. **374**(1-3): p. 61–64.

110. Analytical, I. *CHARACTERIZATION OF MATERIALS BY FT-IR*.

111. www.pananalytical.com/index. *PANanalytical*. 30:08:2010.

112. Instruments, P., *Raman spectroscopy basics*, www.piacton.com, 08:08:2010.

113. Gupta, A., Chen G, Joshi, P., Tadigadapa, S., Eklund, P. C *Raman scattering from high-frequency phonons in supported n-graphene layer films.* Nano Letters 2006. **6**: p. 2667.

114. Calizo, I., Miao, F., Bao, W., Lau, C. N., Balandin, A. A *The effect of substrates on the Raman spectrum of graphene: Graphene-on-sapphire and graphene-on-glass.* Appl. Phys. Lett., 2007 **91**: p. 201904.

115. *The Atomic Force Microscopy Resource Library*. 2010 [cited 2010 27:10:2010].

116. Tycko, R., *Biomolecular solid state NMR: Advances in structural methodology and applications to peptide and protein fibrils.* Annual Review of Physical Chemistry, 2001.

117. http://pubs.acs.org/doi/abs/10.1021/nn900728d., *Nanometer Graphene Makes Novel OLEDs Display*, in *Stanford University*. March 19, 2010

118. Wang, X.et al., *Transparent, Conductive Graphene Electrodes for Dye-Sensitized Solar Cells.* Nano Letters, 2007. **8**(1): p. 323.

119. Eda G, F.G., Chhowalla M *Large-area ultrathin films of reduced graphene oxide as a transparent and flexible electronic material.* Nat Nanotechnol 2008. **3**(5): p. 270-4.

120. Stoller, M.D.; Park., S.; Zhu, Y.; An, J.; Ruoff, R. S. *Graphene-Based Ultracapacitors.* Nano Lett 2008. **8**(10): p. 3498.

121. Schedin, F.et al., *Detection of individual gas molecules adsorbed on graphene.* Nature Materials, 2007. **6**(9): p. 652–655.

122. Carbon-Based Electronics: Researchers Develop Foundation for Circuitry and Devices Based on Graphite March 14.

123. Wang, H.N., D.; Kong, J.; Palacios, T. , *Graphene Frequency Multipliers.* IEEE Electr. Device. L, 2009. **30**: p. 547.

124. IBM. Retrieved April 15, from http://www.sciencedaily.com¬/releases/2010/02/100205113551.htm, *Scientists demonstrate world's fastest graphene transistor; holds promise for improving performance of transistors.*, in *ScienceDaily.* 2010, February 7.

125. Kovtyukhova, N.I.; Ollivier., P. J.; Martin, B. J.; Mallouk, T. E.; Chizhik, S. A.; Buzaneva, E. V.; Gorchinskiy, A. D, *Layer-by-layer assembly of ultrathin composite films from mictron-size graphite.* Chemical Materials, 1999. **11**: p. 771.

126. Chen, W.Y., L.; Bangal, P. R, *Preparation of graphene by the rapid and mild thermal reduction of graphene oxide induced by microwaves.* CARBON 2010. **48**: p. 1146 – 1152.

127. Fan, Z.; Wang., K.; Wei, T.; Yan, J.; Song, L.; Shao, B, *An environmentally friendly and efficient route for the reduction of graphene oxide by aluminum powder.* CARBON, 2010. **48**: p. 1670-1692.

128. Stankovich, S., Dikin, D. A., Piner, R. D., Kohlhaas, K. A., Kleinhammes, A., Jia, Y., Wu, Y., Nguyen, S-B. T., Ruoff, R. S, *Synthesis of graphene-based nanosheets via chemical reduction of exfoliated graphite oxide.* Carbon, 2007. **45**: p. 1558-1565.

129.   Heyong He, T.R., Anton Lerf, and Jacek Klinowski, *Solid-State NMR Studies of the Structure of Graphite Oxide.* Journal of Physical Chemistry, 1996. **100**: p. 19954-19958.

130.   Stankovich, S.; Dikin.A.D.; Piner, R.D.; Kohlhaas, K.A.; Kleinhammes, A.; Jia, Y.; Wu, Y.; Nguyen, S-B,T.; Ruoff, R. S. *Synthesis of graphene-based nanosheets via chemical reduction of exfoliated graphite oxide.* Carbon, (2007). **45**: p. 1558-1565.

131.   Fischer, E.; van.den.Berg., C.M.G. *Anodic stripping voltammetry of lead and cadmium using a mercury film electrode and thiocyanate.* Analytica Chimica Acta, 1999. **385**: p. 273-280.

132.   Cooksey, R.S.a.B.G., *Adsorption of lead on container surfaces* Journal of Electroanalytical Chemistry, 1980. **106**: p. 251-262

133.   Svancara, L.; Baldrianova., E.; Tesarova, S.B.; Hocevar, S. A. A.; Elsuccary, A.; Economou, S.; Sotiropoulos, B.; Ogorevc.; K. Vytras *Recent Advances in Anodic Stripping Voltammetry with Bismuth-Modified Carbon Paste Electrodes.* Electroanalysis, 2006. **18**: p. 177.

134.   Lee, G.K.; Lee., H. M.; Rhee, C. K, *Bismuth nano-powder electrode for trace anaysis of heavy metals using anodic stripping voltammetry.* Electrochemical Communication, 2007. **9**: p. 2514-2518.

135.   Wu, Y.; Li., N. B.; Luo, H. Q. *Simultaneous measurement of Pb, Cd and Zn using differential pulse anodic stripping voltammetry at a bismuth/poly (p-aminobenzene sulfonic acid) film electrode.* Sensors and Actuators, 2008. **133**: p. 677-681.

136. Rico, M.A.G.Olivares-Marin., M.; Gil, E. P. *Modification of carbon screen printed electrodes by adsorption of chemically synthesized Bi nanoparticles for the voltammetric stripping detection of Zn (II), Cd (II) and Pb (II).* Talanta, 2009. **80**: p. 631-635.

137. Tall, O.E.I.; Jaffreziv-Renault., N.; Sigaud, M.; Vittori, O. *Anodic stripping voltammetry of heavy metals at nanocrystalline boron-doped diamond electrode.* Electroanalysis, 2007. **18**: p. 177-185.

138. Rahacek, V.;Hotovy., I.; Vojs, M.; Mika, F. *Bismuth film electrodes for heavy metal determination.* Microsystem Technology, 2008. **14**: p. 491-498.

139. McGaw, E.; Swain., G. M, *A comparison of boron-doped diamond thin film and Hg-coated glassy carbon electrodes for anodic stripping voltammetric determination of heavy metals in aqueous media.* Analytica Chimica Acta, 2006. **575**: p. 180-189.

140. Siriangkhawut, W.; Pencharee., S.; Grudpan, K.; Jakmunee, J. *Sequential injection monosegmented flow voltammetric determination of cadmium and lead using a bismuth film working electrode.* Talanta, 2009. **79**: p. 1118-1124.

141. Torma, F.; Kadar., M.; Toth, K.; Tatar, E. *Nafion/2,2'-bipyridyl-modified bismuth film electrode for anodic stripping volatmmetry.* Analytica Chimica Acta, 2008. **619**: p. 173-182.

142. Kefala, G.; Economou., A. *Polymer-coated bismuth film electrode for the determination of trace matals by sequentail-injection analysis/ anodic stripping volatmmetry.* Analytica Chimica Acta, 2006. **576**: p. 283-289.

143. *Reducing agent.* http://en.wikipedia.org/wiki/Reducing_agent, 29-11-2010.